A controllable fluid dynamics system for processing pharmaceutical powders in a single vessel

Kay, Graham Richard

Award date:
2001

Awarding institution:
University of Bath

A CONTROLLABLE FLUID DYNAMICS SYSTEM FOR PROCESSING PHARMACEUTICAL POWDERS IN A SINGLE VESSEL

Submitted by Graham Richard Kay
for the degree of Ph.D.
of the University of Bath
2001

Author : ..... Date : 31.07.2001

ProQuest LLC
789 East Eisenhower Parkway
P.O. Box 1346
Ann Arbor, MI 48106-1346

ACKNOWLEDGEMENTS

It is impossible to name and thank all of the people who have helped and inspired me on the long road to the completion of this work. Nevertheless my grateful thanks are extended to them all, but particularly to the following:

To my supervisor, Professor John Staniforth, for being the ideas man and for his attempts to broaden me.

To the Tobyns; to Sal for providing first class billeting on many occasions and to Mikee for being my 'surrogate supervisor' and for his (successful) attempts to broaden himself.

To Drs. Linda Newnes and Stuart MacGregor for taking care of the engineering side of things, to Dr. Ming 'The Merciless' Li for driving the CFD package, to Gerald Atherton for drawing and building the processors and to the other members of the SVP Project Team for their valued contributions.

To Dr. Martin Clarke for sharing with me his expert knowledge of DPI formulation and for his unique demonstration of the principle of 'time of flight'. Also to the staff and students, past and present, of the Department of Pharmacy and Pharmacology at Bath, many of whom will be friends for life.

To my brother, Andy, for encouraging me to 'do yerself a favour and do sum wurk'.

To my parents for their incredible support, especially my dad, without whose guidance and resolute project management I would have failed in this undertaking.

I reserve special gratitude for Sonia, firstly for her crucial contribution during the frantic completion of this tome but also for agreeing to manage me on a full time basis later this year.

SUMMARY

Processing of dry powder inhaler formulations often requires equipment that is able to impart a high shearing force into the mixing bed in order to adequately disperse the active ingredient and/or other performance modifying ingredients. In addition, particle size of drug and excipient powders must be closely controlled in DPI formulation systems.

The selection of processing equipment available to achieve these conditions is limited and it often difficult to closely control the amount of shear generated within the processing environment.

A series of single vessel processors, so called due to their versatility in performing multiple powder processing operations, was developed, two of which were characterised for their performance in producing blends of an asthma drug, nedocromil sodium, in a formulation designed for dry powder inhalation.

The first vessel (FBSVP-A) was a fluidised bed system with a series of 12 tangential high pressure air nozzles supplying the energy for powder movement. This was found to provide some dry powder blending and particle size reduction performance but the existence of extensive areas of powder stagnation made the equipment inefficient and modification of the vessel was required.

These modifications resulted in fabrication of a second vessel, the FBSVP-B, in which a filter bag replaced the cyclone separator used in the previous design. This was found to offer some improvement in particle size reduction performance. The FBSVP-B was used to manufacture nedocromil sodium blends and was found to produce blends of poor overall homogeneity and variable *in-vitro* aerosol performance. Again, some areas of flow stagnation were found to exist, although these were much reduced from the previous design.

Modelling of the FBSVP-B using computational fluid dynamics was able to successfully predict these areas of low flow activity, thus providing verification of the use of this software in simulating flow regimes in this application.

The CFD software was then used in the design of a final vessel, the SBSVP which utilised high volume air flows in place of the vertical fluidised bed and doubled the number of high pressure air nozzles from the previous vessel designs.

Nedocromil sodium blends processed in this vessel were found to exhibit excellent homogeneity and *in-vitro* aerosol characteristics that were at least equivalent to those found in blends produced in conventional high shear equipment. Rate and extent of particle size reduction were also shown to be enhanced considerably in this vessel design.

It was therefore concluded that further development of the SBSVP may result in a practical alternative to conventional equipment in the preparation of DPI and other formulation systems where controllable high shear inputs are required.

CONTENTS

1. INTRODUCTION

1.1 Inhalation therapy

Delivery of aerosolised drugs to the respiratory tract by inhalation is a well-established route of administering pharmaceutical treatments and has now become the therapy of choice for delivery of medications whose site of action is in lung tissue (Asking and Olsson, 1997).

Inhalation therapy is also being used increasingly for delivery of large-molecule new chemical entities, such as proteins and peptides produced through biotechnology, since many of these materials have demonstrated good lung absorption compared to poor oral bioavailability (Johnson, 1997, Smith, 1997; Berressem, 1999). Other novel therapies have exhibited reduced dosage requirements when inhaled compared to intravenous administration (Nyce, 2000).

The most important uses of inhalation therapy are currently in the treatment of lung diseases such as asthma and chronic obstructive airways disease (Smith and Bernstein, 1996). There is a number of advantages of inhalation over other drug delivery routes for treatment of these and other diseases since the drug is delivered directly to the site of action thus providing a rapid and predictable therapeutic response and avoiding hepatic first-pass and gastrointestinal degradation of the active (Timsina *et al.*, 1994).

1.2 Aerosol delivery systems

The three main systems used for generating medicinal aerosols are nebulisers, pressurised metered dose inhalers (pMDIs) and dry powder inhalers (DPIs), each of which has advantages and disadvantages.

It is generally considered that pMDIs are compact, portable and inexpensive to produce. However, many patients are found to experience difficulties in co-ordinating inhalation with device actuation, which can lead to increased deposition of the dose in the patient's mouth and throat rather than in the deep lung (Crompton, 1982). More recently breath actuated pMDIs have become available that are able to counteract these problems (Hickey and Dunbar, 1997).

pMDIs are often found to discharge large droplets which leave the device at high initial velocities. This can lead to considerable loss of the dose to the oropharynx (Leach, 1999), although the use of spacer devices has been seen to mitigate these effects (Vidgren *et al.*, 1987a).

Concerns regarding the adverse environmental effects of chlorofluorocarbon (CFC) propellants used in pMDIs have led to international regulations (Tansey, 1997) requiring these to be replaced with alternative methods of aerosolisation (Leach, 1999). Although a number of formulations containing hydrofluorocarbon propellants have successfully replaced CFC products (Leach, 1999), presentations that do not require chemical propellants, such as DPIs, are clearly more desirable from an environmental perspective.

DPIs allow generation of an aerosol without using a propellant and problems of co-ordination of patient inspiration with device actuation are avoided since DPIs are breath-actuated. (Steckel and Müller, 1997).

Typical disadvantages of DPIs are a dependency on the patient's inspiratory flow rate for efficient drug delivery, greater problems in dose uniformity than in pMDIs, less protection from environmental effects and increased expense compared to pMDIs (Ashurst *et al.*, 2000).

1.3 Factors influencing lung deposition of inhaled particles

1.3.1 Lung anatomy

The human respiratory tract is composed of a series of branching tubular airways, which become progressively smaller in diameter as they develop into the innermost regions of the lung. The lung can be divided into three sections of gradually decreasing airway diameter; these are the oropharynx, the tracheobronchial airways and the alveolar region, also known as the deep lung (Gerrity, 1990).

The airway diameter will cause particles to be deposited in different parts of the lung anatomy, dependent on a number of factors (Vidgren *et al.*, 1988a).

Particles of >5μm tend to deposit in the upper airways through inertial impaction (Hinds, 1982), since their momentum prevents particles greater than this size from following an airstream as it is drawn through tight turns in the airways. In order to become deposited in the deep lung, it is generally recognised that particles need to be in the size range 1-5μm (Gonda, 1992; Hinds, 1982). It has been found that particles below 0.5μm fail to deposit in the lung in large numbers and are mostly exhaled (Zanen *et al.*, 1994).

1.3.2 Aerosol properties

The physical properties of drug powders for inhalation determine the deposition characteristics of aerosol clouds generated from these powders. The most critical physical property is particle size (Hinds, 1982; Staniforth, 1996).

When characterising particles used in inhalation the most appropriate measure of particle size is represented by the aerodynamic equivalent diameter, D_{ae}, which is defined as the diameter of a perfect sphere of density $1gcm^{-3}$ that has a terminal velocity in still air equal to that of the particle examined; this parameter therefore considers the properties of size, shape and density of a particle (Gonda, 1988).

It is widely accepted that drug particles with a D_{ae} $\oslash 5\mu m$ are most likely to be deposited within the deep lung when inhaled (Ganderton and Kassem, 1992).

Although the particle size of drug and excipient materials used in DPI systems can be carefully engineered, the interactions between particles can have a critical effect on aerosol properties (Stewart, 1986). These interactions will be influenced in turn by a number of factors such as the formulation, processing techniques, electrostatic charging and/or environmental conditions (Makin *et al.*, 1997).

1.4 Formulation factors influencing DPI performance

When undertaking formulation of powders for inhalation, three critical factors must be considered. The powder formulation must: (a) be homogeneous, (b) be capable of reliable, consistent filling into and delivery from a DPI device and (c) allow delivered drug particles to be available for deposition into the deep lung in a reliable, consistent manner.

The theory of random mixing, first proposed by Lacey in 1943, assumes that there is a small probability that an infinitely long mixing time will result in the production of an ideal mix through random events brought about by the mixing process (Staniforth, 1982). However, this theory does not take into account attractive interactions that are likely to occur between the fine particles in a DPI formulation (Staniforth, 1987).

Such interactions are considered in more modern mixing theories, where fine particles have been shown to adhere to the surfaces of coarser ('carrier') particles (Travers and White, 1971); this phenomenon has been termed ordered mixing (Hersey, 1975). In an ordered mix, fine particles are bound to the carrier particles by interparticle forces that result from surface electrical attractions.

Staniforth (1982) proposed that both random and ordered mixing processes were likely to occur in combination as a dynamic equilibrium in any mixing system, since it is unlikely that formation of ideal random or partially ordered mixes occurs in pharmaceutical powders; this theory was termed total mixing (Staniforth, 1981).

Drug particles of a size suitable for inhalation (i.e. in the range 1 to 5μm) tend to exist as cohesive powder systems with poor flow, which can result in difficulties during processing of the powders into DPI delivery systems. The inherent cohesiveness of fine particles can also lead to the formation of self-aggregates from which respirable particles must be released upon patient inhalation to facilitate deep lung deposition (Hickey *et al.*, 1994).

Two general approaches have been adopted to address these issues through formulation. The first approach entails formulations containing only the active drug powder. These are processed in such a way so as to encourage the formation of loosely bound drug agglomerates that are able to become dispersed into their primary fine particles upon inhalation (Trofast and Falk, 1996; Yang and Kenyon, 2000).

The second, and more common approach to formulation requires the micronised drug particles to be mixed with other excipient powders. These excipients are generally coarse particles of a size range 30 to 100μm and have a role as carrier particles in the formation of ordered powder mixes (Hersey, 1975). The fine drug particles are bound to active sites on the carrier surfaces (Staniforth, 1996). Such systems are dependant on a proportion of the fine drug becoming detached from the carrier surface upon inhalation of the formulation so that these particles can be carried to the deep lung. The carrier particles are generally designed to remain in the device or deposit in the mouth or upper airways once they have dissociated from the fines.

Such systems are often found to be inefficient since large numbers of the drug particles fail to separate from carrier surfaces and those particles that do become

dislodged may do so as aggregates or may re-form into aggregates, which are themselves too large to travel to the deep lung.

Many of the drug presentations used in inhalation therapy are highly potent and require only small doses for therapeutic efficacy. Such low doses generally require to be formulated with a large proportion of excipient powders, typically resulting in drug to carrier ratios of between 1:50 and 1:500. It is possible for mixing of such systems to result in the formation of ideal interactive mixtures in which a monolayer of drug particles is distributed over carrier surfaces (Wong et al., 1995a).

In contrast drugs requiring higher doses, where drug to carrier ratios may range from 1:10 to 1:1, are unable to form pure monolayer interactive mixtures since the drug particles are too numerous. Drug particles in these formulations may exist in a variety of possible states: (a) individual drug particles, (b) drug-drug agglomerates, (c) drug particles bound to individual carrier particles in mono- or multi-layer configurations and (d) as combined drug and carrier agglomerates (French *et al.*, 1996; Wong *et al.*, 1995b).

Low and high dose carrier based systems have been further improved by the addition of fine particle ternary excipients to the formulations (Lord and Staniforth, 1996; Lucas et al., 1998; Zeng et al., 1998; Peart, 1996; Louey et al., 2000). It has been proposed that these fine particle excipients act by occupying highly active binding sites on carrier particle surfaces, leaving more passive sites available for adhesion of drug particles at lower energy levels, thus facilitating separation of the drug during dose delivery (Staniforth, 1996).

Lucas *et al.* (1998) reported the formation of multiplets of drug particles with fine particle lactose which were thought to bring about improved deposition characteristics since drug particles were more easily liberated from the surfaces of fine particle lactose than from coarser particles.

The use of fine particle lactose as the excipient component in a binary mixture with nedocromil sodium has been shown by Clarke *et al.* (1998) to be effective in improving *in-vitro* deposition performance. It was proposed that this was brought about through intercalation of the fine particle lactose into the structure of drug agglomerates, which reduced their cohesive strength and resulted in an increase in the liberation of fine drug particles on application of a dispersive force (Lucas *et al.*, 1998; Clarke *et al.*, 1998). The processing and binding characteristics of nedocromil sodium are considered in some detail below.

The forces of attraction that develop between particles in any DPI formulation system must be carefully controlled since cohesive drug-drug or adhesive drug-carrier interactions that are of too great a magnitude will prevent adequate dispersal of the drug particles (Zanen *et al.*, 1992).

1.5 Nedocromil sodium

1.5.1 Therapeutic use of nedocromil sodium

Current strategies for the pharmacological management of asthma are concentrated around symptomatic relief and preservation of lung function (Smith and Bernstein, 1996). Acute symptoms are treated with selective β_2-adrenergic agonists, anticholinergic agents, theophylline and other xanthine-oxidase inhibitors. The most common treatments for long-term prophylaxis of asthma employ anti-inflammatory preparations containing corticosteroids and/or the anti-allergic drugs, cromolyn sodium or nedocromil sodium (Holgate, 1996; Smith and Bernstein, 1996).

Nedocromil sodium has a pharmacological action similar to that of sodium chromoglycate, thought to act by stabilising mast cell membranes and thus preventing release of pharmacological mediators of bronchospasm. The only formulation currently available for inhalation use containing nedocromil sodium is a pMDI presentation (Tilade ®, Patheon Healthcare Limited, London, U.K.). This is usually administered to adults at a dose of 4 mg twice to four times daily for the prophylactic treatment of asthma (Cairns *et al.*, 1985; British National Formulary, 2001).

1.5.2 Physical properties of nedocromil sodium drug substance

Nedocromil sodium (disodium 9-ethyl-4, 6-dioxo-10-propyl-4H, 6H-pyrano[3,2-g]quinoline-2, 8-dicarboxylate) is a hydrophilic drug that has been found to exist in

four states of hydration dependent on humidity conditions; these are summarised in table 1.1 below.

% Relative Humidity at 22°C	Hydration state
< 6.4	Monohydrate
6.4 - 80	Trihydrate
80 - 92.9	Heptahemihydrate
92.9	Saturated solution
> 92.9	Unsaturated solution

Table 1.1. Hydration states of nedocromil sodium at different percent relative humidities at 22°C.

1.5.3 DPI formulations containing nedocromil sodium

The aerosol performance of dry powder blends containing nedocromil sodium trihydrate was investigated by Clarke (1998); the findings from this work are summarised below.

This study investigated nedocromil sodium formulations in pure drug form, as mono-component or bi-component coarse carrier systems, as fine particle lactose carrier systems and as aggregated powder systems. Processing of these formulations was carried out in a range of blending equipment; these were a pestle and mortar, a turbulent tumbling mixer and a rotary bladed high shear mixer.

The effects of relative humidity were also investigated and this parameter was carefully controlled in conditioning and testing of the powders. All formulations were characterised for *in-vitro* aerosol performance during delivery of an 8mg dose to a modified twin stage impinger apparatus through a Cyclohaler® DPI device.

Carrier based formulations were prepared incorporating a high percentage of nedocromil sodium trihydrate (40%$^{w}/_{w}$) with α-lactose monohydrate powders.

These studies indicated an optimised formulation using fine particle lactose. Blending conditions that provided the highest amounts of shear were found to improve aerosol performance of the blends and deposition characteristics were also found to be enhanced with increased mixing times.

The mechanism for formation of the optimised blends was proposed as one of intercalation of fine particle lactose particles into the lattice of self-agglomerated nedocromil particles so causing the attractive forces between nedocromil particles to be weakened hence allowing greater deaggregation by a turbulent airstream during delivery from the DPI system.

It was clear that distribution of the fine particle lactose in relation to the nedocromil particles was critical to achieving optimal blend performance and that very high shear forces needed to be imparted into the formulation during blending to achieve ideal dispersal of ingredients.

1.6 Powder blending equipment

1.6.1 Turbulent tumbling mixers

Tumbling mixers are frequently used in generating powder blends for inhalation. Various designs of tumbling mixers are available, all of which basically incorporate a mixer vessel, or shell, which is rotated so that the powder bed within it exceeds its angle of repose, thus causing it to flow over itself. The mechanism of mixing in this case is division and recombination of the powder bed by shearing in the bulk of the material and diffusion at the surfaces, brought about by turbulent conditions provided by the tumbling action of the mixer vessel (Scott, 1957).

The mixer vessel may be one of a number of geometrical shapes, such as a cylindrical drum, double cone, y-cone or cube, which is rotated about an axis, the selection of which depends upon the desired powder flow pattern. The movement of the vessel may be more complex than a simple rotation, for example, the Turbula® mixer comprises a cylinder which is rapidly turned in a 'figure-8' type motion allowing it to develop more shear force than conventional rotation patterns.

These mixers are most suitable for dry, free-flowing materials and are often used where a mild action is necessary. Segregation of materials is often a problem in tumbling mixers, especially with free-flowing materials with large size or density differences. The inclusion of baffles in the chamber design can have the effect of increasing convective mixing, which may help to reduce segregation (Williams, 1968). Mixing of cohesive powders, such as those often used in DPI products may

often require more shear than can be provided by tumbling mixers (Rees, 1977), although some have been fitted with high speed agitator devices which may facilitate the mixing of cohesive powders and limit the amount of segregation (Harnby, 1967).

The simplicity of the mixing vessel and the absence of moving parts within it allow easy cleaning of most tumbling mixers, although this benefit is reduced in designs which include baffles or agitators.

1.6.2 Agitator mixers

A second class of mixers, agitator mixers, convey a mixing action to a powder bed by using blades or paddles of various designs which move within a stationary mixing vessel.

Agitator mixers are generally able to impart high shear forces into a mixing process which makes them particularly useful for mixing cohesive powders.

Planetary mixers are agitator mixers which operate using a mixing shaft which simultaneously rotates about itself and around the circumference of a circular mixing bowl. Although it is possible to operate these blenders using variable shear they are rarely used for dry powder blending purposes (Lantz and Schwartz, 1981).

A number of designs of mixing equipment are available which are described as high speed or high shear mixers. Since these mixers have traditionally been used in preparation of wet granulations for tableting or encapsulation, they are often termed

high shear mixer/granulators. Most designs of this type of granulator consist basically of a mixing chamber or bowl, a main impeller and a chopping tool.

The orientation of the mixing bowl may be horizontal as in the Loedige® mixer, or vertical as in the Diosna® and Gral® type mixers. Vertical mixers are more accessible and so are easier to clean than the Loedige®, and the design of the Gral® mixer is such that the mixing blades and chopper are top driven, hence are removable from the bowl, further simplifying cleaning (Stanley-Wood, 1990).

Powder mixing is achieved through the use of shear and compaction forces generated from the rapidly rotating main impeller. The dry powder is placed into the bowl and mixed using the main impeller at speeds generally in the range of 100 to 500 rpm.

High shear blenders often contain chopper blades that can be rotated at very high speeds (up to approximately 4000 rpm) in a different plane to the main impeller; this action is thought to break up any large agglomerates, although it has also been suggested that its main role is to prevent a uniform flow pattern being created within the mixing chamber (Holm, 1987).

The main operational influences on mixing in this type of equipment are shape, size and orientation of mixing chamber, design and speed of impeller and chopper and the amount of powder to be processed (Schæfer, 1988).

One of the disadvantages of high-shear mixer/granulators is that a large amount of frictional heat may be generated during their operation, which may damage some

materials and may require a cooling jacket to be included in the design. Also, the presence of moving parts within the mixing vessel can make cleaning difficult and may lead to contamination of the granules by material still resident from previous batches as well as from wear of the mixing blades themselves. The correct design of the seals or glands around the mixing impellers is an important factor in preventing cross-contamination of the product (Hauser, 1992) and these are often air-flushed in modern equipment.

1.6.3 Air mixers

A final category of mixer operates using fluid flows to agitate powdered material. Although no published evidence of the use of air mixers in producing blends for inhalation can be found, a review of these mixers is included here since it is the intention of this study to investigate the potential use of an air driven system for DPI blend manufacture.

The technique of fluidisation is widely used in pharmaceutical operations where fluid/solid contact is required; general aspects of fluidisation are considered elsewhere (e.g. Davidson *et al.*, 1985).

Fluidisation processing is usually carried out within a vessel in which the powder rests on a perforated base (distributor plate), which also serves to direct the gas flow to give a uniform velocity distribution throughout the cross-section of the powder bed. The design of the distributor plate has an important effect on the operation of the fluidised bed (Whitehead, 1985).

Powder mixing using fluid flows may be described as being achieved by either a fluidisation or an agitation technique. Fluidisation techniques are considered here as being those in which a high volume of low pressure fluid is applied across a bed of powder. Agitation techniques are those in which particle movement is elicited by the injection of high pressure gas streams into the powder mass.

Segregation of material may be a problem in fluidised beds where particles of widely differing sizes and/or densities occur (Rowe and Nienow, 1976) and fluidised bed mixing is therefore precluded as a method suitable for processing of such materials in the dry state (Simon, 1975) unless additional turbulent flows are introduced to the processing environment. Mixing of solid particles within a gas fluidised bed is also influenced by the nature of the material, the most important properties being particle size and density (Shakhova and Minayev, 1972).

Another type of mixer has been described in which material is pneumatically conveyed upwards through a vertical tube in the centre of a mixing chamber by a radial fan. Blending is achieved mainly by transverse mixing, so an adequate homogeneity is only achieved after a number of circulations of material through this central tube. Increasing longitudinal mixing with the inclusion of an outer annular cone can reduce the number of circulations necessary for adequate mixing, since material is returned to the main chamber at two different heights (Krambrock, 1976).

Mixing may also be achieved by agitation of powder within a vessel by the injection of pressurised air into the vessel. One technique of pneumatic mixing, the Airmix

mixer, uses a number of upwardly tilted air jet nozzles, which are arranged in a ring-shape at the bottom of a frusta-conical vessel (Anon., 1966). The material to be mixed forms a cone on the floor of the mixer from where it is carried up along the walls of the mixer by compressed air fed through the jet nozzles. The turbulent region arising from the jet nozzles imparts a mixing action to the particles causing the material to be deposited back onto the centre of the cone. To prevent centrifugal segregation of material of different densities or particle sizes, the jets may be pulsed to give short blasts of air (Anon., 1966; Teichmann, 1967). The performance of the Airmix mixer has been shown to be influenced by the operating pressure of the air nozzles (Ashton and Valentin, 1966).

An alternative design uses negative air pressure to mix powders (Akiyama *et al.*, 1982; Akiyama and Tada, 1984; Akiyama and Tada, 1985; Akiyama *et al.*, 1986). In this system, air is drawn through a series of tangential ports located around a conical mixing vessel. The main advantage of the negative pressure air mixer over a conventional, positive pressure air mixer, is a reduced need for bag filtration.

In a comparison of the performance of a number of mixer types using differently coloured, non-segregating particles, an air mixer was found to be the fastest mixer of the seven types investigated (Miles and Schofield, 1970). An advantage of this type of mixer is the absence of moving parts within the product chamber; this reduces cross-contamination and allows easier cleaning. Additional advantages are reduced damage to the particles; the possibility of transporting the material by air; and the large batch sizes that can be handled (Akiyama *et al.*, 1982).

Unpublished data has described the use of cone mills in aiding dispersal of fine particles in DPI formulations. Cone mills employ an impeller blade which forces material through a screen of variable size and this application attempted to take advantage of the high shear conditions resulting from operation of this type of equipment.

1.7 Fluid energy milling

A brief review of particle size reduction by fluid energy milling is presented here since the processor under investigation in this study had an intended application for particle size reduction of DPI excipients and the mode of action was considered to possess some similarities with fluid energy milling equipment.

Fluid flows may be used to reduce particle size using the technique of fluid energy milling, also known as jet milling or micronising. The fluid energy mill operates by the acceleration of particles using a high pressure jet of gaseous fluid, usually air, so that they collide with each other or with a part of the grinding chamber, causing comminution by particle impaction and attrition. Fluid may be introduced at pressures ranging from 25 to 300 pounds per square inch, producing regions of turbulence in which sonic or supersonic velocities impart sufficient kinetic energy to the feed material to effect particle size reduction (Albus, 1964).

The fluid energy mill or 'microniser' is the type of mill most suitable for ultrafine impact milling of materials to a size less than 5 μm. Most conventional impact mills are capable only of size reduction to approximately 50 μm because neither the impact velocity nor the solids concentration is sufficiently high to accomplish ultrafine grinding (Rumpf, 1959; Leschonski and Menzel, 1986). Particles produced by micronising typically have a narrow size distribution and are smooth and round in shape (Akbarieh and Tawashi, 1987).

Fluid energy mills are particularly useful in the fine milling of heat sensitive pharmaceuticals since the expansion of compressed air upon entering the milling chamber causes it to cool and counteracts the heat generated by milling. The milling atmosphere can easily be controlled by selection of the grinding fluid. For example, hygroscopic or hydrolysable materials can be milled using very dry air, and materials susceptible to oxidation could be milled using high pressure nitrogen. The turbulent conditions generated within a fluid energy mill may also provide an excellent environment for mixing of the ingredients (Albus, 1964).

A further advantage of fluid energy mills is the absence of moving parts in the grinding area which makes cleaning easier and reduces the likelihood of cross contamination (Dotson, 1962). These mills can be adapted to operate under aseptic conditions by sterilisation of the mill components and the use of sterilised air or high temperature water vapour as the jet fluid (McDonald, 1971).

Most fluid energy mills incorporate a size classifier that removes sufficiently comminuted material and retains the remainder for further size reduction. This allows efficient production of material with a narrow size distribution. Efficient operation of a fluid energy mill often requires the feed material to be premilled. The degree to which a material should be premilled is determined by the mill specifications, the characteristics of the material and the particle size reduction required. Typically, the particle size of the feed material should be between 150 to 850 μm (Parrott, 1976).

There are several basic designs of jet mill, including target jet mills, opposed jet mills, tangential jet mills and fluidised bed jet mills (Prior et al., 1990).

In a target jet mill, a single jet directed onto a target plate causes particles to collide with the target and bring about particle fracture by impaction. Size reduction is achieved in an opposed jet mill by head-on impact of particles through entrainment in two opposing jet streams. Sufficiently fine particles will be carried towards the centre of the classification chamber by entrainment in the air leaving the mill, whereas larger particles will be forced towards the outside of this chamber by centrifugal force and then returned to the impact site. The fine particles are then collected from the escaping air by separating devices such as cyclones and bag filters.

Several types of fluid energy mill apply a tangential jet nozzle design. One such design is based upon a vertical, hollow toroid (Albus, 1964) although the milling chamber may also be cylindrical (Nair and Ramanujam, 1986). Material is fluidised and fed into the chamber by a high pressure air injector whereupon a number of jet nozzles at the base of the mill provide a region of turbulence in which size reduction takes place as a result of high energy particle collisions. The central classifier removes fines in a similar manner to that in the opposed jet mill described previously. An attempt has recently been made to characterise the classification system of a circular (cylindrical) fluid energy mill (Nair and Ramanujam, 1991).

The efficiency of an alternative tangential system, designed to operate horizontally, was been shown to be affected by the angle of the nozzles (Smit, 1986). This type of mill was the subject of a recent study, which demonstrated that particle size reduction was increased with increasing fluid pressure and by the installation of deflectors in the milling chamber (Yoon, 1994). This report also concluded that increasing the feed

rate of material decreased the level of comminution but other workers have reported that, in some cases, increasing the concentration of solids in the grinding chamber produces finer particles due to increased collision frequency (Akbarieh and Tawashi, 1987). An accelerating particle must have sufficient time before collision to reach a velocity high enough to attain maximum impact energy, and if the system is very highly loaded this velocity may not be achieved, so reducing the extent of comminution (Rumpf, 1960).

It is likely that maximum particle size reduction occurs at an intermediate level of particulate loading at which there is an optimal balance between the amounts of energy transferred to each particle and the rate of particle collisions.

Jet mills have also been designed in which grinding occurs within a fluidised bed incorporating a motor-driven air classifier (Ghosh, 1993). One advantage of this design is decreased wear of the mill parts, so that product contamination from this source is reduced. This benefit results from the reduction in the speed of particles as they get closer to the mill walls so that particle-mill collisions are prevented and virtually all size reduction is achieved through particle-particle collisions (Prior *et al.*, 1990). In addition, these mills produce particles of narrower size distributions (Prem and Eddington, 1988) and are more energy efficient than standard jet mills (Prem, 1984).

The mode of action of fluid energy mills will result in some mixing of the materials being processed and suitably adapted mills have been used for this purpose (Albus, 1964).

1.8 Aims of the study

It is clear that the amount of shear imparted to a blending process during manufacture of powders for inhalation is critical to:

(a) Attaining a homogeneous ordered mixture by adequately dispersing fine powders onto carrier particle surfaces

(b) Avoiding the formation of overly large interactive forces between particles which may hinder liberation of fine drug particles from the formulation during patient use.

The choice of mixing equipment capable of providing the large amounts of shear for this process is restrictive. Furthermore it has often been found difficult to balance reliably the shear input within equipment which is currently available since such equipment usually has been designed for other purposes.

Where performance modifying agents such as fine particle lactose are added to a DPI formulation, the distribution of these in relation to the other components in the formulation is postulated to be critical to their effectiveness and hence control of the amount of shear available during processing of such systems is likely to be crucial.

Furthermore, the size of both drug and excipient particle ingredients is important to the performance of a DPI formulation and although a range of equipment is available to effect manipulation of particle size, it is not yet possible for this to be performed

within mixing equipment; such an application may have benefits in control of DPI blend manufacture.

Research into enhancing the performance of DPI systems has often been directed at formulation improvement or developments in device design rather than investigation of novel processing alternatives.

Consequently an attempt was made within this study to design, develop and characterise alternative equipment that was able to provide controllable and reliable levels of shear capable of achieving the required mixing and/or control particle size reduction processes.

These characterisations were performed using a nedocromil sodium formulation in order to provide a direct comparison with the established conventional processing techniques investigated by Clarke (1998), which are discussed in section 1.5.3.

Size reduction investigations were also undertaken within the novel processing equipment using a commonly used inhalation excipient, lactose powder.

2. MATERIALS AND GENERAL METHODS

2.1 Materials

2.1.1 Analytical materials

Cyclohexane, used in sample preparation for wet cell particle size analysis of nedocromil sodium trihydrate, was HPLC grade (BDH Limited, Poole, U.K.).

HPLC grade propan-2-ol (BDH Limited, Poole, U.K.) was used as a dispersant liquid in wet cell particle size analysis of fine particle lactose.

Lecithin, used as a dispersal aid during wet cell particle size analysis, was obtained from BDH Limited, Poole, U.K.

Water was freshly deionised.

Magnesium nitrate, used to prepare the saturated salt solutions, was obtained from BDH Limited, Poole, U.K.

2.1.2 Materials used during processing

Table 2.1 describes the raw materials used for particle size reduction and dry blending processing.

Type of experiment	Material	Supplier's grade	Batch number	Supplier
Size reduction	α-lactose monohydrate	* Prismalac 40 ®	Not known	Meggle GMBH, Wasserberg, Germany
Dry blending	α-lactose monohydrate	SorboLac 400 ®	L7589	Meggle GMBH, Wasserberg, Germany
	Nedocromil sodium trihydrate	Micronised	GMR 5021G	Rhône-Poulenc Rorer, Cheshire, U.K.

Table 2.1. Description of materials used during processing.

* Note: Prismalac 40® is the replacement proprietary name for CrystaLac 40® (used in the FBSVP-A milling experiments); these are claimed by the manufacturer to be equivalent materials in all other respects.

2.1.3 Other materials used during testing

Cyclohaler® dry powder inhalers (PCH Pharmachemie, Haarlem, Netherlands).

Size 3 hard gelatin capsules (Davcaps®, Hertfordshire, U.K.).

Volumetric glassware was Class A (Fisher Scientific Ltd, UK).

2.1.4 Formulation

All blending studies were carried out using the common formulation set out below:

Nedocromil sodium trihydrate	40% $^{w}/_{w}$
SorboLac 400 α-lactose monohydrate	60% $^{w}/_{w}$

2.2 Control of relative humidity

2.2.1 Storage of drug and excipient powders

Materials used in the dry blending experiments were stored in desiccators within an environment of controlled relative humidity (RH) for at least 24 hours before processing. Optimum conditions for stable storage of nedocromil sodium trihydate have been determined at 22 degrees C, 50% RH (Khankari *et al.*, 1998). A RH of approximately 55% was readily achieved by placing a saturated solution of magnesium nitrate in the base of a sealed desiccator vessel. Temperature was not controlled, but was maintained at an ambient laboratory level, which was monitored to confirm that this did not deviate outside 15 - 30 degrees C. This provided a RH of between 52 – 56% within the desiccator environment (Pharmaceutical Handbook, 1980).

2.2.2 Storage of hard gelatin capsules

Hard gelatin capsules were also stored under conditions of approximately 55% RH. This was to avoid extremes of RH which have been found to cause brittleness of capsules at RH < 40% and moisture sorption leading to swelling of capsules at RH > 85% (Konty and Mulski, 1989). It was thought that capsule brittleness could lead to inconsistent piercing of the capsules during operation of the Cyclohaler® device, which may then affect the aerodynamic behaviour of the powders during aerosolisation.

It was also considered prudent to fill powders into the capsules immediately before testing to minimise any effects brought about by moisture transfer between the gelatin and the test powder.

2.2.3 Processing and testing

All processing and testing was performed under ambient laboratory conditions. Humidity and temperature changes within the laboratory for the year 1998 were recorded and ranged from 19 to 63% RH and 16 to 29 degrees C.

Materials were kept within the above described desiccator environment until immediately before processing and samples were placed under similar conditions within 30 minutes after the completion of processing. Samples were subsequently exposed to the laboratory environment only during the time taken to perform individual test determinations.

2.3 Particle size analysis

Techniques of Low Angle Laser Light Scattering (LALLS) were employed to determine the particle size distribution of powder samples. LALLS particle size analysis relies on the interaction of a beam of laser light with a suspended sample of particles. Projection of laser light onto a particle will cause a diffraction pattern to be superimposed onto the geometrical image of the particle. This pattern is large compared to the image and the diffraction angle, obtained by focusing the undeflected and forward scattered light through a lens, is inversely related to the particle size.

The pattern formed by this technique is known as a Fraunhöfer diffraction pattern. Fraunhöfer theory relates particle size to diffraction on a number of assumptions, namely that the particle is much larger than the wavelength of the light, that all sizes of particles scatter with equal efficiencies and that particles are opaque and do not transmit light (Allen, 1990).

For particles of a size approaching the wavelength of laser light (i.e. particles below about 3 μm diameter), the scattering becomes more complex and may be described by Mie scatter theory (Allen, 1990). One limitation of Mie theory is that the refractive index of the sample and dispersal medium must be known to allow accurate calculations.

Two types of LALLS equipment were employed during initial materials characterisation, a Malvern Mastersizer X (Model MSX02SM, Serial number 6278, Malvern Instruments

Ltd., Malvern, UK) and a Sympatec HELOS (HELOS System H0100, Sympatec GmbH, Bury, UK). Both of these instruments comprised a helium-neon laser light source, a sample cell, a focusing lens and a photodetector (Figure 1.5); they may be used to analyse samples as dry powders or as powders suspended in liquids.

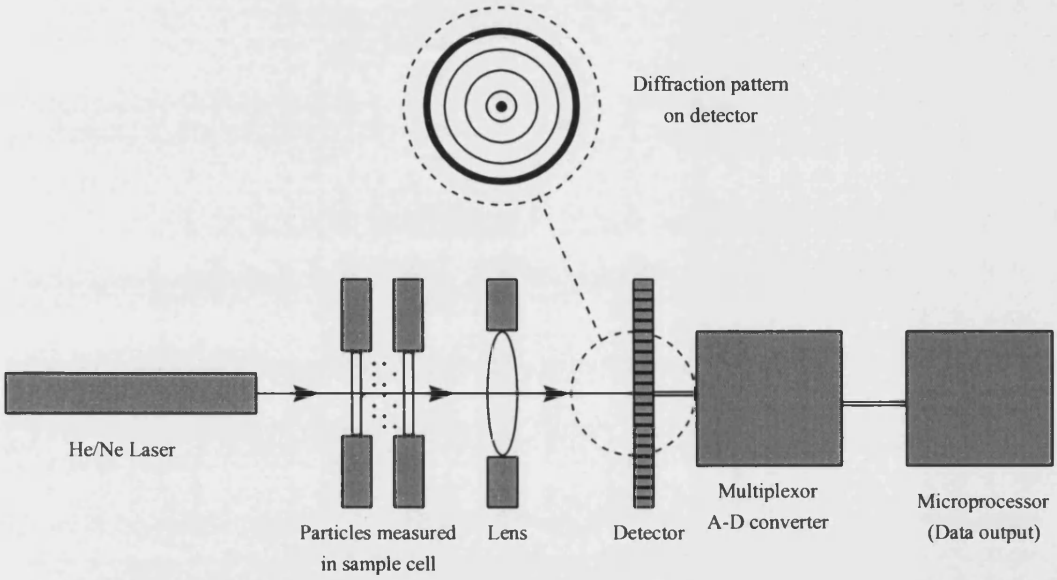

Figure 2.1. Schematic diagram of LALLS particle size analyser.

The simplest way to expose a powder sample to a laser beam is to draw it through the sample cell suspended in a stream of air. In those cases where the sample powder is cohesive and forms agglomerates, as is often the case for very fine powders, then practical and effective measurement of the primary particle size usually requires dispersal in a contacting non-solvent within a sample cell or some other form of powder dispersal system.

The powder dispersal systems in both instruments were found to be adequate for analysis of the lactose powders before and after milling. However, whilst it was found that the Sympatec dry powder system was able to efficiently disperse micronised nedocromil sodium trihydrate powders, it was necessary to employ a wet cell method when using the Malvern equipment for analysis of this material in order to obtain consistent and reliable results.

The availability of equipment meant that Malvern analysis was used for routine particle size analysis during size reduction experimentation, although both systems were employed during initial size characterisation of materials.

2.3.1 Particle size characterisation of micronised nedocromil sodium trihydrate

2.3.1.1 Malvern Mastersizer particle size analyser

The large volume circulating cell was used to analyse micronised nedocromil sodium, using a solution of 1% $^{w}/_{v}$ lecithin in cyclohexane as the dispersant liquid; cyclohexane was used since it has been established that it does not dissolve nedocromil sodium trihydrate; lecithin was introduced as a wetting agent. The solution was filtered (Type A/E glass 76 mm diameter, Gelman Sciences, Michigan, U.S.A.) before use and its refractive index measured using an optical refractometer to determine an appropriate presentation for the particle size calculations.

A 45 mm lens was fitted into the Malvern instrument, which provided a detectable particle size range of 0.1 to 80 μm, and the reservoir of the large volume circulating cell was filled with an appropriate amount (approximately 1 litre) of the filtered dispersant liquid. With the cell fixed into position the optics in the instrument were aligned and the diffracted light measured in the absence of a sample in order to establish a background reading.

Approximately 5ml of dispersant liquid was filled into a small test tube and approximately 1 mg of micronised nedocromil sodium added. The tube was manually agitated and subsequently placed in an ultrasonic water bath for 10 minutes, which was maintained at a temperature between 20 and 25°C in order to reduce the likelihood of any dissolution of the material. Following sonication a number of drops of the suspension were immediately added to the reservoir of the large volume circulating cell until an obscuration level of between 15% and 25% was obtained. All samples were prepared and analysed in duplicate.

2.3.1.2 Sympatec particle size analyser

The Sympatec HELOS system was used in conjunction with the RODOS dry disperser system (Sympatec GmbH, Bury, UK). The R2 lens (measuring range 0.25 – 87.5 µm) was selected and the disperser pressure set at 3.0 bar. Trigger conditions were set at 1% optical concentration for 100ms. The vibrator was set with a feed rate of 50% with a

funnel height of 1.00mm. A reference measurement was taken then samples of approximately 0.5 g each analysed in triplicate.

2.3.2 Particle size characterisation of fine particle lactose

2.3.2.1 Malvern Mastersizer particle size analyser

The particle size of the SorboLac 400 lactose raw material was measured using the small volume stirred cell in conjunction with the 100 mm lens (particle size range 0.5 to 120 μm). The stirred cell was filled with approximately 15 ml propan-2-ol, the optics aligned and a background reading established with the stirrer operating at speed 3. Approximately 1 mg of lactose sample was placed into a test tube, which was half filled with propan-2-ol. This was manually shaken then sonicated for 2 minutes. Several drops of the suspended sample were added to the stirred cell until an obscuration level of between 15 and 25% was obtained and the sample analysed using 2000 sweeps of the light beam.

2.3.2.2 Sympatec particle size analyser

The Sympatec HELOS system and RODOS dry disperser system were set up as described in section 2.3.1.2, using identical operating conditions except that the vibrator was set with a feed rate of 75% and a funnel height of 1.00mm. A reference

measurement was taken to establish the background reading then samples of approximately 0.5 g each analysed in triplicate.

2.3.3 Particle size characterisation of coarse lactose raw material and products of milling experiments

The Malvern Mastersizer X was used, employing a dry powder feeder technique to present powder to the measurement array. This utilised a vacuum device (Nilfisk Type GS80, 700 W, Nilfisk Ltd., Suffolk, UK) to draw powder samples across two parallel optical glass panes within the dry powder feeder manifold (Model MSX64, Malvern Instruments Ltd., Malvern, UK). A flow rate of approximately 100 litres min^{-1} was found to provide the required Mastersizer obscuration value of between 15 and 25 % during sample detection.

The 300 mm lens (particle size range 1.2 to 600 μm) was fitted to the instrument and a sample of approximately 0.5 g of the test powder drawn through the sample cell. Otherwise, the instrument was operated as described in section 2.3.1.1 above. Measurements were obtained in triplicate.

2.3.3 Particle size analysis of raw materials – results

Raw Material	LALLS instrument	d(0.1)(μm)		d(0.5)(μm)		d(0.9)(μm)	
		Mean	SD	Mean	SD	Mean	SD
SorboLac 400®	Malvern Mastersizer	1.1	0.04	6.5	0.3	19.1	2.5
	Sympatec	1.3	0.01	7.1	0.1	17.7	0.2
Nedocromil sodium trihydrate (micronised)	Malvern Mastersizer	0.7	0.01	2.7	0.2	8.1	2.0
	Sympatec	0.7	0.05	1.4	0.05	3.0	0.03
Prismalac 40®	Malvern Mastersizer	-	-	460	7.1	-	-

Table 2.2. Particle size analysis of raw materials by Malvern Mastersizer and/or Sympatec LALLS instruments.

Key:

d(0.1) = diameter below which 10% of particles are sized by mass

d(0.5) = diameter below which 50% of particles are sized by mass (mass median particle diameter)

d(0.9) = diameter below which 90% of particles are sized by mass

2.4 Nedocromil sodium assay

2.4.1 Equipment and materials

Helios UV spectrophotometer (Helios α, Unichem Limited, Cambridge, U.K.)

10mm path length synthetic far-UV quartz cell (Type 100-QG, Hellma UK Limited, Essex, U.K.)

Freshly deionised water

2.4.2 Method

2.4.2.1 Wavelength determination

Nedocromil sodium trihydrate was stored at 55% RH. The UV spectrophotometer was blanked with deionised water. 10mm quartz sample cells were used. A 0.002% w/v solution of nedocromil sodium trihydrate was prepared in deionised water and analysed using the UV spectrophotometer over the range 250 – 450 nm to determine the absorption maxima. Peaks were found at 245nm, 280nm, 340nm and 373nm. A wavelength of 373nm was selected for determination of nedocromil sodium trihydrate assay.

2.4.2.2 Calibration

Method

A 0.040% solution of lactose in deionised water was prepared and analysed on the UV spectrophotometer for absorption at 373nm. No absorption was found.

Three nedocromil sodium stock solutions, A. B and C, were prepared at a concentration of 0.1% w/v using deionised water . Duplicate sets of dilutions (A1, A2, B1, B2, C1 and C2) were made from each of the three stock solutions at concentrations of 0.001%, 0.002%, 0.003%, 0.004% and 0.005%. Each set of solutions A1, A2, B1, B2, C1 and C2 was assayed three times using the UV spectrophotometer (λ = 373nm) and the mean absorbance recorded. This enabled the statistical determination of $E_{1cm}^{1\%}$, taking into account the accuracy of weighing and preparation of dilutions.

Results

Table 2.1 summarises the linear regression data obtained from the calibration plots for the solutions of nedocromil sodium prepared above. Linear regression was performed using Origin® v6.1 (OriginLab Corporation, MA, U.S.A.).

Stock	Dilution	Slope ($E^{1\%}_{1cm}$)		Intercept		Coefficient of
		Value	SD	Value	SD	correlation
A	1	158.2	0.28	0.017	0.0092	0.99954
A	2	156.5	0.27	0.0275	0.0089	0.99956
B	1	157.2	0.24	0.025	0.0079	0.99965
B	2	157.2	0.25	0.0266	0.0081	0.99964
C	1	157.2	0.27	0.0314	0.0090	0.99956
C	2	157.5	0.25	0.0323	0.0082	0.99963
Mean		**157.3**		**0.0266**		

Table 2.2. Linear regression data for calibration of UV spectrophotometer for assay of nedocromil sodium content (0.001 to 0.005 % $^{w}/_{v}$).

These calibration data enabled calculation of nedocromil sodium content of samples analysed for absorbance using the UV spectrophotometer according to the following formula:

$$\text{Nedocromil sodium content } (\%\,{}^{w}/_{v}) = \frac{\text{UV Absorbance} - 0.0266}{157.3} \qquad \text{[Equation 2.1]}$$

2.5 *In-vitro* aerosol characterisation

A single dose capsule based dry powder inhaler device, the Cyclohaler®, was used to assess the *in-vitro* performance of blends.

All *in-vitro* aerosol investigations were performed using a method based on that described for Apparatus A in the British Pharmacopoeia 1993, Appendix XVIIC (Figure 2.2). The standard Apparatus A has an effective cut-off diameter for 50% of the aerosol mass (ECD_{50}) of 6.4μm at the prescribed flow rate of 60 litres min^{-1}. Providing the apparatus conforms to impactor theory, an alternative ECD_{50} can be obtained by altering the internal diameter of the jet within stage 1 according to the following equation:

$$ECD_{50} = 0.95 W^{1.5} Q^{-0.5}, \qquad \text{[Equation 2.2]}$$

where W is the internal jet diameter (mm) and Q is the air flow rate (litres min^{-1}) (Hallworth and Westmoreland, 1987). Using this equation, the internal diameter of the stage 1 jets was modified to 11.6mm to provide a calculated ECD_{50} of 4.80μm at 60 litres min^{-1}. Calibration of Apparatus A using the 11.6mm stage 1 jets was performed using monosized methylene blue droplets produced with a vibrating orifice aerosol generator by AEA Technology (Harwell, UK). An ECD_{50} of 5.3μm was measured for the modified Apparatus A at 60 litres min^{-1}. All other dimensions in the modified Apparatus A conformed to pharmacopoeial specifications.

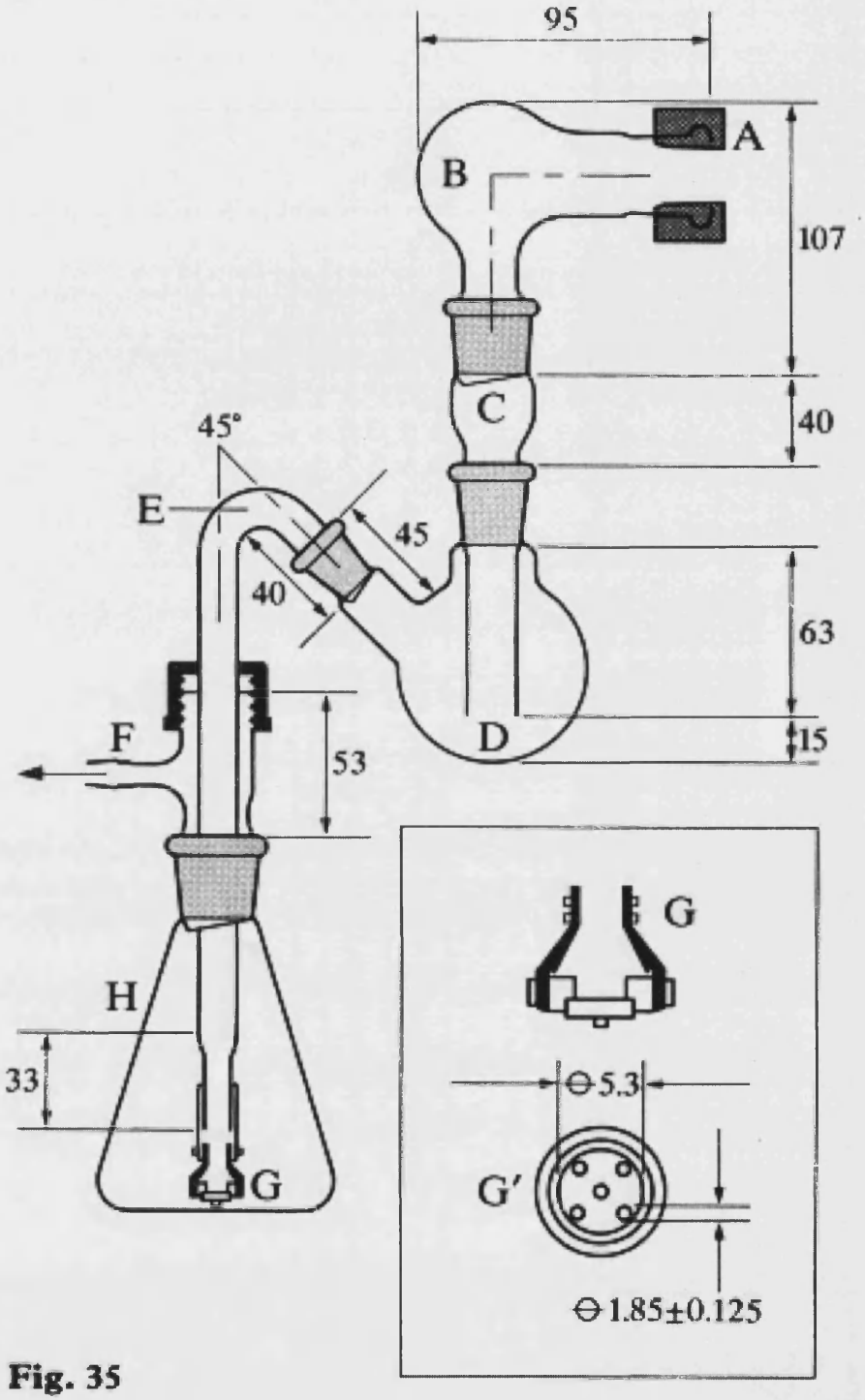

Fig. 35

Figure 2.3. Diagram of Apparatus A (British Pharmacopoeia 1993, Appendix XVIIC).

Table 12F-1 Component specificatiob for Figs. 12F-1/3

Code	Item	Description	Dimensions[a] mm
A	Mouthpiece adapter	Moulded rubber adapter for actuator mouthpiece	
B	Throat	Modified round-bottomed flask	50 ml
		ground-glass inlet socket	29/32
		ground-glass outlet cone	24/29
C	Neck	Modified glass adaptor	
		ground-glass inlet socket	24/29
		ground-glass outlet cone	24/29
		Lower outlet section of precision-bore glass tubing	
		bore diameter	14
		Selected-bore light-wall glass tubing	
		external diameter	17
D	Upper impingement chamber	Modified round-bottomed flask	100 ml
		ground-glass inlet socket	24/29
		ground-glass outlet cone	24/29
E	Coupling tube	Medium wall glass tubing	
		ground-glass cone	14/23
		Bent section and upper vertical section	
		external diameter	13
		Lower vertical section	
		external diameter	8
F	Screwthread, side-arm adapter	Plastic screw cap	28/13
		Silicone rubber ring	28/11
		PTFE washer	28/11
		Glass screwhead, *threadsize*	28
		Side-arm outlet to vacuum pump,	
		minimum bore diameter	5
G	Lower jet assembly	Modified polypropylene[3] filter holder connected to lower vertical section of coupling tube by PTFE tubing	See Fig 12F-1
		Acetal circular disc with the centres of four jets arranged on a projected circle of diameter 5.3 mm with an integral jet spacer peg	10
		peg diameter	2
		peg protrusion	2
H	Lower impingement chamber	Conical flask	250 ml
		ground-glass inlet socket	24/29

Note: A modified part C (stage 1 jet) was used, having an internal bore diameter of 11.6mm and an external diameter of 14.6mm.

Figure 2.4. Component specification for figure 2.3.

The flow rate of the system was adjusted daily before testing using the following method. The modified Apparatus A was assembled and charged with 7ml deionised water in stage 1 and 30ml deionised water in stage 2. A vacuum pump (Gast Manufacturing Inc., Michigan, USA) was attached to the system via a timer controlled solenoid valve and a flow rate adjustment valve. An empty size 3 hard gelatin capsule was loaded into a Cyclohaler® device, which was attached to the modified Apparatus A using a moulded silicone rubber adapter. A calibrated rotameter was attached to the apparatus, sealed over the Cyclohaler®, and the flow rate adjusted to obtain a reading of 60 ±5 litres min^{-1}. The apparatus was then disassembled, emptied and dried prior to use for testing.

The modified Apparatus A was assembled and charged with 7ml deionised water in stage 1 and 30ml deionised water in stage 2. A size 3 hard gelatin capsule (stored in RH controlled environment until immediately before testing as described in section 2.2.2) was filled with 20mg of powder blend. This was loaded into the Cyclohaler® and the device primed. The capsule was then inspected and if brittle fracture of the capsule had occurred the test was aborted.

The vacuum pump was switched on and allowed at least 5 seconds to achieve a steady flow rate. The solenoid valve was then opened for 4.0 seconds, which gave sufficient time for 4 litres of air to be drawn through the system. The apparatus was then dismantled and the various components rinsed with deionised water into volumetric flasks and made up to volume with deionised water as follows:

Device	50ml volumetric flask
Capsule	50ml volumetric flask
Stage 1 (Parts A, B, C & D*)	100ml volumetric flask
Stage 2 (Parts E, F, G and H*)	100ml volumetric flask

* See figure 2.3.

Assay of these solutions allowed calculation of the following parameters to describe the *in-vitro* aerosol performance of each sample.

Delivered Dose

The total quantity of drug recovered from the modified Apparatus A (i.e. the amount of drug found in stages 1 and 2) was expressed as the Delivered Dose (DD).

Fine Particle Fraction

The amount of drug recovered in stage 2 of the modified Apparatus A indicated the potentially respirable or fine particle component of the sample. This was expressed as a percentage of the DD (Fine Particle Fraction, FPF).

2.6 Content uniformity testing

A 20mg aliquot of sample material was accurately weighed on a calibrated four figure analytical balance into a 100ml volumetric flask which was accurately diluted to volume using freshly deionised water.

Each solution was assayed for nedocromil sodium trihydrate content using a UV spectrophotometer as described in section 2.4.

3. SVP CONCEPT:

DESIGN STRATEGY AND

PRELIMINARY WORK

3.1 Design constraints

The objective was to develop a series of novel powder processors within the following design criteria or constraints:

(a) Should be capable of performing multiple pharmaceutical powder processing operations in a single vessel. These operations may include particle size reduction (agglomerate break-up and/or micronisation), dry powder blending, wet granulation and drying.

(b) Should employ directed airflows for all kinetic energy input.

(c) Should operate without moving parts in contact with the product; i.e. it should be a 'bladeless' system.

(d) Should attempt to reproduce similar product movement and particulate interaction conditions to those attained in conventional high-shear mixer/granulators.

(e) Should use materials of fabrication that allow visualisation of the flow fields inducing powder movement by imaging equipment as well as by the naked eye.

(f) Should operate using only those utilities that would be expected to be found within a typical cGMP pharmaceutical manufacturing environment.

(g) Although initial prototypes would be expected to be at a small batch scale, these should be designed with consideration for effective scale-up.

(h) Should allow operation within a range of definable and mensurable process conditions.

3.2 Early development studies

A series of basic prototypes was developed in order to demonstrate 'proof of principle' for a design strategy based around directed high-pressure air nozzles, intended to replace and mimic the blades in a conventional high-shear blender.

3.2.1 Previous work

A number of alternative designs were considered during a Final Year Engineering Design Project (Bates and Ball, 1993). One of these was selected for further development and constructed as shown in Figure 3.1.

The main vessel comprised two conical sections of 10° and 45° slope so as to reduce the velocity of entrained powder in the top region of the vessel and thus reduce the amount of powder leaving the vessel. A cyclone separator with jet pump attachment was connected to the exit duct to collect and recycle particulate material from the air escaping from the vessel. Air was ducted, via a gas distributor, into a base plenum using a radial fan to provide fluidisation of the powder bed. It was possible to introduce granulation liquid through an atomising nozzle and the fluidising air could be heated to facilitate air drying. A series of nine jet nozzles was arranged tangentially around the circumference of the vessel in order to induce a turbulent swirling airflow motion.

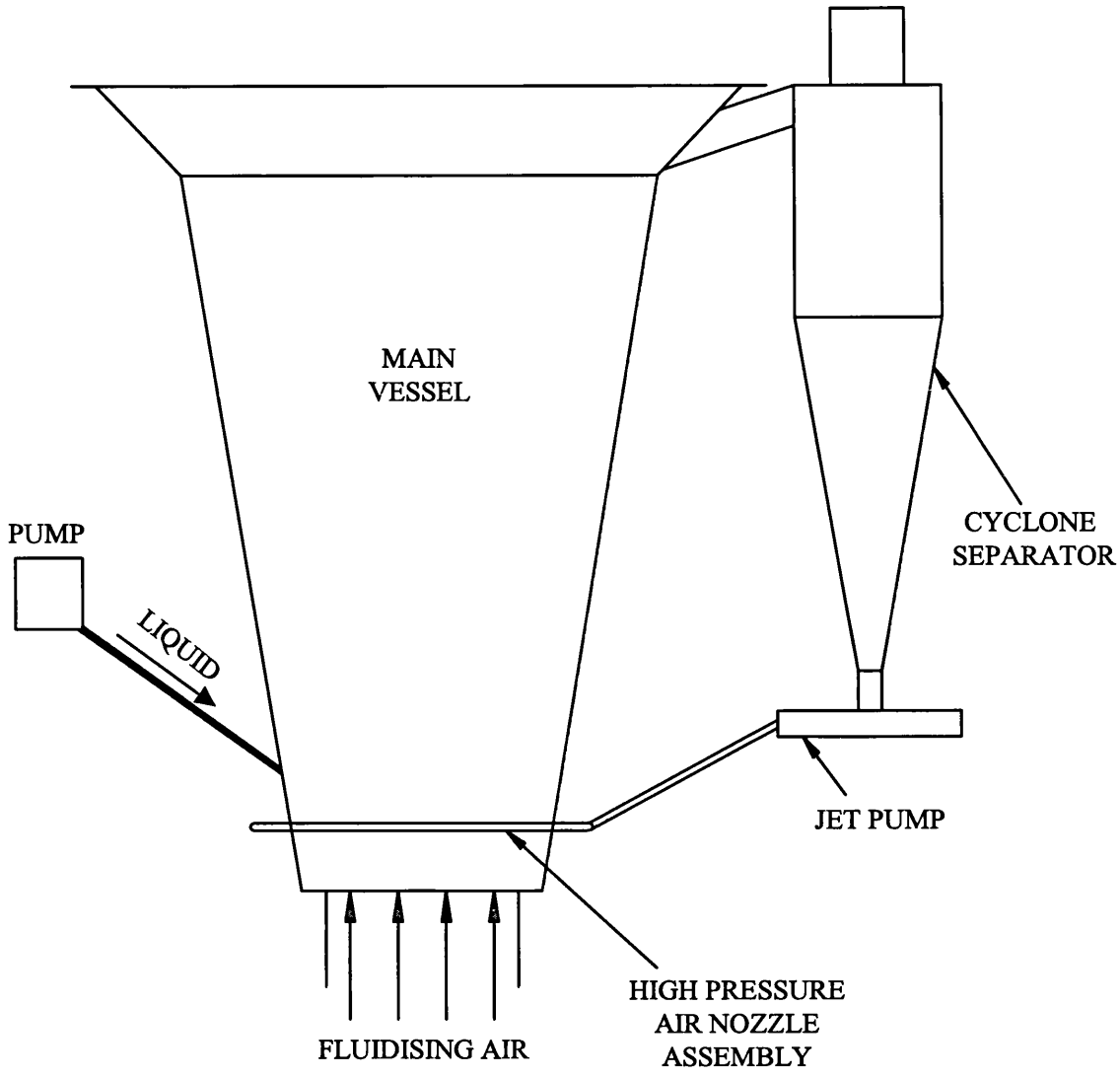

Figure 3.1. Schematic diagram of 'Bates and Ball' SVP design.

Although this design displayed some improved characteristics over previous models in terms of mixing and particle size reduction there was still a number of problems encountered. One major defect was that a large amount of powder escaped from the vessel via the lid seal, the base ducting and the gas outlet of the cyclone. Powder was also found to adhere to the vessel walls in significant quantities and to accumulate in the upper conical section and around the base ducting. Another defect in the design

was that it was necessary to provide continuous fluidising air whilst the vessel was loaded in order to prevent material falling through the base of the processor.

3.2.2 Pre-prototype 1

An initial prototype (Figure 3.2) was constructed from a Perspex cylinder, approximately 300 mm in diameter and 250 mm high. The cylinder was fitted with a wooden base through which six L-shaped nozzles were positioned, equally spaced in a circular arrangement approximately 30 mm from the vessel wall. The nozzles were aligned in the horizontal plane in a tangential direction to the circumference around the nozzle stems so as to generate a vortex air motion. A cloth filter was provided across the top of the vessel.

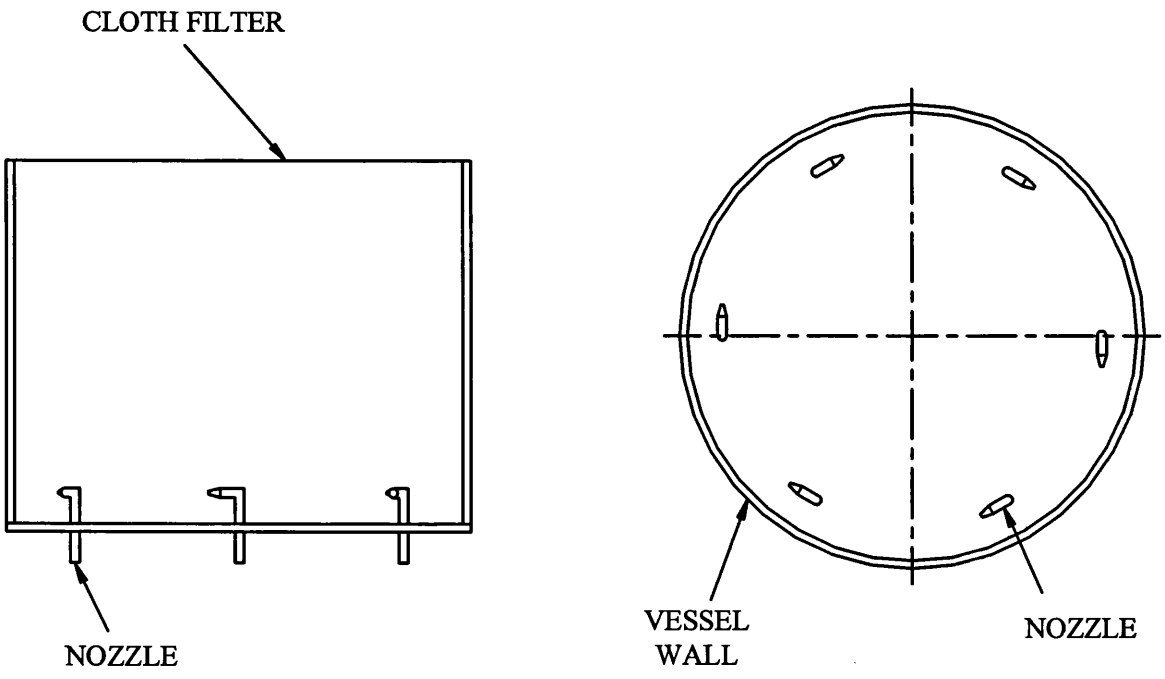

Figure 3.2. Schematic diagram of SVP Pre-prototype 1.

The airflows generated in this vessel when the nozzles were operated at a pressure of approximately 210 kPa displayed a large zone having little or no air flow resulting in the formation of a static region or 'dead spot' in the centre of the cylinder. In addition, the system did not generate a sufficiently well defined or controlled movement of powder and so failed to achieve any of the required processing operations. Consequently, a number of modifications were made and these are described below.

3.2.3 Pre-prototype 2

In order to eliminate the large central dead zone found in the first design, the vessel base was fitted with a central cone so creating a flat annular region separating the cone rim from the cylindrical wall of the vessel (Figure 3.3). This cone and brim arrangement effectively space-filled the dead zone and so induced a toroidal movement of powder under the action of the tangential jet stream. Although this design feature reduced the main dead zone, regions of low velocity were still found to exist behind the nozzles and around the cone brim. In addition the cloth filter was found to be inadequate for collection of very fine particles until it had collected a certain amount of material. Furthermore, with prolonged usage, the filter became increasingly blocked, eventually leading to powder leakage from other parts of the vessel.

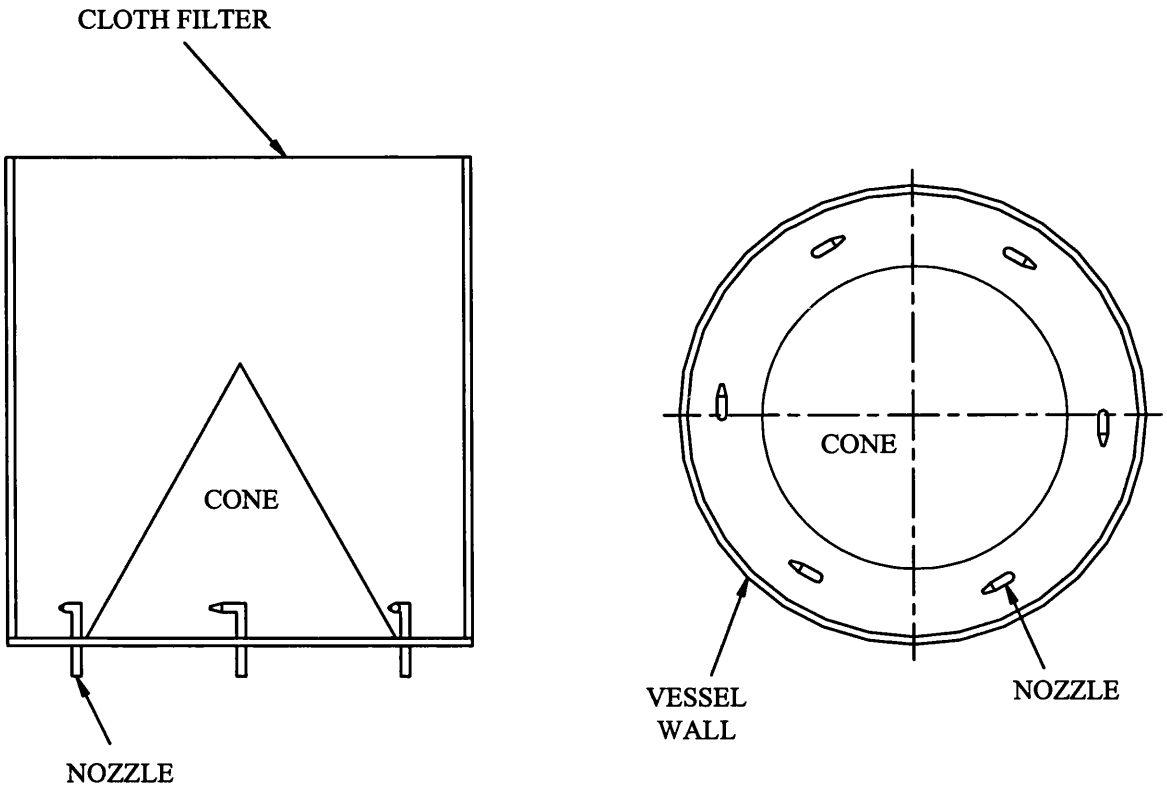

Figure 3.3. Schematic diagram of SVP Pre-prototype 2.

Although SVP Pre-prototype 2 produced air movements that were found to be inadequate for effective efficient powder mixing encouraging results were found in particle size reduction indicating that sufficient velocities could be obtained for this purpose using the nozzles as designed and fitted.

3.3 Fluid Bed SVP Model A

Although the findings from the initial prototypes including SVP Pre-prototype 2 were mainly a result of *ad hoc* investigations and observations they yielded sufficient information to enable the development of a fourth vessel, the Fluid Bed SVP Model A (FBSVP-A). A summary of the design and practical investigations into the particle size reduction and powder blending capabilities of this vessel is given below.

3.3.1 Design

A prototype processor, the FBSVP-A, was constructed to the design shown in figure 3.4.

A hollow cylinder of clear Perspex of wall thickness 6 mm was used for the main vessel wall so that powder movements could be observed during operation of the processor. This was fitted with a mesh base of 100μm aperture diameter that provided support for powder within the vessel, whilst allowing uniform fluidisation of the powder bed when air was introduced through the base. A lid provided with a rubber o-ring seal was attached to the top of the vessel using four case clasps. A polyethylene cone was fixed to the centre of the vessel base to prevent the formation of a dead zone in this part of the vessel.

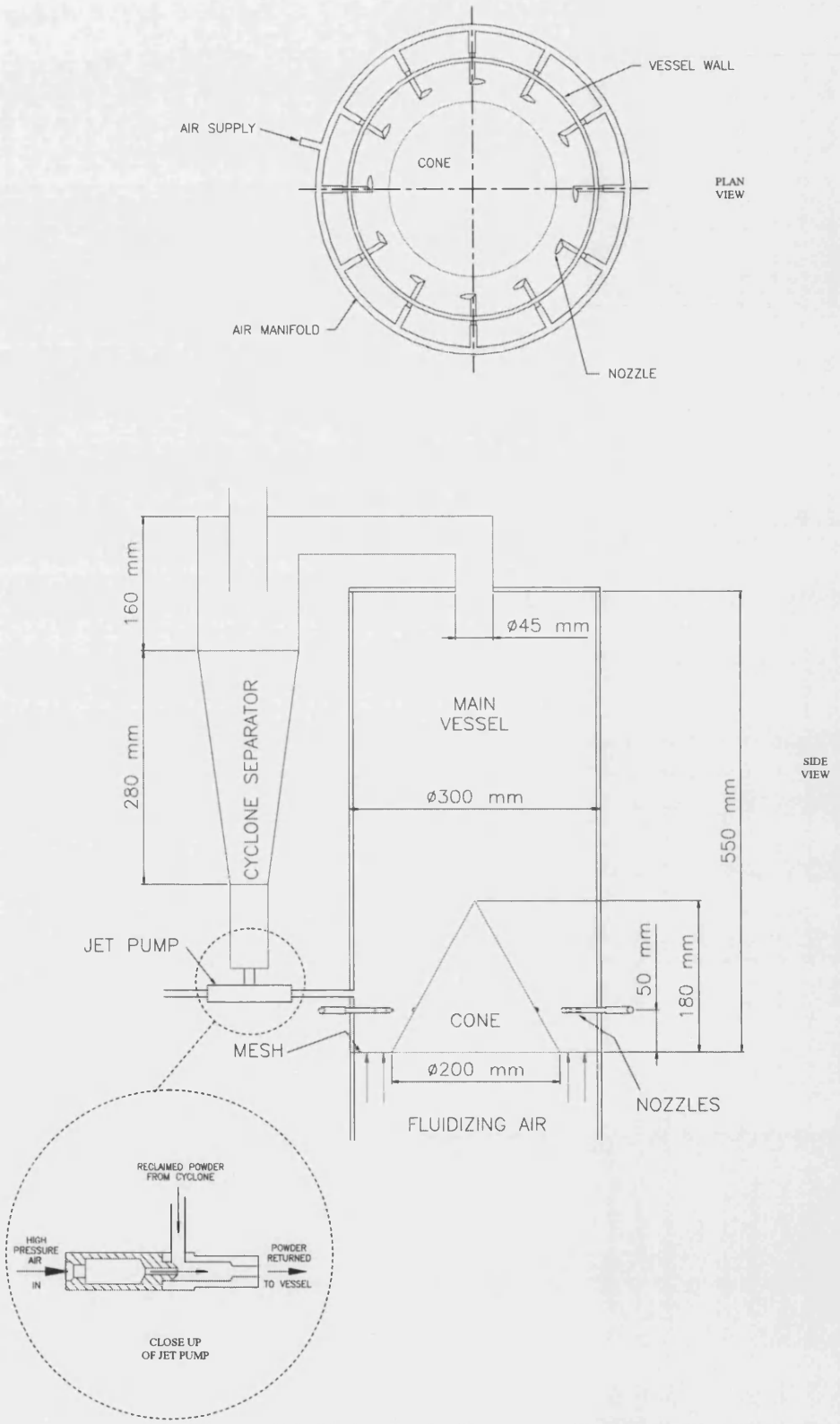

Figure 3.4. Schematic diagram of FBSVP-A.

Fluidising air was ducted into the bottom of the vessel from a centrifugal fan that could be operated at a maximum rotational speed of 2800 r.p.m.; this produced a calculated maximum air flow rate of 0.0456 m^3/s. Twelve L-shaped high-pressure jet nozzles of 1 mm output diameter were located around the base of the vessel and connected to a compressed air manifold. A compressed air feed of approximately 550 kPa was able to supply each nozzle at an air pressure of up to 210 kPa. The design of the nozzles was such that they could be adjusted in angle and depth within the vessel as required. A needle valve allowed control of the nozzle output air flow rate.

The attachment of a cyclone separator to the vessel lid was intended to enable the arrestment and return of entrained particles from the air leaving the vessel during operation of the air inputs. The gas outlet of the cyclone was allowed to vent to atmosphere and the dust outlet was attached to a jet pump. High-pressure air was directed through the jet pump nozzle causing air to be drawn through the top hole. This produced a suction effect that returned arrested powder from the cyclone dust outlet back into the main vessel.

The FBSVP-A was found to provide more uniform and widespread powder movements than previous designs and powder losses from the vessel were also greatly reduced. A further advantage of this design over the previous fluidised bed vessel was that it was not necessary to maintain a fluidising air input at all times, thus making it easier to control the process and to remove powder at the end of processing.

3.3.2 Particle size reduction

3.3.2.1 Materials.

Two grades of granular α-lactose monohydrate were selected as model test materials. These were of similar particle size ranges, but were prepared by different methods and consequently could be expected to exhibit different physical properties.

The first test material was a pharmaceutical quality commercially available granular lactose (CAGL), CrystaLac 40 (Meggle, Wasserberg, Germany). The second material was granulated lactose manufactured using SorboLac 400 lactose powder (Meggle, Wasserberg, Germany). This particular grade of material exhibited a higher specific surface area and finer particle size than CAGL. The granulation was performed in a high-shear mixer/granulator, using water ($20\%^{w}/_{w}$) as the binding liquid. The granules were fluid-bed dried to a moisture content of less than 5% w/w and granules outside the size fraction 250 – 500μm were removed by sieving. This material was termed high-shear mixer/granulated lactose (HSMGL).

3.3.2.2 Methods

500g lots of lactose were placed in the processor and size reduction carried out over a 30 minute period. Three lots of each material were processed in the vessel at nozzle pressures of 70, 140 or 210 kPa, corresponding to gauge readings of approximately 10, 20 or 30 p.s.i. respectively. These nozzle input air pressures had been previously verified using a calibrated pressure transducer.

Representative samples of approximately 1.5g of the powder were obtained from four positions in the powder bed using a sampling thief at 0, 60, 120, 180, 240, 300, 450, 600, 900, 1200, 1500 and 1800 seconds after the initialisation of size reduction.

Particle size analyses were performed in triplicate using low angle laser light scattering (LALLS) equipment and a dry powder feed technique.

Scanning Electron Microscopy (SEM) was used to obtain images of particles at different stages of milling.

3.3.2.3 Results

Data describing the changes in median particle diameter during milling are presented in Tables 3.1 and 3.2 for CAGL and HSMGL respectively.

Milling time (seconds)	Nozzle air pressure (kPa) 70	140	210
	Mean mass median particle diameter (μm)		
0	459	459	459
60	401	345	297
120	415	358	227
180	390	287	197
240	330	261	199
300	314	281	182
450	283	211	180
600	272	233	172
900	230	196	163
1200	236	194	157
1500	221	174	160
1800	199	167	157

Table 3.1. Summary of change in mean mass median particle diameter of CAGL with milling time in FBSVP-A at different nozzle air velocities.

Milling time (seconds)	Nozzle air pressure (kPa)		
	70	140	210
	Mean mass median particle diameter (μm)		
0	373	373	373
60	355	316	245
120	304	251	238
180	317	249	202
240	339	198	164
300	274	188	155
450	297	163	134
600	241	141	131
900	195	121	107
1200	151	118	115
1500	154	115	117
1800	127	109	107

Table 3.2. Summary of change in mean mass median particle diameter of HSMGL with milling time in FBSVP-A at different nozzle air velocities.

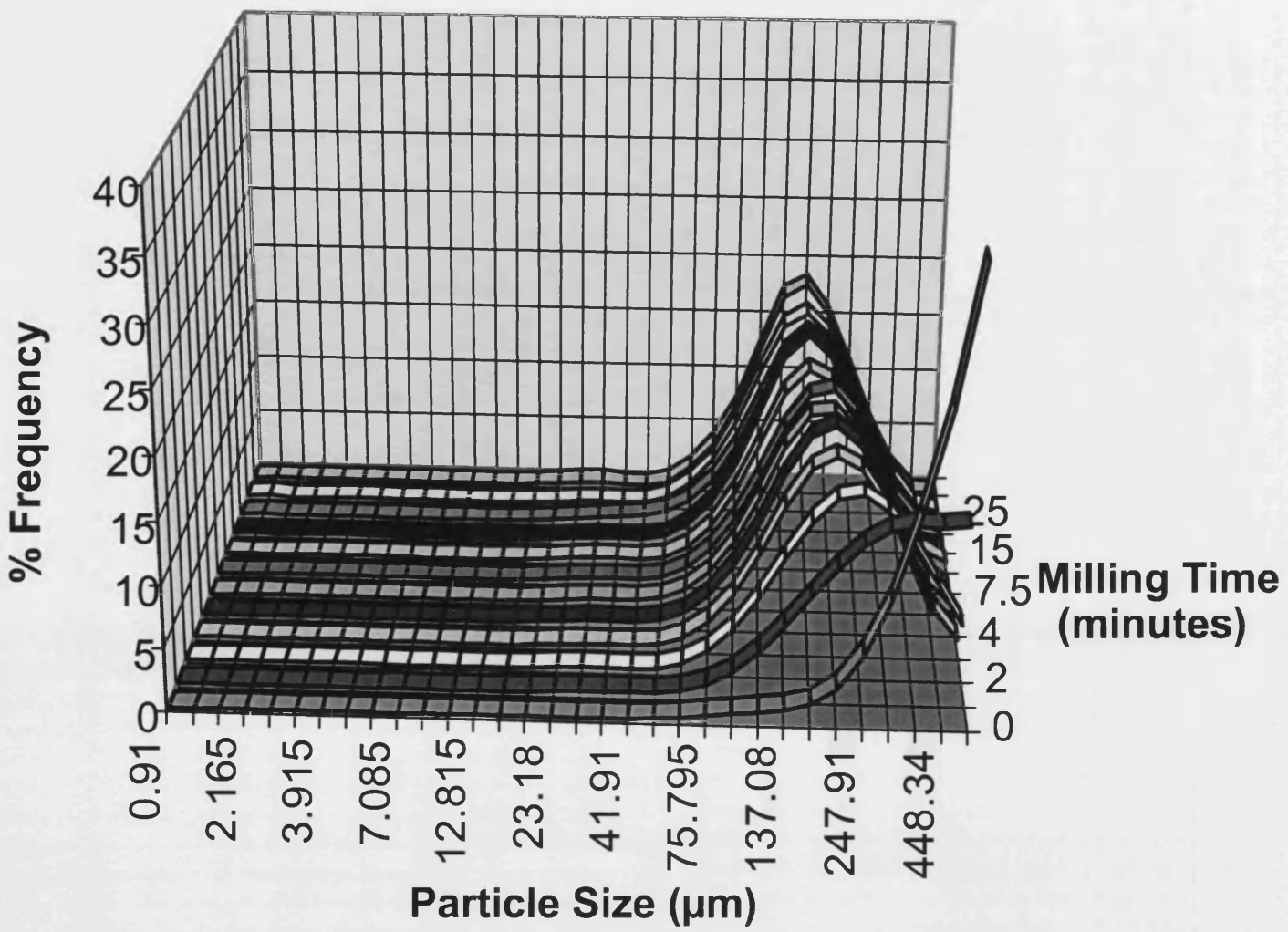

Figure 3.5. Graph showing change in particle size distribution of CAGL with milling time in FBSVP-A, operating at 30 p.s.I.

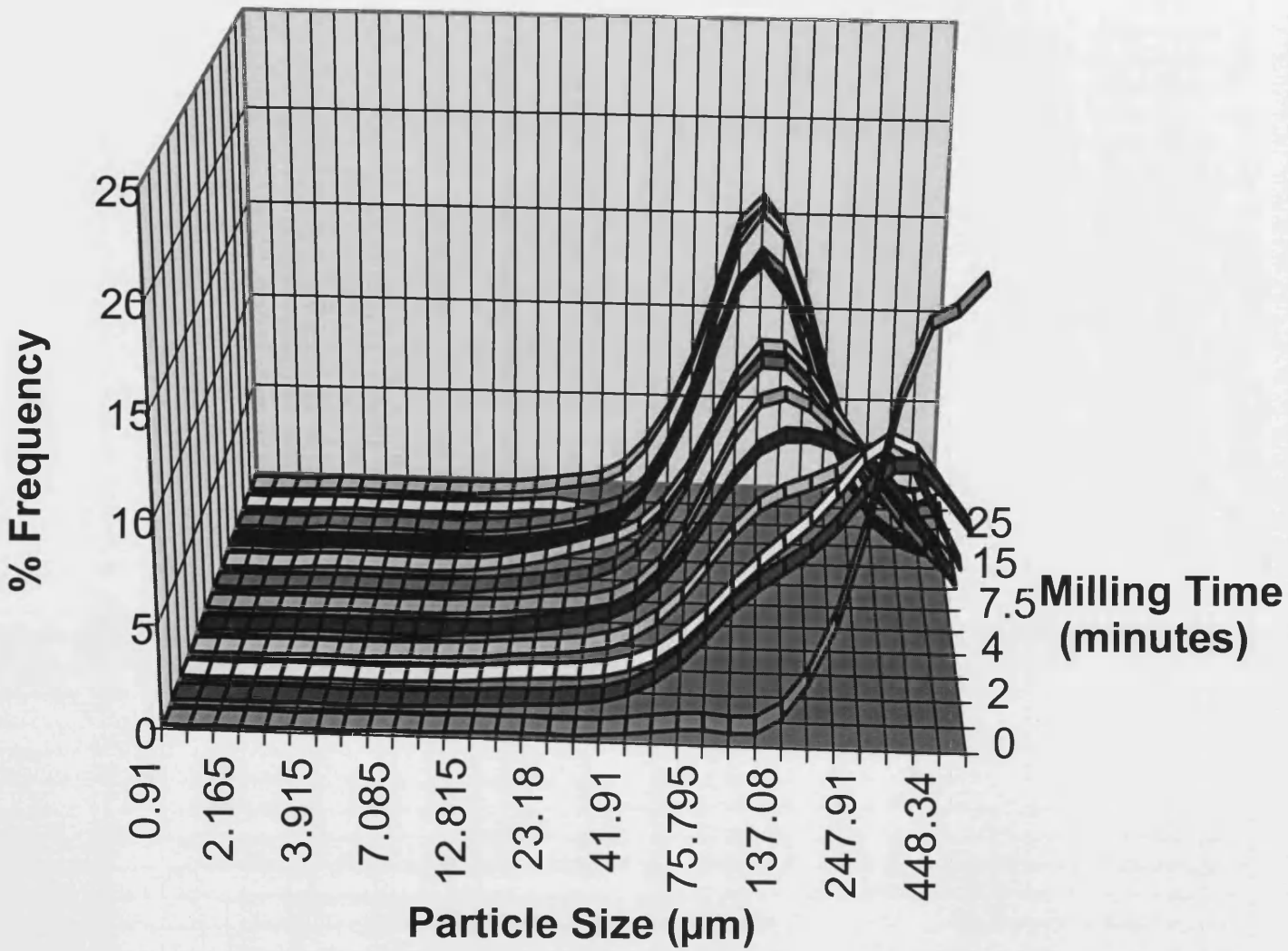

Figure 3.6. Graph showing change in particle size distribution of HSMGL with milling time in FBSVP-A, operating at 30 p.s.I.

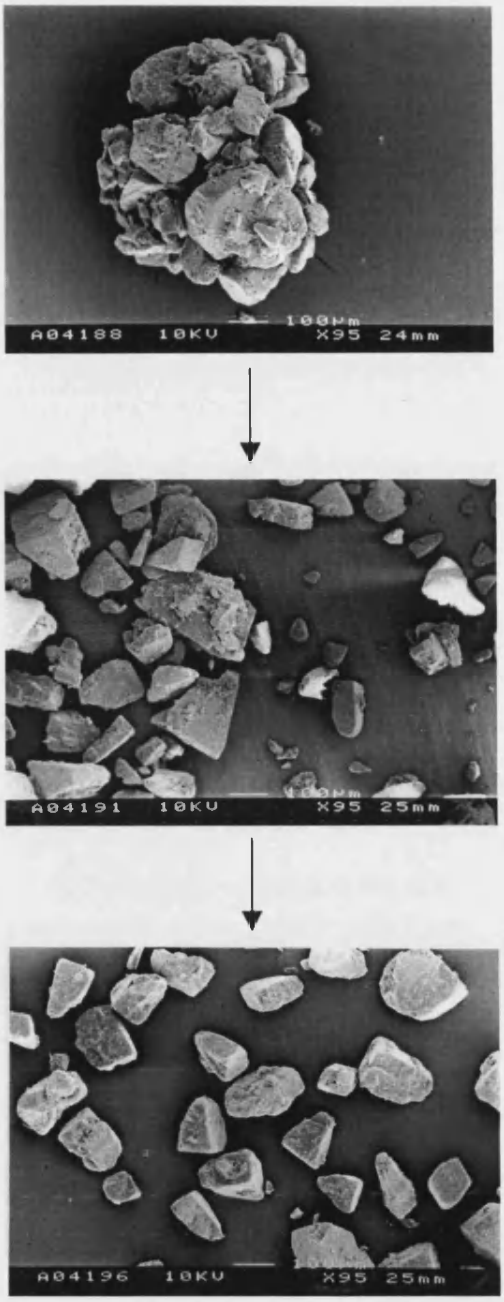

(a) unprocessed particle.

(b) after 1 minute processing at nozzle pressure 30 p.s.i.

(c) after 30 minutes processing at nozzle pressure 30 p.s.i.

Figure 3.7. Scanning electron photomicrographs of CAGL before and after milling.

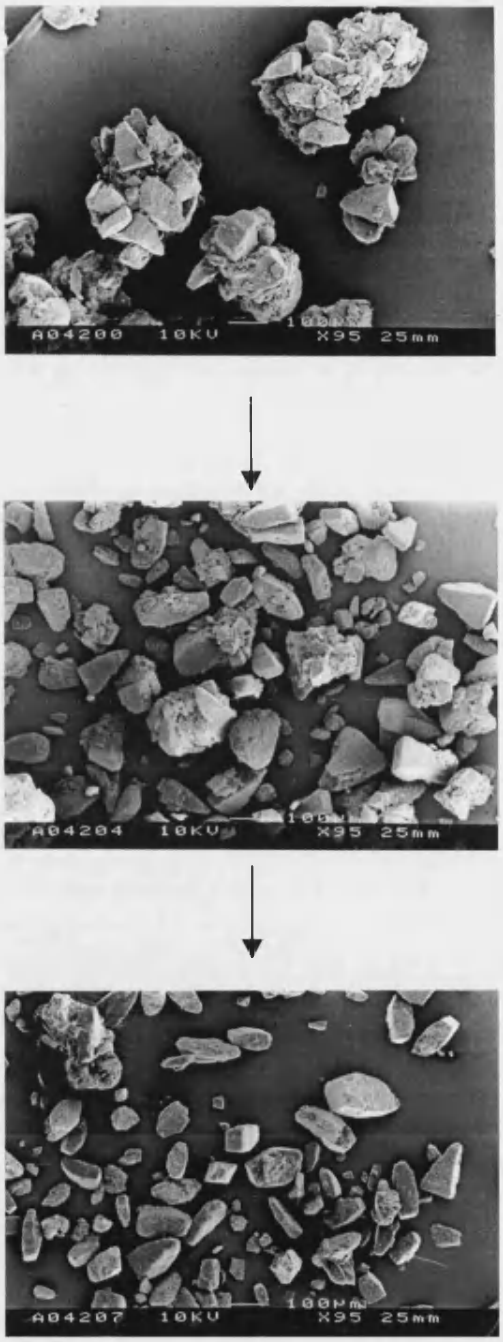

(a) unprocessed particle.

(b) after 1 minute processing at nozzle pressure 30 p.s.i.

(c) after 30 minutes processing at nozzle pressure 30 p.s.i.

Figure 3.8. Scanning electron photomicrographs of HSMGL before and after milling.

3.3.2.3 Discussion

The change in size distribution of CAGL when milled over 30 minutes at a nozzle pressure of 30 p.s.i was demonstrated (see Figure 3.5). It was shown that after 1 minute of milling, the modal size of the CAGL was reduced and the material exhibited a unimodal particle size distribution. This latter observation was considered noteworthy since powders usually display bimodal distributions during the early stages of milling; this may therefore have been indicative of a non-standard size reduction mechanism or a characteristic of the proprietary material (see below).

The effect of milling time at a nozzle pressure of 210 kPa on the particle size distribution of HSMGL is shown in Figure 3.6. The size distribution analysis indicated a bimodal character after 1 minute of milling. This was considered a classical response profile for the early stages of a milling process.

This evidence was suggested that in the case of CAGL most of the agglomerates were reduced to their constituent crystallites within the first minute of milling at 210 kPa nozzle pressure. This stage in the milling process when practically all individual crystallites had been liberated from their agglomerates was termed the 'Point of Complete Deagglomeration' (POCD) and was considered to be a key parameter in the process under study.

In contrast to CAGL the HSMGL agglomerates appeared to be broken down less easily into their constituent crystallites. After a milling time of 1 minute the material exhibited a bimodal distribution in which many of the agglomerates were still largely

intact with a small proportion broken into individual crystallites. The implication was that the bonding strengths between crystallites in HGMGL were stronger than those in CAGL. This theory was further supported by SEM photomicrographs (Figures 3.7 and 3.8), which showed a larger proportion of agglomerates in the HSMGL after 1 minute of milling than were present in CAGL.

Figure 3.5 shows a downward trend for the modal size of CAGL. However, after about 1 minute of milling, the modal and median sizes were less affected by increasing milling time. This suggested that most of the agglomerates had been broken down into their constituent crystals after 1 minute and that any further reduction in particle size was due to fragmentation of the individual crystallites by edge abrasion as shown in figure 3.9.

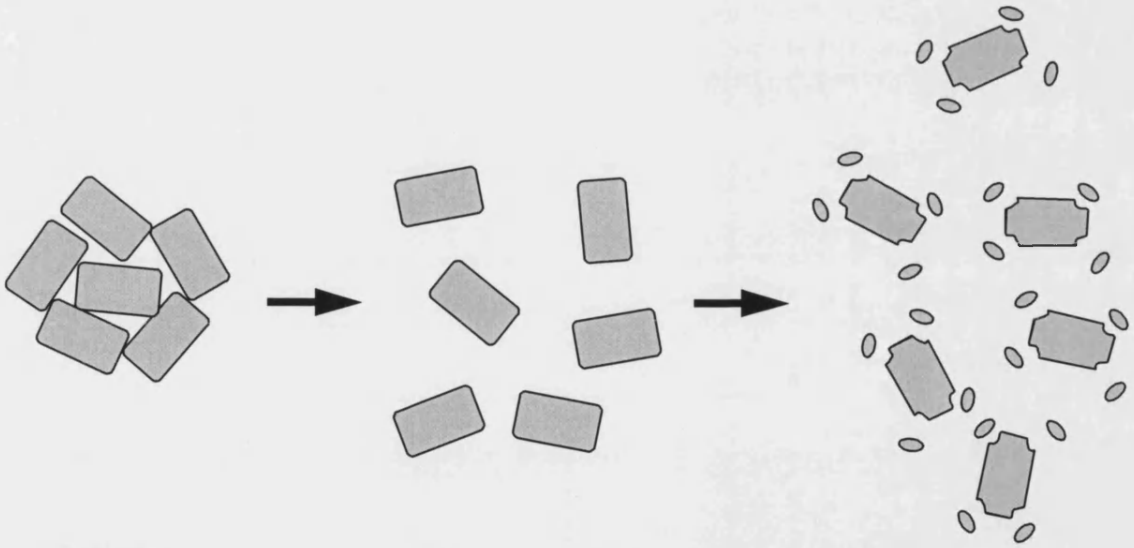

Figure 3.9. Proposed milling mechanism of CAGL and HSMGL in FBSVP-A showing POCD and edge abrasion after further milling.

This mechanism suggests that fragmentation of the component crystals would lead to the formation of a fine particle fraction in the later stages of milling and hence a bimodal size distribution. Since there was no evidence in the particle size data to suggest that this was the case the phenomenon could be caused by a preferential removal of fines from the processor since observation of the apparatus during milling indicated that a certain amount of fine material was seen to be entrained in the air leaving the cyclone separator.

The effect of reducing the milling nozzle pressure was investigated and as expected the rate of milling was reduced with decreasing nozzle pressures for both materials. The times taken to reach the POCD for CAGL and HSMGL at different nozzle pressures and the median particle diameter of the materials at these times are summarised in Table 3.3.

Material	Nozzle air pressure (kPa)	Time taken to reach POCD (sec)	Mean mass median particle diameter at POCD (μm)
CAGL	210	60	297
HSMGL	210	300	155
CAGL	140	180	287
HSMGL	140	600	141
CAGL	70	300	314
HSMGL	70	1200	151

Table 3.3. Summary of time taken to reach POCD for CAGL and HSMGL at different nozzle air pressures in FBSVP-A.

These milling data indicated that for CAGL, the maximum milling capability of the processor was able to mill the material to a median particle diameter of approximately 160μm. This appeared to have been achieved at nozzle pressures between 140 and 210 kPa. The maximum milling capability of the apparatus for HSMGL appeared to be to a median particle diameter of approximately 110μm. It was speculated that altering the milling conditions by increasing the nozzle pressures or by changing the geometry of the vessel could have resulted in an increase in the milling capacity as well as an increase in the rate of milling.

3.3.3 Mixing

3.3.3.1 Materials

HSMGL was used as the major component (90%) and milled sodium chloride crystals (Lot No. 40414 40408011, Aldrich Chemical Company Limited, Gillingham, Dorset. U.K.) the minor model drug component (10%) of a 500g mass of the binary powder mix. Sodium chloride was selected as a model drug to allow conductivimetric analysis over a wide concentration range without requiring sample dilutions. The mass median particle diameter of the lactose was 373μm and the sodium chloride was hammer-milled to a mass median particle diameter of approximately 30μm as measured by LALLS.

This differential in the mass median particle diameter of the two components was selected so as to encourage the formation of interactive mixes in which finer particles became adhered to the surfaces of coarser 'carrier' particles.

3.3.3.2 Methods

The efficiency of the FBSVP-A for mixing two dry powders was compared with two other mixing techniques with known efficiencies namely geometric mixing and turbulent tumbling mixing.

3.3.3.2.1 Geometric mixing

Geometric mixing was performed by placing 50g of milled sodium chloride crystals and 50g of lactose granules into a large mortar and triturating thoroughly by hand for 5 minutes using a pestle. A further 100g of lactose was added and similarly mixed, followed by a 200g quantity of lactose, which was also mixed for 5 minutes. A final quantity of 100g lactose was added and thoroughly mixed for a further 15 minutes. Thus, the total mixing time was 30 minutes.

3.3.3.2.2 Turbulent tumbling mixing

Milled sodium chloride crystals 50g and lactose granules 450g were placed into a two litre glass jar and the lid sealed. The jar was then loaded onto a turbulent tumbling mixer (Turbula® Mixer, Type T2C, Glen Creston Limited, Stanmore, Middlesex, U.K.), which was operated at speed II for 30 minutes.

3.3.3.2.3 FBSVP-A mixing

450g of lactose granules were placed into the FBSVP-A, and 50g of milled sodium chloride were gently added. The fluidising fan was turned on at its maximum speed providing an air volume throughput of approximately 0.02 m^3sec^{-1}; the jet nozzles were supplied with air at a pressure of 210 kPa.

The above conditions were maintained for a period of 30 minutes after which the air supplies were terminated and the powder removed from the vessel for sampling and analysis.

3.3.3.2.4 Powder sampling

The material obtained from each mixing experiment was emptied onto a clean, flat surface with a minimum of agitation so that samples could be taken from the resulting powder. Thirty samples of approximately 500mg were taken at random from the mixture using a sample thief.

3.3.3.2.5 Model drug assay

500mg samples were placed in a 50ml volumetric flask, and diluted to 50ml using freshly deionised water at 25°C. A conductivity meter and cell were calibrated and each sample solution assayed for sodium chloride content based on the conductivity of the solution. Controls showed that lactose did not affect the conductivity reading.

The homogeneity obtained from each mixing technique was measured by calculating the percent relative standard deviation (%RSD) of the mean of each set of thirty results.

3.3.3.3 Results

Mixing method	Mean content	%RSD
Manual geometric mixing	9.4%	0.9%
Turbulent tumbling mixing	9.5%	15.2%
Mixing in FBSVP-A	8.2%	2.5%

Table 3.4. Mean content and %RSD obtained from each mixing technique.

3.3.3.4 Discussion

As expected, the most efficient mixing of the materials tested was obtained by manual geometric mixing, which provided a %RSD of 0.9%. The value of this technique was to provide evidence that a homogeneous mixture could be obtained using the materials under investigation. The results using manual geometric mixing were considered to be a point of reference for other mixing techniques.

Since the method of homogeneity testing was considered to give values that were a composite for mixing and segregation, any segregation phenomena that occurred during the mixing process were considered to have been taken into account.

It was notable that the results indicated a mean content that was slightly less than the theoretical value of 10.0% sodium chloride. This was thought to have occurred through agitation of the material causing entrainment of fine particles into the air, which were then lost to the external environment since the mixing vessel was not enclosed during the mixing process. This preferential loss of fine material from the

bulk powder was considered to account for the low content assay since this material was likely to have been predominantly composed of sodium chloride particles.

The quality of mix obtained by using the turbulent tumbling technique was poor, being characterised by a %RSD of 15.2%. This was probably due to a lack of internal shear forces being provided by tumbling mixing, particularly between initial fine particle agglomerates of sodium chloride. Such forces were considered necessary for the formation of an interactive powder mixture in this particulate system (see below).

The effect of a shearing force imparted onto a powder mixture containing two components one of which was much finer than the other is shown diagrammatically (see Figure 3.10). This figure shows an agglomerate of the fine component, surrounded by larger carrier particles. A low shear force was represented as taking the energetically easiest route through the powder, which in this case was shown to be around the exterior of the carrier particles and the fines agglomerate. A high shear force was shown as able to pass between individual particles in the agglomerate and hence break it up so that it could be distributed over the carrier surfaces and form an interactive mix.

It is suggested that a geometric manual mixing technique imparted large shear forces on the powder by the grinding action of the mortar and pestle, causing the more adhesive component (milled sodium chloride) to be redistributed onto the carrier particle surface.

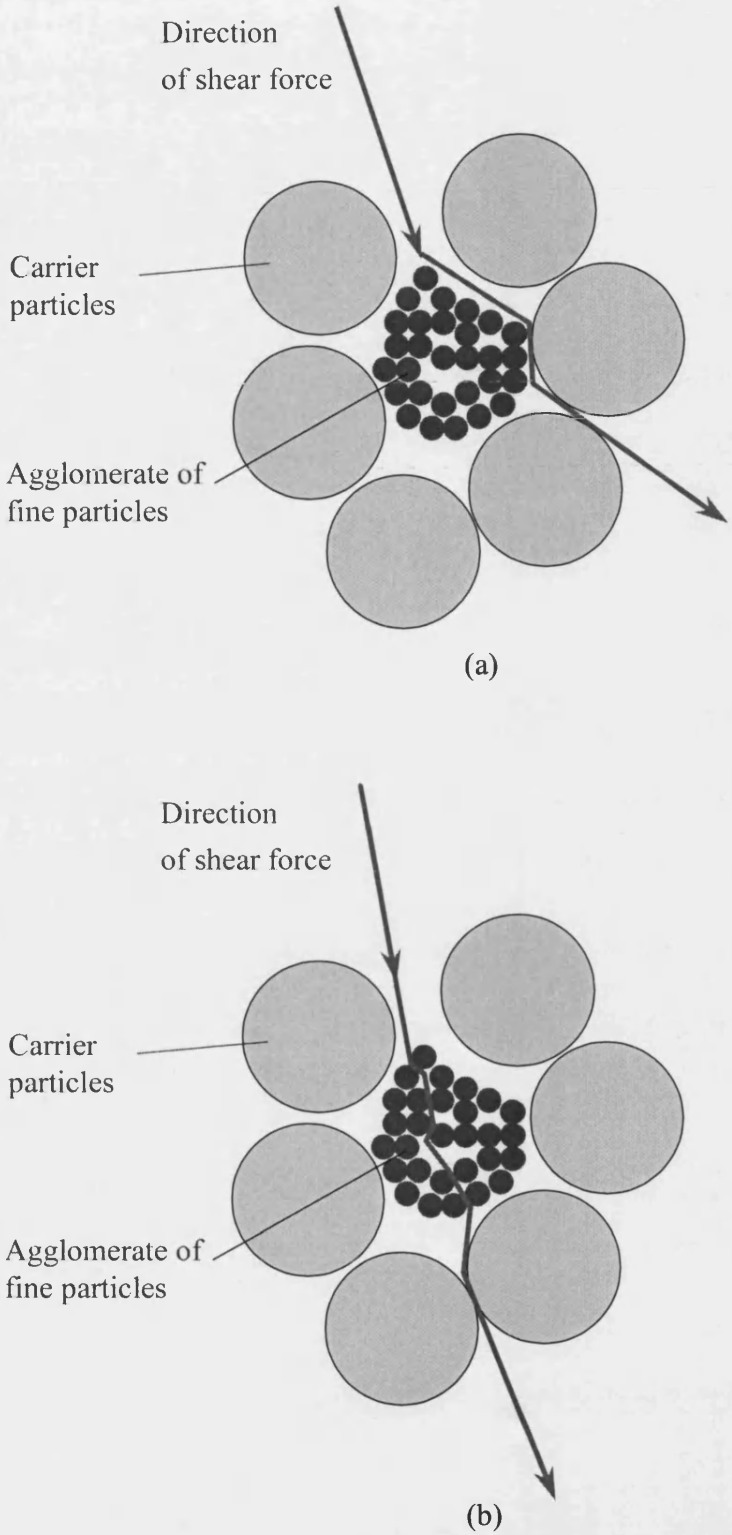

Figure 3.10. Schematic representation of application of (a) a low shear force and (b) a high shear force in ordered mixing.

Aggregates that were of a similar particle size to the carrier lactose particles were postulated to remain intact in the turbulent tumbling technique due to this lack of shear, so reducing the homogeneity of the mix.

It was considered that the high shear conditions created by the high pressure air nozzles within the FBSVP-A were able to break up the agglomerates during the mixing evaluation in a similar fashion to that which would be expected in a bladed high-shear mixer.

A value for %RSD of less than 5% is generally considered adequate in most pharmaceutical powder mixing processes. The FBSVP-A provided a mixing capability characterised by a %RSD of 2.5%. As shown in Table 3.4, this represented an improved mixing efficiency over turbulent tumbling mixing. The motion of powder within the vessel during its operation was observed to display large regions of recirculating flow, which encouraged efficient mixing to occur.

The combination of fluidising air, which was supplied to all of the flat regions of the vessel base, with the swirling flow fields generated by the high pressure air nozzles ensured that the flow patterns within the vessel attained sufficiently turbulent conditions and fluctuating velocities within the powder bed to perform the mixing process. The high shear created by the action of the high pressure air nozzles facilitated the mixing of a binary powder system consisting of powders of widely differing particle sizes, thus enabling the formation of interactive powder mixes.

3.3.3.5 Conclusion

The prototype FBSVP-A was found to be capable of performing the sub-operations of granule size reduction and dry powder mixing. There was also evidence that the processor was capable of providing some primary size reduction of materials, probably by edge abrasion.

The flow patterns induced in the powder within the FBSVP-A could be readily observed and displayed a strong turbulent flow field that was well fluidised. Conditions such as these are generally considered to be beneficial in mixing operations.

Particle size reduction was found to be rapid for the 500g batch size investigated; the speed and extent of granule size reduction was considered to be at least equivalent to that which could be attained using conventional techniques of secondary size reduction in granulation. It is projected that greater size reduction could be obtained by increasing the nozzle pressures.

The mixing achieved within the processor was found to be more homogeneous than that achievable with a similar powder system using a conventional low shear mixing technique (turbulent tumbling).

The principle of using controllable fluid dynamics to perform multi-task processing of powders was demonstrated. The FBSVP-A was thought to offer a system with the

potential for the batchwise preparation of powders for pharmaceutical use within a single vessel.

The arrestment and return to the powder bed of very fine particles from the gas stream using a cyclone separator was not as effective as needed and this aspect requires further attention; future designs may require the inclusion of a fibrous filter system.

The SVP concept was considered to form the basis for the design of a continuous bladeless processor, capable of integration into a closed, automated and controllable manufacturing system in which raw materials could be processed without manual intervention.

4. FLUID BED SVP MODEL B DESIGN AND FABRICATION

4.1 Rationale

The preliminary work detailed in Chapter 3 described a number of successful design features of the FBSVP-A that made it suitable for certain powder processing operations and recognised some design limitations.

One of the major limitations was identified when attempting to use the FBSVP-A for wet granulation activities. It became evident that an attempted resolution to this problem was likely to encompass a substantial investigation in its own right and it was therefore decided not to include such work within the scope of this thesis. Consequently it was proposed to investigate the benefits of the technology with respect to those procedures for which the FBSVP-A had been demonstrated to be potentially effective i.e. the dry processes of particle size reduction and powder blending.

One aspect of pharmaceutical technology that has not received significant attention in recent years is the development of alternative equipment for the treatment of powders for use in inhalation therapy. Much of the processing associated with dry powder inhalation products concerns particle size control and efficient dry blending and therefore it was intended to develop the FBSVP-A into a modified processor, the

Fluid Bed SVP Model B (FBSVP-B), with particular emphasis on its application in processing powders for inhalation thus encompassing powder blending and particle size reduction of active compounds and/or excipient powders.

4.2 Modifications to FBSVP-A

4.2.1 Gas – solids separation

The cyclone/jet pump arrangement utilised in the FBSVP-A was found to be inefficient particularly in its application to very fine particles such as those produced during size reduction experiments. Cyclone systems are often used in conjunction with bag filters in fluid energy mills; however, such a combination could not easily be incorporated into the SVP design.

Similar types of equipment found in current pharmaceutical production that utilise high-volume airflows, such as fluid bed granulators and driers, are generally fitted with bag-house filters.

For these reasons, and particularly since it was the intention to process fine particle drug compounds in the processor the vessel was fitted with a bag filtration system as described in section 4.3.2 below.

It was expected that a reduction in the pressure build-up within the vessel resulting from this modification would reduce leakage of material from the vessel.

4.2.2 Repositioning of nozzles

Since a significant portion of the FBSVP-A base was subject to stagnation of material movement during operation of the airflows the positions of the high-pressure air

nozzles were adjusted in the FBSVP-B. It was found that positioning these nozzles closer to the base of the vessel provided a more comprehensive movement of powder in the area around the base of the cone and behind the nozzles.

4.3 Fabrication

4.3.1 Main vessel assembly

A schematic diagram of the FBSVP-B is presented in figure 4.1.

The vessel wall comprised a Perspex® cylinder of 300mm external diameter, 550mm height and a wall thickness of 6mm. This was fitted with a stainless steel (Grade 304) mesh (John Staniar & Co., Manchester, U.K.) base of 100μm aperture width.

The mesh was supported by a coarser mesh of stainless steel wire (Grade 304) of 1mm gauge and providing a 10mm aperture width (John Staniar & Co., Manchester, U.K.).

A cylindrical Perspex® skirt of 50mm height was fixed to the underneath of the base and fitted with an o-ring and four case clasps to enable sealed attachment of the fluidising air plenum.

A polyethylene cone of 200mm base diameter and 180mm height was located in the centre of the mesh base providing an annular ring of 44mm width through which fluidising air could be introduced.

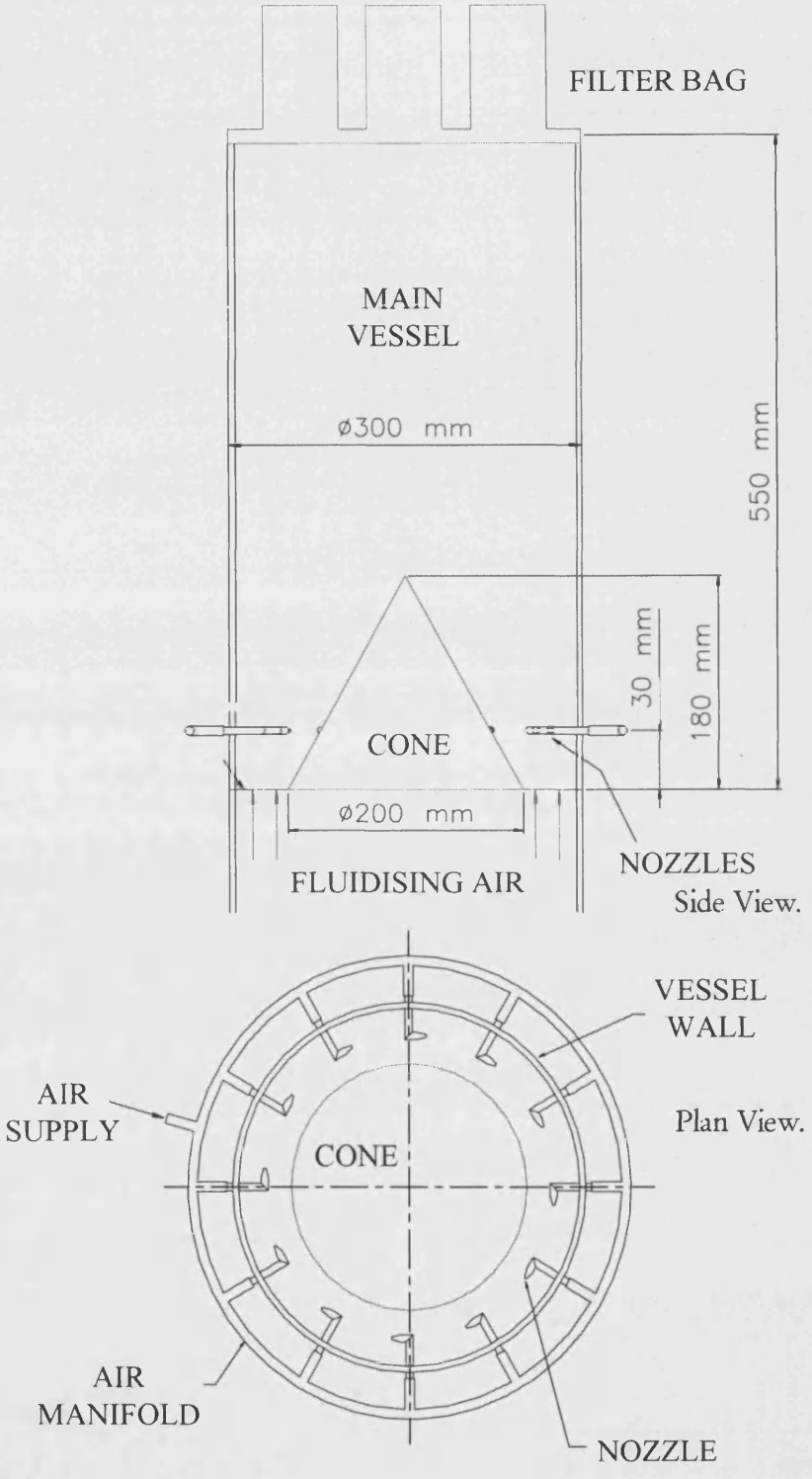

Figure 4.1. Drawing of FBSVP-B.

Twelve holes of 7mm diameter were drilled equidistantly around the circumference of the vessel wall 30mm from the base. Each hole was fitted with a rubber sealing flange into which one of the high-pressure nozzles was seated. The nozzles were fabricated from 5mm O.D. brass tubing and were designed with a nozzle outlet diameter of 1.0mm. A diagram of the nozzle design is shown in figure 4.2.

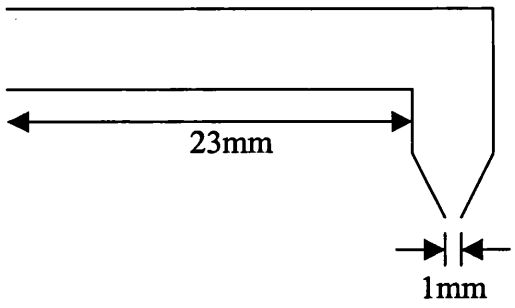

Figure 4.2. Schematic diagram of nozzle dimensions

The nozzles were positioned in the rubber flanges so that the centre of each nozzle outlet was pointing at an angle of 45° below the horizontal. Each nozzle was also positioned so that the centre of the nozzle outlet bisected the area between the cone and the wall at the height of the nozzle outlet. This approximated to an insertion depth of 23mm as indicated in figure 4.2.

A view of the nozzle arrangement is shown in figure 4.3.

Four case clasps were arranged around the circumference, towards the top of the vessel and the top face of the vessel wall was fitted with a rubber o-ring of 2.9 mm diameter to allow the filter assembly to be secured and sealed.

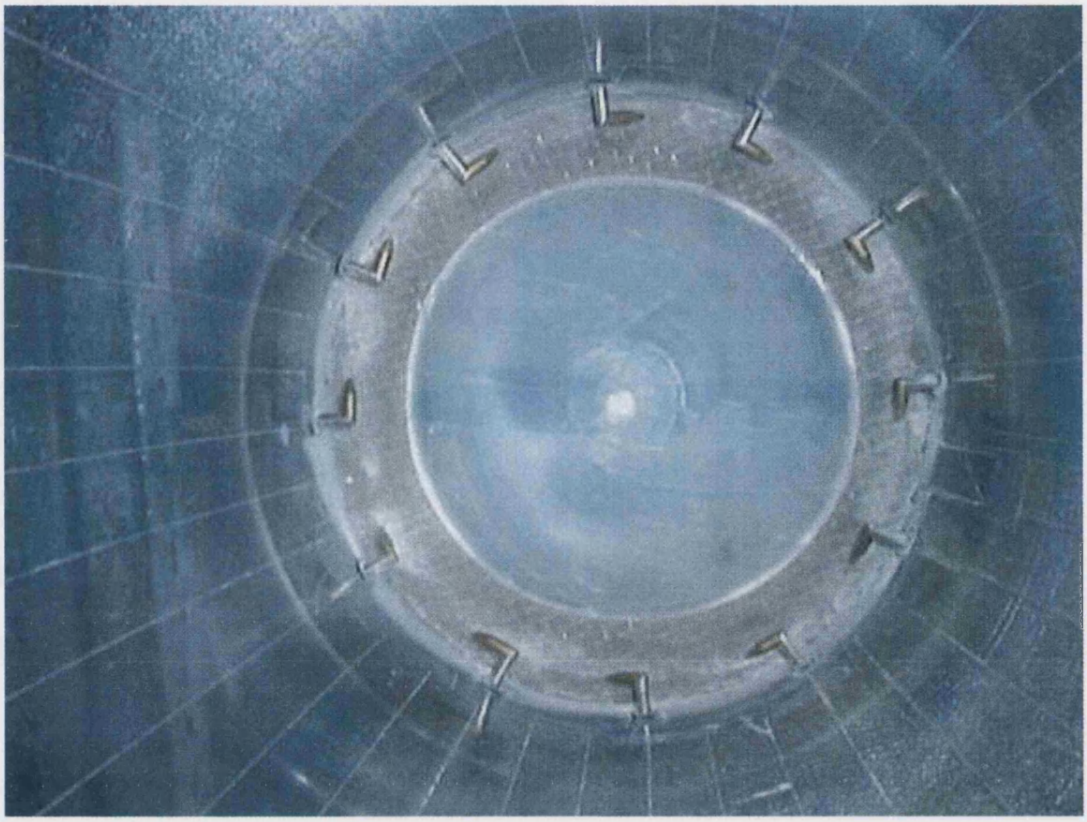

Figure 4.3. Photograph of nozzle arrangement in FBSVP-B.

4.3.2 Filter assembly

An 80 mm high cylindrical Perspex section was fitted with a seal and clasps so as to enable attachment to the top of the main vessel. A woven nylon filter containing carbon fibre insertions to reduce static build-up (Samuel Hill Ltd., Rochdale, U.K.) with an approximate air permeability of 120 l dm^{-2} min^{-1} was sealed into this section.

The approximate dimensions of the filter bag are shown in figure 4.4 (six outer tubes: d = 80mm, h = 130mm; one central tube: d = 80mm, h = 90mm; overall diameter = 300mm). The approximate surface area of the filter bag was calculated as $0.3m^2$.

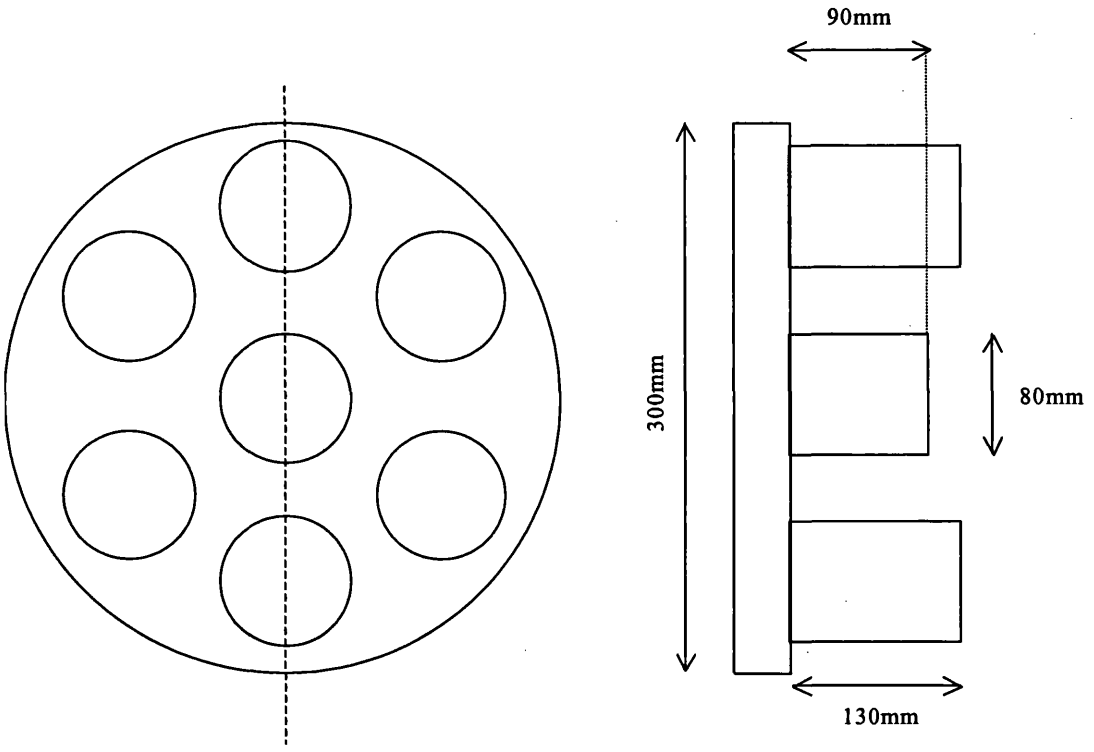

Figure 4.4. Schematic diagram of filter bag.

4.3.3 High pressure air manifold

The twelve high-pressure nozzles were split into two banks of six. The nozzles in each bank were interconnected using 6mm polyethylene fittings and flexible tubing. Each bank was then connected using standard brass fittings to a needle valve (Part number B-4JNR2-RT, Nupro Company, Ohio, U.S.A.) and pressure gauge (0-160

p.s.i., Martonair, Birmingham, U.K.) in order to allow the air supply to each bank to be independently regulated to a known and reproducible air pressure.

Two compressed air supplies were available which were combined to enable the nozzle pressure to be regulated up to a maximum of approximately 35 p.s.i.

4.3.4 Fluidising air fan and plenum

Fluidising air was supplied to the base of the main vessel from a centrifugal fan (Type D28 0.75 kW, Robert Stahlschmidt Elektromotorenwerk, 4801 Altenhagen, Germany) having the following specification:

Fan diameter: 180 mm

Blade width: 12 mm (blade angle of 20°)

Maximum blade speed: 2800 revolutions per minute

Regulation of the input voltage enabled control of the theoretical flow output from the fan between zero and approximately 50 $Lsec^{-1}$.

The outlet was positioned horizontally and directed through a flexible corrugated aluminium duct of 120mm diameter into to the expansion plenum consisting of a frusta-conical chamber of 410 mm height so increasing the duct diameter from 120 to 300mm. This arrangement is shown schematically in figure 4.5. The expansion plenum was connected to the bottom of the main vessel using four clasps and a rubber seal.

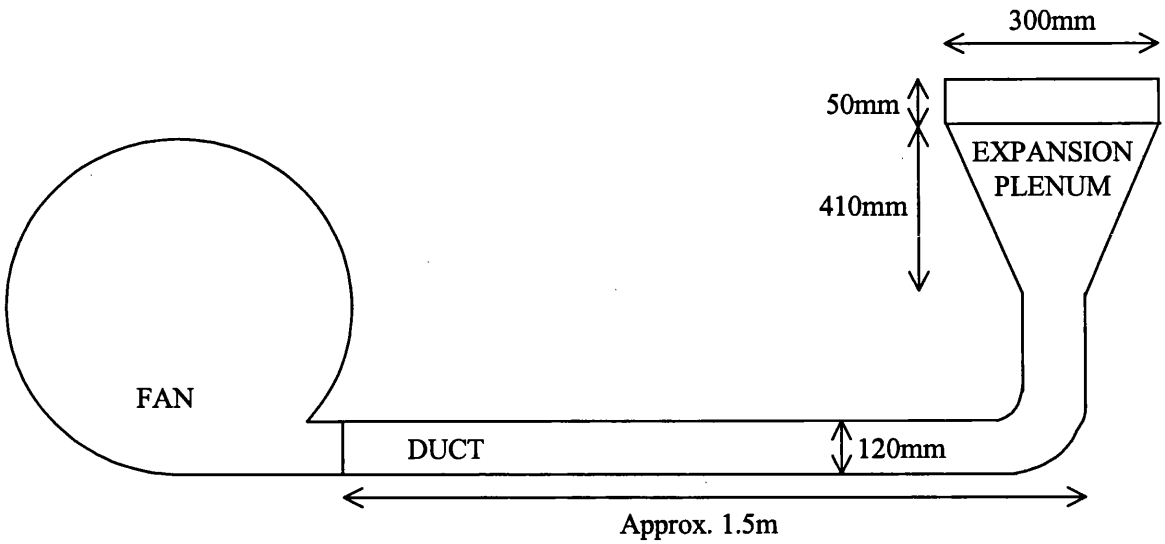

Figure 4.5. Schematic diagram of fan, ducting and expansion plenum.

4.3.5 Anti-static treatment

One phenomenon that had been noted during previous studies had been the propensity for material to become adhered to the vessel walls and cone, due to the generation of electrostatic charge on the plastics surfaces.

In order to reduce the magnitude of this charge and make it easier to dislodge material from affected surfaces all insulating surfaces in product-contact zones were covered with an anti-static adhesive tape (12mm width, RS Components Limited, Northants., U.K.). The tape reduced electrostatic effects by distributing more evenly any charges generated across the tape surface.

The effect of coating the internal vessel wall with this antistatic tape is shown in figure 4.6. In this case one section of the vessel was coated with antistatic tape with the remaining part of the vessel wall remaining untreated. The photograph shown in figure 4.6 was taken after processing lactose powder in the FBSVP-B for a period of 5 minutes and then knocking the vessel wall with a rubber mallet. This photograph clearly shows that material had cleared to a much greater extent from the treated vessel wall than from the untreated portion.

Although the anti-static tape was found to reduce visual acuity through the vessel walls it was still sufficiently transparent to allow clear observation of powder movements. However, since the tape was cellulose based, it was not possible to clean down the vessel with water between experiments and therefore cleaning of powder residues from the vessel after use was performed by brushing and vacuum extraction.

Whilst it was recognised that such cleaning procedures would be unacceptable in a pharmaceutical production application it was envisaged that any production vessel would be constructed from earthed stainless steel, thus allowing electrostatic charges to be discharged to earth.

The interaction of the anti-static tape with water was found to cause a gradual degradation of the tape over several weeks, due to the ambient humidity of the laboratory. This resulted in some detachment of the tape from the surface leading to entrapment of powder and so necessitating periodic replacement of the tape.

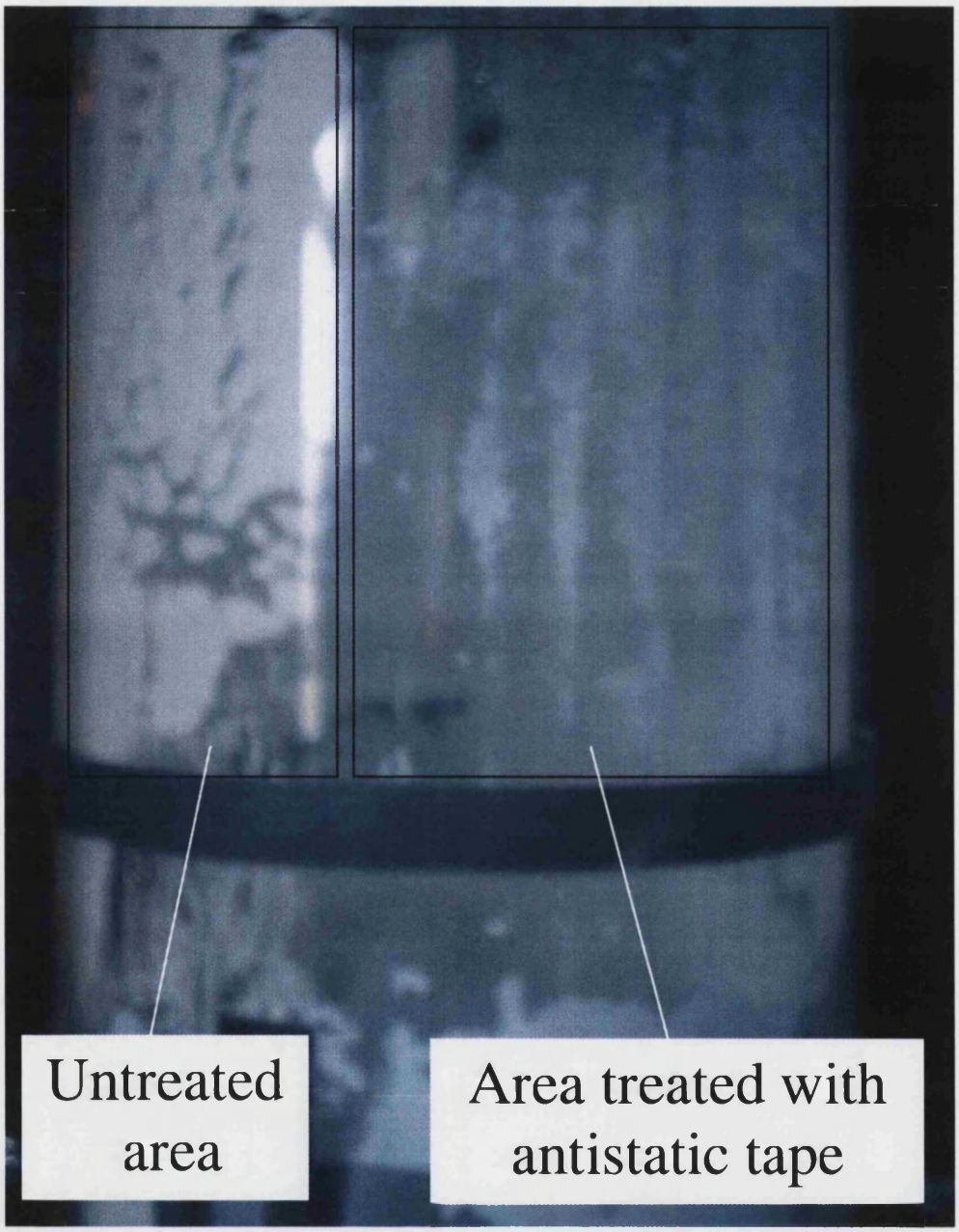

Figure 4.6. Photograph of side view of FBSVP-B showing untreated area and area treated with antistatic tape following operation of vessel containing lactose powder.

4.4 Air flow determination

4.4.1 High-pressure nozzles

The air output flows from the high-pressure nozzles could be varied using needle valves the effects of which could be monitored on in-line pressure gauges. Whilst these gauges could be used to monitor the pressure within the air manifold the pressure readings did not give an indication of the velocity of the air at the nozzle exit. In order to measure the actual air output velocities it was necessary to measure the pressure drop immediately across the nozzle exits; this was undertaken as explained below by the use of a pitot tube.

A mercury U-tube manometer (Department of Mechanical Engineering, University of Bath, Bath, U.K.) was attached to a pitot tube and the opening of the pitot tube was directed in opposition to the air stream as close to the nozzle opening as possible without blocking the flow. The head height of mercury was recorded for each nozzle at a series of gauge pressures and air velocities were calculated by application of Bernoulli's equation:

$$P_t = P_s + \tfrac{1}{2}\rho_{air} v^2 \qquad \text{[Equation 4.1]}$$

where P_t is the gauge pressure in Nm^{-2}; P_s is atmospheric pressure in Nm^{-2}; ρ_{air} is the density of air in kgm^{-3}; v is air velocity in $msec^{-1}$.

Calculation of atmospheric pressure.

Atmospheric pressure was measured using a mercury barometer (Department of Mechanical Engineering, University of Bath, Bath, U.K.), which provided an atmospheric pressure value in mmHg. This reading was converted to Nm^{-2} using the following equation:

$$P_s = \rho_{Hg} g h_{baro} \qquad \text{[Equation 4.2]}$$

where P_s = atmospheric pressure (Nm^{-2}); ρ_{Hg} = density of mercury (= 13560 kgm^{-3} at 15°C); g = gravitational acceleration (= 9.81 ms^{-2}); h_{baro} = head height of mercury in barometer (mHg).

Calculation of density of air.

The ambient temperature was measured using a calibrated mercury in glass thermometer. The density of air at ambient temperature and pressure was calculated for each set of experiments using the equation of state:

$$P_s V = mRT \qquad \text{[Equation 4.3]}$$

where V = volume of air in m^3; m = mass of air in kg; R = gas constant for air (= 287 J/kgK); T = temperature (K).

Since $m = \frac{\rho_{air}}{V}$, where ρ_{air} = density of air (kgm^{-3}),

$$\rho_{air} = \frac{P_s}{RT} \qquad \text{[Equation 4.4]}$$

Calculation of gauge pressure of each nozzle.

The values for gauge pressure obtained using the mercury manometer were converted from mmHg to Nm^{-2} using the following equation:

$$P_t = \rho_{Hg} g h_{man} \qquad \text{[Equation 4.5]}$$

where P_t = gauge pressure (Nm^{-2}); h_{man} = head height of mercury manometer (mHg).

Calculation of air velocity.

The velocity of air exiting each nozzle was calculated using Bernoulli's equation:

$$P_t = \frac{1}{2}\rho_{air} v^2 \qquad \text{[Equation 4.6]}$$

hence,

$$v = \sqrt{\frac{P_t}{\frac{1}{2}\rho_{air}}}$$ [Equation 4.7]

A summary of the air velocities at each nozzle pressure setting is shown in table 4.1.

Nominal nozzle pressure		
10 p.s.i.	20 p.s.i.	30 p.s.i.

Nozzle number	Mean *v* (m/s)	SD	Mean *v* (m/s)	SD	Mean *v* (m/s)	SD
1	69.5	8.2	120.7	6.6	149.0	2.1
2	78.9	4.5	120.7	4.3	148.0	6.1
3	82.7	0.8	116.5	6.4	146.8	1.5
4	83.1	4.5	116.5	4.6	145.6	1.1
5	79.3	1.2	99.7	15.6	127.9	3.1
6	82.9	5.1	77.3	2.4	130.6	15.2
7	80.5	3.3	85.1	23.5	116.5	3.8
8	76.0	2.0	97.2	3.4	132.0	0.9
9	81.6	3.9	98.7	1.2	134.7	4.2
10	76.9	3.5	96.5	3.6	134.2	0.9
11	80.0	1.0	133.6	2.0	144.9	2.3
12	61.9	1.6	117.7	4.8	146.6	3.6
Approx. overall mean	78		107		138	

Table 4.1. Summary of measured air velocities of each nozzle at different nominal nozzle ring air pressures.

4.4.2 Fluidising air

The flow rate of the fluidising air was measured by attaching a rotameter (Dept. of Mechanical Engineering, University of Bath, Bath, U.K.) to the output from the top of the vessel. The maximum flow rate of the fan (i.e. voltage output set at maximum) was measured at 0.02 m^3sec^{-1}.

4.5 Computational Fluid Dynamics

Following the initial design investigations, and having identified the need to redesign the processor, it was considered advantageous to facilitate design development by using computer aided design engineering techniques.

Computational Fluid Dynamics (CFD) technology for modelling air flow fields and particle movements was exploited to project the air velocity profile of vessel designs during a range of operational conditions and also to predict likely effects of changes to the vessel geometry, design and operating parameters prior to undertaking any fabrication and testing.

The first stage in utilising the CFD technology was to prepare a model of an existing processor configuration and compare the modelling predictions with observed experimental results.

4.5.1 Introduction to CFD

Only a brief description of the mechanics of CFD is given since more general texts are able to provide greater detail (e.g. Versteeg and Malalasekera, 1995).

The use of CFD is now widespread in engineering design where systems involving fluid flows are being developed. Applications of the technique include investigation of aerodynamics of aircraft and automobiles, internal combustion engines and mixing processes. CFD has recently been used in the modelling of human and *in vitro* lung systems for the development of medical aerosol technology and to predict the air flows obtained during actuation of pressurised metered dose inhalers (Versteeg *et al.*, 2000). In this latter study good agreement was found between the CFD predictions and observations using advanced image visualisation techniques.

CFD can offer a number of advantages to a design process:

(a) reduced number of prototypes and design cycles

(b) simulation of flow conditions that are difficult to study experimentally

(c) provision of comprehensive data throughout the flow domain with respect to gas only, gas-solid and gas-solid-liquid interactions.

CFD software codes are structured in order to process the numerical algorithms that describe fluid flow. The codes are used to solve the partial-differential equations for conservation of mass, momentum, energy and species concentration. A CFD code generally contains three elements: a *pre-processor*, a *solver* and a *post-processor*.

The *pre-processor* allows input of the various parameters involved within the flow system under investigation. The first input requirements are a definition of the region of interest (or computational domain) and its sub-division into a mesh (or grid) of non-overlapping cells. The physical and chemical phenomena (e.g. velocity) that are to be modelled are then selected and the physical properties of the fluid system defined (e.g. density, viscosity). The final requirement is to establish the specification for the boundary conditions at cells that coincide with or touch the domain boundary (e.g. solid surface, porous surface).

Each cell within a CFD model contains a cell-centred node at which the solutions of given flow parameters are calculated. The accuracy of a CFD model depends on the number of cells in the mesh, i.e. the fineness of the mesh. Meshes are often non-uniform in cell size such that areas of large variations in fluid activity are subject to grid refinement.

The *solver* uses various numerical solution techniques to express the mathematical models (e.g. turbulence models) or equations (e.g. Navier-Stokes equation) used to describe the flow processes. One of these techniques is termed the finite volume method, which is the process used to perform the modelling in this study. This method considers each cell as a finite volume and solves the governing equations of conservation for each cell using iterative processes.

A *post-processor* is used to present and manipulate the solved data. Some of the data visualisation tools that have been employed in this study include domain geometry, grid display, vector plots and particle tracking.

The simplest CFD models are constructed in two dimensions, however the emergence of powerful microprocessors has allowed CFD to provide three-dimensional analysis of fluid flow problems, which are more useful for the application described in this thesis. It is possible to construct CFD models that predict gas flows only (single-phase), gas flows containing solid particles (two-phase) and gas flows containing solid and liquid elements (three-phase models).

4.5.2 The computational model

A comprehensive description of the CFD model, including the governing equations used, is outside the scope of this thesis, but can be found in related publications (MacGregor *et al.*, 1999); a summary is provided below.

Single-phase models were initially constructed, which provided predictive information pertaining to the fluid (i.e. air only) flows within the domain. These were then developed into more complicated two-phase models in order to predict the movement of powder particles within the processor under different operating conditions. The construction of three-phase models was considered to be outside the scope of the current work but the model was constructed such that it could be readily expanded into three phase models if this became desirable in future work in order to model the effects of the addition of liquids (e.g. granulating fluids) to the processor.

In their introductory text to CFD, Versteeg and Malalasekera (1995) state that '...the results generated by a CFD code are at best as good as the physics (and chemistry) embedded in it and at worst as good as its operator'. Although CFD has been used widely in industries such as aerospace, its use in pharmaceutical equipment design had met with limited success to date. This may be attributable more to a lack of the specialist knowledge and skills required to operate the technique in this sector than to a limitation of the technique itself. For this reason an understanding of the technique and verification of its use in modelling the operation of a powder processor design through comparison with practical observations was undertaken.

An investigation was undertaken to utilise information that had been gathered in the initial phase of the current work. The FBSVP-B was used as a starting point for the application and for verification of CFD simulation.

The computational model was set up using Star-CD-v3000 (Computational Dynamics Limited, London, UK), which is a finite volume based commercial CFD package.

The following simplifications were assumed for the computational model of the SVP in order to make most efficient use of the processing capabilities available:

(a) The vessel outlet was constructed in the model as a simple circular opening of 45mm diameter rather than attempting to model a cyclone system or bag filter.

(b) The mesh base was characterised using a baffle feature incorporated in the CFD software, which represented the mesh as a porous material across which there would be a pressure drop as fluid flowed through.

(c) The high-pressure air nozzles were cylindrical, which made them difficult to model and therefore rectangular bodies were used to approximate nozzles with roughly the same cross-sectional area.

Since the main vessel was essentially axisymmetrical, only one twelfth of the cylinder was generated in the computational grid (see figure 4.7). The most complex parts of the model were at the base, where the tangential nozzles and mesh were located. The computational grid was made finer in these areas to facilitate the geometry generation and computing convergence. A local refinement to the grid was made at the top of the vessel in order to address some convergence problems that were encountered in this area.

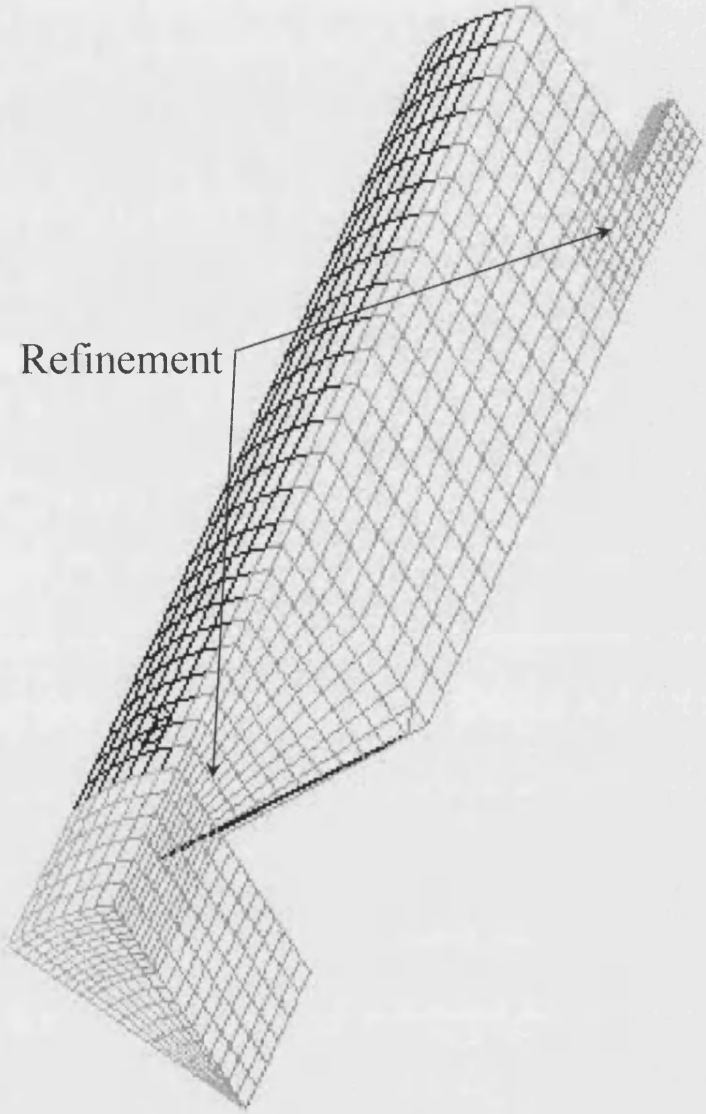

Figure 4.7. CFD computational mesh for of FBSVP-B.

Models with 2600, 4000 and 8000 cells were tested and the model with 4000 cells chosen as the final computational model since it represented a compromise between computing time and convergence.

Single-phase models were constructed in which only the flow of air was investigated. The flow of a mixture of air and solid powder (i.e. two-phase model) was also modelled. The air was programmed as a continuous phase and the powder particles as a disperse phase. The modelling strategy was based on the Lagrangian/Eulerian kind, in which the fluid governing equations for the air phase were solved in the Eulerian co-ordinate system and the particle phase was modelled in Lagrangian co-ordinate systems that move with individual particles.

4.5.3 CFD model verification

A single phase CFD simulation was constructed as described above to predict the air velocities that would develop at different heights in the FBSVP-B when operated at a nozzle outlet velocity of $3msec^{-1}$ and a fluidising air velocity of $0.3msec^{-1}$.

The velocity magnitudes and fluid flow directions predicted from this simulation are shown in figure 4.8 below. Figure 4.9 shows the height position that is represented by each of the four models given in figure 4.8.

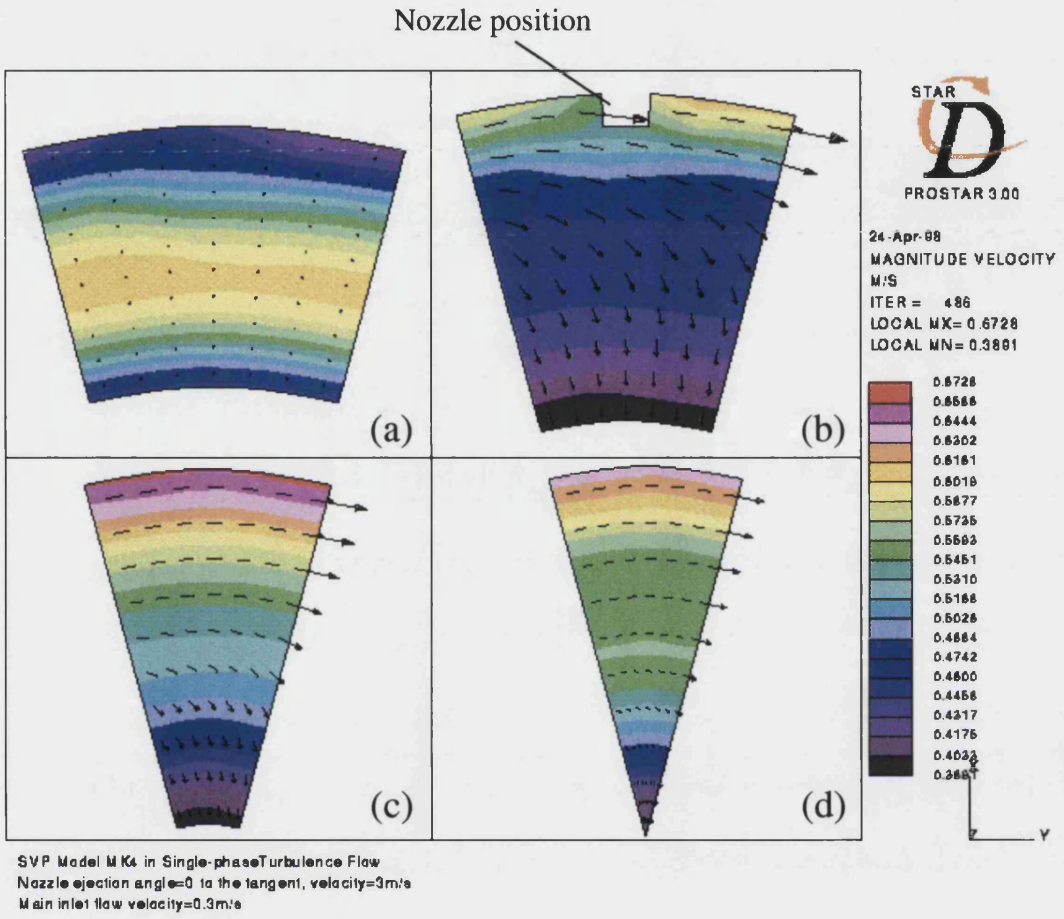

Figure 4.7. Example of CFD model of FBSVP-B simulating for single phase flows. Model shows $^{1}/_{12}$ cross-sections of vessel in the plan view at different heights corresponding to locations (a), (b), (c) and (d) as shown in figure 4.8.

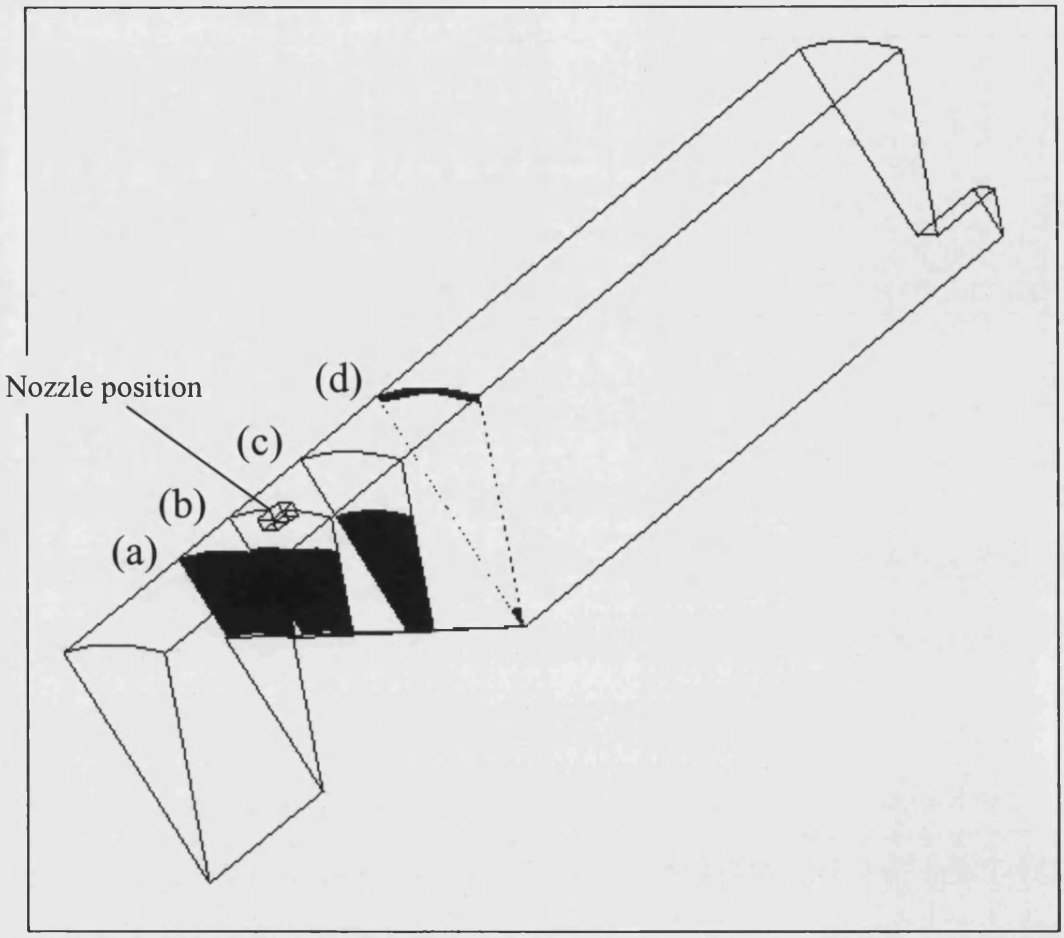

Figure 4.8. Cross-sectional heights corresponding to single phase flow regimes shown in CFD model of FBSVP-B shown in figure 4.7.

These predictions compared well with the powder movement observed during operation of the FBSVP-B. It was found that the fluid flows developed during FBSVP-B operation caused collection of powder residue in areas of low velocity after processing lactose in the vessel.

A photograph of a typical deposition pattern of lactose powder after a period of vessel operation is shown in figure 4.9 below.

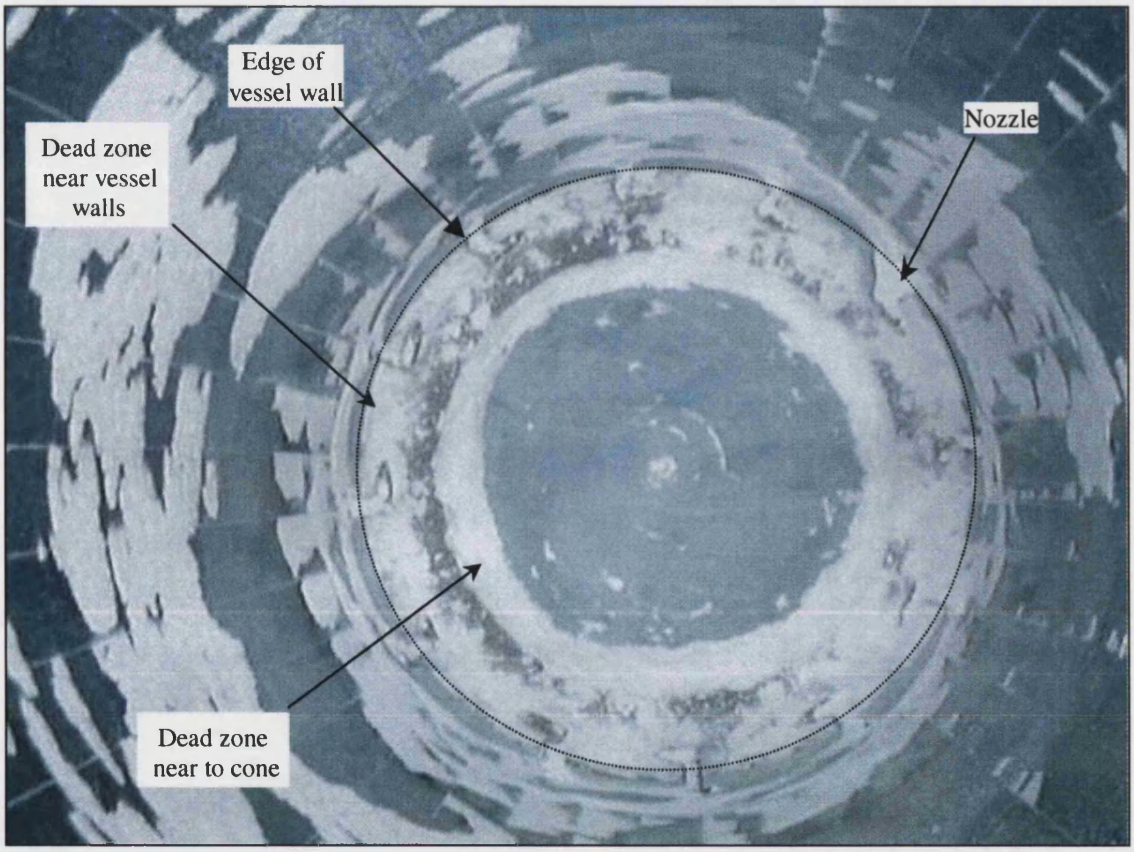

Figure 4.9. Photograph of typical pattern of powder deposition following processing of lactose granules in FBSVP-B.

The deposition pattern showed that dead zones had developed near to the base of the vessel wall, near to the base of the cone and directly behind the nozzle outlets. A comparison of figure 4.7 with figure 4.9 indicates that the observed dead zones apparent in figure 4.9 coincided with the zones of lowest velocity predicted by the CFD simulation in figure 4.7 (a) and (b).

The photograph presented in figure 4.10 shows the flow of lactose powder during operation of FBSVP-B under typical conditions (see section 5.1.2). Powder was found to rotate as a cloud mass and areas of low and high powder density were found to form transiently; in the figure below a low density area of the mass is clearly identifiable.

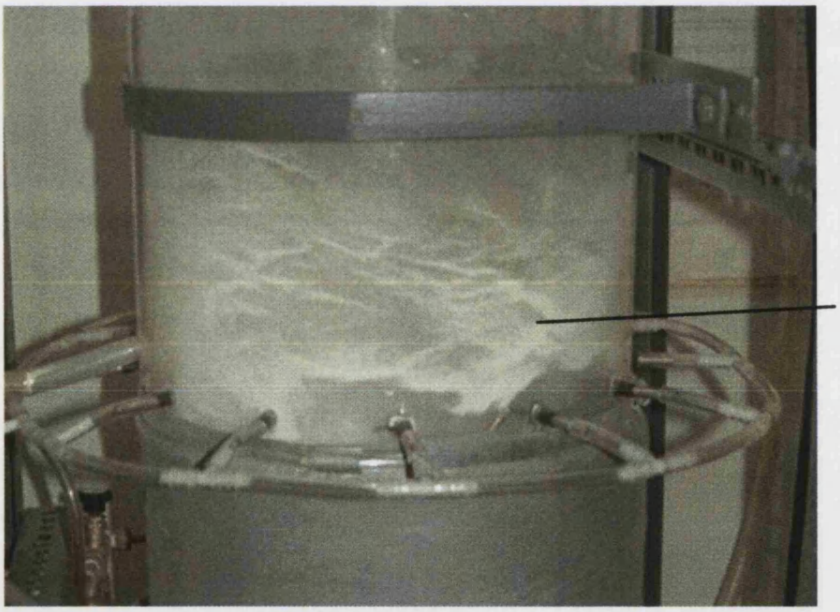

Figure 4.10. Photograph of flow patterns of lactose powder generated during operation of FBSVP-B.

If it had been possible to show the overhead view of the vessel contents it would have been demonstrable that there was a significant flow field close to the vessel wall in the region between the nozzle array and the middle of the vessel height, in the area indicated by the label 'CAGL plumes' on figure 4.10. Referral to segments (c) and (d) of figure 4.7 indicated that the CFD simulation predicted similar flow fields in these areas.

4.5.4 Conclusion

The apparent agreement of the simulations with observed fluid flows in FBSVP-B gave verification of the ability of the CFD model to predict fluid flows in this application.

5. FLUID BED SVP MODEL B CHARACTERISATION

5.1 Particle size reduction

5.1.1 FBSVP-B set up

Any powder residue was cleared from the inside surfaces of the vessel using a combination of dry wiping and vacuum extraction until visibly clean. The filter bag was washed in warm water until visibly clean, rinsed with deionised water and dried in an oven. It was allowed to cool before re-attachment to the filter assembly.

The vessel was assembled and the clips attaching the fluidising plenum and the filter assembly to the main vessel secured. The fluidising fan was set at maximum output and the nozzle pressure set to the appropriate value using the needle valves and making reference to the pressure gauges. The system was manually inspected for leaks before being loaded with test material.

5.1.2 Experimental conditions

The test material in all particle size reduction experiments was Prismalac 40® lactose (see Section 2.1.2), which was loaded in 500g quantities into the processor and spread

over the mesh base using a spatula to give an approximately constant bed height across the base.

Ambient environmental temperature and relative humidity conditions were monitored during all testing and recorded, but not controlled.

The flow fields arising during processing were visually monitored and any dead spots or other unusual occurrences recorded.

The efficiency of the FBSVP-B for particle size reduction of the test material was investigated for the following processing parameters:

Nozzle ring pressure (kPa)	Nozzle air velocity ($msec^{-1}$)	Fluidising air flow rate (m^3sec^{-1})
70	78	0.02
140	107	0.02
210	138	0.02

Table 5.1. FBSVP-B processing parameters for particle size reduction testing.

Three batches of test material were processed at each nozzle pressure setting and processing halted to allow samples to be taken for particle size analysis at the following processing times:

0, 30, 60, 120, 180, 240, 300, 450, 600, 900, 1200, 1500 and 1800 seconds

Sampling necessitated removal of the filter bag assembly (see section 5.1.3 below). After each set of samples had been taken from the processor, the filter assembly was replaced and shaken to allow adhered material to fall back into the bulk powder bed. The walls of the processor were then knocked with a rubber mallet to allow material adhering to the internal surfaces of the processor to return to the powder bed.

5.1.3 Sampling

Four samples of approximately 1.5g were removed from prescribed positions (see figure 5.1) in the powder bed at each time point using a sample thief, the design of which is described below. The four samples from each time point were pooled into a 25ml screw-top glass vial and analysed in triplicate for particle size distribution as described in section 2.3.3.

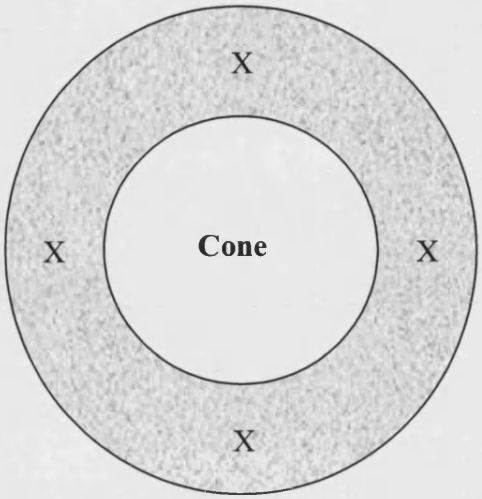

Plan View

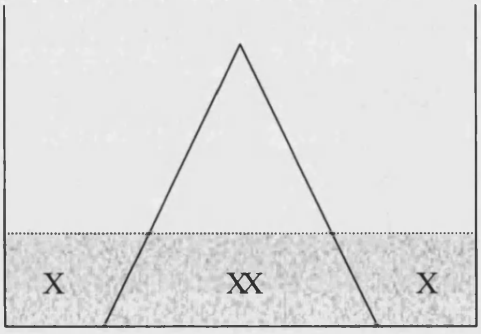

Side View

X = Sampling position

Figure 5.1. Schematic representation of sampling positions used for particle size analysis of lactose granules during particle size reduction testing.

A sample thief was designed with a flat bottom since the powder bed being sampled was too shallow to allow for the tapered end normally associated with commercially available sample thief designs.

The sample thief comprised a hollow, cylindrical, aluminium outer sheath of internal diameter 15mm and a cylindrical, stainless steel inner core of external diameter 14mm. A circular hole of 10mm diameter was made in the inner core with its centre 15mm from the base of the cylinder. The outer sheath was placed over the inner core and a hole of 10mm diameter was cut into the sheath. This hole was at such a height that when the sheath was turned to the 'open' position it coincided with the hole in the inner core so enabling a sample to be collected in the thief. The sheath was returned to the 'closed' position to retain a sample in the thief. A retaining bolt connected the sheath to the inner core and allowed movement of the sheath to the 'open' or 'shut' position.

This arrangement allowed collection of samples of approximately $3cm^3$, corresponding to sample weights of approximately 1.5g.

5.1.4 Results

Expt. No.	Run 1	Run 2	Run 3	Mean	SD
Milling time (seconds)	Mass median particle diameter (μm)				
0	468	454	458	460	7.1
30	243	296	234	258	34.0
60	243	234	239	239	4.7
120	196	194	193	194	1.4
180	181	196	196	191	8.5
240	188	168	180	179	10.0
300	173	156	173	167	9.9
450	168	162	173	168	5.6
600	172	156	167	165	8.0
900	160	144	164	156	10.3
1200	155	138	129	141	13.6
1500	149	141	155	148	6.8
1800	173	126	155	151	23.7

Table 5.2. Mass median particle diameters obtained at different times during milling period of 30 minutes in FBSVP-B at nozzle pressure of 140 kPa.

5.1.5 Discussion

The following changes were effected in the design of FBSVP-B in order to overcome shortcomings identified during the operation of FBSVP-A:

(a) Replacement of the cyclone separator with a filter bag

This change was initiated in order firstly to reduce the backpressure within the vessel brought about by the high flow resistance characteristics of the cyclone separator system and secondly to reduce the quantity of fines lost from the vessel due to the inefficiency of the cyclone system.

The high backpressure encountered in the FBSVP-A caused increased loss of fines due to leakage and reduced fluidisation within the powder bed.

In addition the filter was expected to provide improved arrestment of fine particles which could then be returned to the powder bed rather than lost from the vessel.

(b) Lowering of the high pressure air nozzle ring assembly

This modification was expected to improve powder movement at the vessel base so leading to a greater proportion of the powder being introduced to the zones of high activity located close to the outlets of the high pressure air nozzles.

In addition, it was expected that any effects of milling through collision of particles with the vessel base would be increased.

(c) Application of antistatic tape to the vessel walls

It was expected that the use of antistatic tape would reduce the quantity of powder adhering to the wall surfaces so improving visual acuity and allowing more powder to remain in circulation within the powder bed.

In summary, if the above changes were effective then it would have been expected to observe the following functional benefits:

(i) Reduced loss of fines

(ii) Improved fluidised bed movement

(iii) Improved visual acuity

(iv) Improved overall milling efficiency

A comparison of the particle size reduction observed in FBSVP-B compared to that obtained in FBSVP-A is shown in table 5.3 and graph 5.1.

Milling time (seconds)	FBSVP-A Mean Mass Median Particle Diameter (μm)	FBSVP-B Mean Mass Median Particle Diameter (μm)	Difference (μm)
0	459	460	N/A
30	Not done	258	N/A
60	345	239	-106
120	358	194	-164
180	287	191	-96
240	261	179	-82
300	281	167	-114
450	211	168	-43
600	233	165	-68
900	196	156	-40
1200	194	141	-53
1500	174	148	-26
1800	167	151	-16

Table 5.3. Comparison of mean mass median particle diameters measured at different processing times during milling of CAGL in FBSVP-A and FBSVP-B.

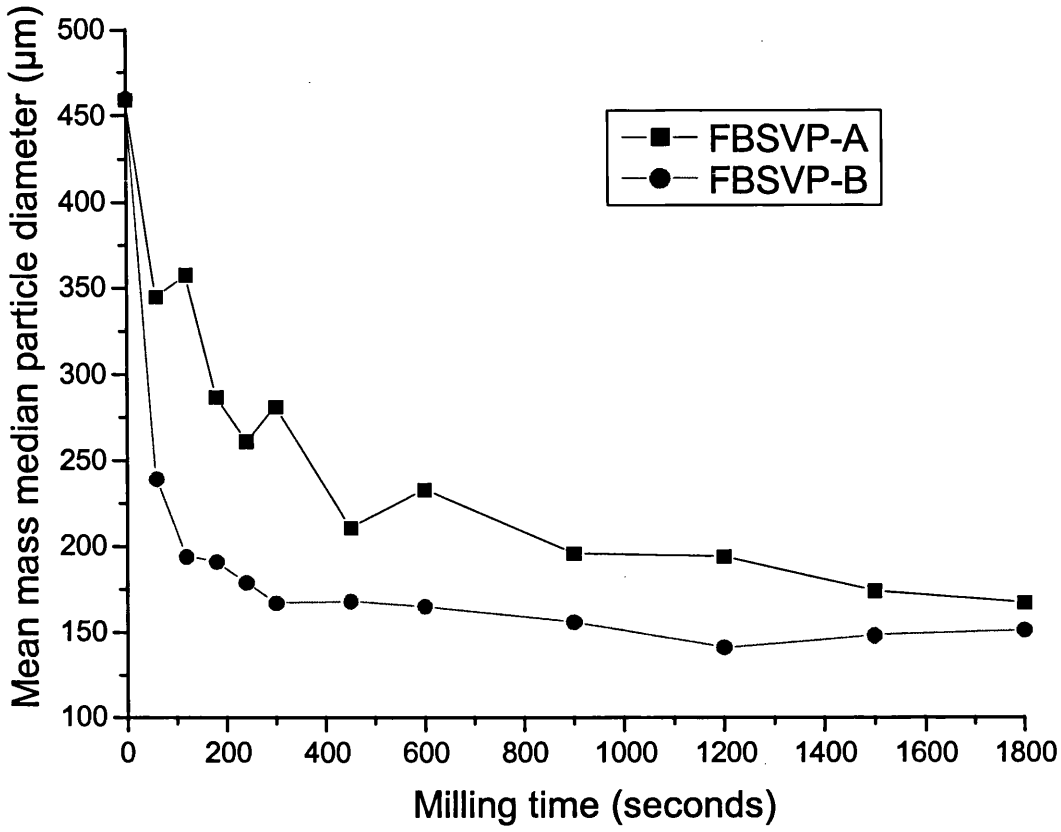

Graph 5.1. Graph showing comparison of mean mass median particle diameters measured at different processing times during milling of CAGL in FBSVP-A and FBSVP-B.

It can be seen from these data that:

(a) In the FBSVP-A, particle size was reduced to 75% of its original size within 60 seconds and to 57% of its original size within 240 seconds

(b) In the FBSVP-B, particle size was reduced to 56% of its original size within 30 seconds and to 52% of its original size within 60 seconds.

(c) Most of the particle size reduction is occurring within the early stages of milling in both vessels. A plateau in size reduction is reached where size reduction has progressed to 90% of its final level after 900 seconds in FBSVP-A and at between 240 and 300 seconds in FBSVP-B.

(d) The maximum particle size reduction achieved in the FBSVP-A was a reduction in median particle diameter to 167μm compared to 141μm in the FBSVP-B.

In addition the following observations were made:

(e) A decrease in the amount of fine material leaving the vessel was observed. Fine material was found to have collected in the filter bag which was easily returned to the vessel by shaking.

(f) Considerably less material was observed to escape due to leakage into the atmosphere surrounding the vessel.

(g) Fluidisation of the powder bed was increased leading to an improvement in powder movement around the base area. However, some dead zones were observed in the locations predicted by CFD simulations (see section 4.5.3).

Consideration of the above information set against the expected benefits is discussed below:

(i) Reduced loss of fines

Visual observation of a reduction in the loss of fines was further supported by a reduction in the median particle diameter recorded at each mixing interval when operating the FBSVP-B compared to FBSVP-A under identical processing conditions.

(ii) Improved powder bed movement

Overall bed movement would appear to have improved significantly on the basis that the time to reach steady state is reduced from a nominal 900 seconds in FBSVP-A to around 300 seconds in FBSVP-B.

In addition the median particle size has decreased indicating some beneficial changes in the overall size reduction capability of the vessel possibly as a result of an increase of the residence time of material in the highly energetic regions close to the nozzle outlets.

However, further improvements in bed movement are needed to eliminate all areas of the vessel displaying low or nil powder movement (dead areas).

(iii) Improved visual acuity

The expected benefits afforded by the application of antistatic tape were achieved as illustrated in figure 4.4.

(iv) Improved overall mixing efficiency

The data would indicate that particle size reduction was more rapid and progressed to a greater extent in the FBSVP-B compared to the FBSVP-A. This is thought to be as a result of increasing the milling efficiency by moving the nozzles closer to the vessel base and by reducing the loss of fine material from the processor.

However, in both vessel designs the overall particle size reduction mechanism may be attributed mainly to deaggregation of agglomerates rather than to milling of the primary crystals (see section 3.3.2.4). For useful application in particle size reduction of excipient ingredients of DPI formulations greater milling efficiency may be required.

5.1.6 Conclusions

The new design of vessel provided the following improvements:

(a) Reduced loss of fines

(b) Improved arrestment of fines

(c) Improved powder bed movement

(d) Enhanced visual acuity

However, the milling performance of the FBSVP-B was unsatisfactory since the particle size reduction was not seen to proceed much beyond the deaggregation of the basic granular material.

Additionally, areas of low powder movement were present in the vessel despite the design modifications made.

These problems are addressed in section 6.

5.2 Blend content uniformity of a dry powder inhaler formulation processed in FBSVP-B

5.2.1 Experimental conditions

The FBSVP-B was set up as described in section 5.1.1. The nozzle air pressure was set at 70 kPa in order to minimise any particle size reduction effects; the fluidising air was set at 0.2 $msec^{-1}$. SorboLac 400 lactose (60g) was introduced into the vessel and the powder bed levelled. Nedocromil sodium trihydrate (40g) was placed evenly on top of the lactose and the layer levelled off across the base.

Five batches of the nedocromil formulation were manufactured using identical processing conditions. Processing was interrupted after the following mixing times:

30, 60, 120, 300, 600 and 1200 seconds

Samples were removed from the powder bed at each mixing time as described in section 5.2.2 below after allowing time for fine powders to settle and removal of the filter assembly.

After removing each set of samples, the filter assembly was shaken and the vessel walls knocked with a rubber mallet to allow adhered material to be returned to the bulk powder bed.

5.2.2 Sampling

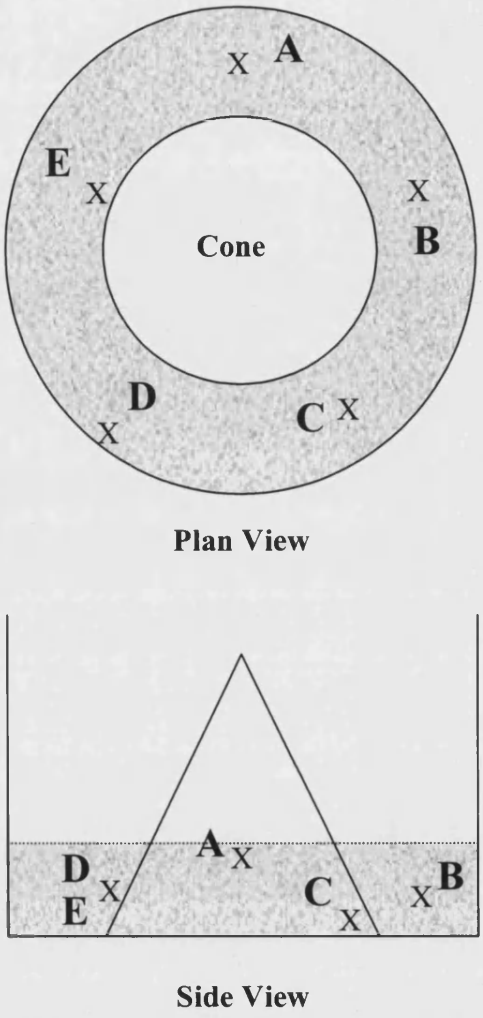

Figure 5.2. Schematic representation of sampling positions for *in-vitro* aerosol characterisation and content uniformity testing of nedocromil sodium trihydrate blends processed in FBSVP-B.

At each sampling time, five samples (A, B, C, D and E) of approximately 1g were removed using a sampling spoon from prescribed positions in the powder bed as shown in figure 5.3. Samples were collected and placed into 25ml screw top glass vials that were hermetically sealed and labelled appropriately.

Samples A, B and C were taken from positions approximately equidistant from the vessel wall and central cone. Sample A was taken from the top, sample B from the middle and sample C from the bottom of the powder bed. Samples D and E were taken from the middle of the powder bed with sample D taken from a position close to the vessel wall and sample E taken from close to the wall of the cone. These latter samples (D and E) were deliberately selected from areas in the processor that were predicted by the CFD work to exhibit least disturbance from the airflows during processing (see section 4.7).

The vials containing the samples were placed into a controlled humidity environment within 30 minutes of processing as described in section 2.2.3.

Two sub-samples of 20 ± 0.5mg were removed from each of samples A to E and tested for content assay as described in section 2.6. The remainder of each sample was reserved for *in-vitro* aerosol characterisation (see section 5.3).

5.2.3 Results

Results from the five mixing experiments are shown in tables 5.2 to 5.6 below and a summary of the %RSD calculated from all five experiments is provided in tables 5.7 and 5.8.

Sample position	Processing time (seconds)					
	30	60	120	300	600	1200
	Nedocromil sodium trihydrate content (%w/w)					
A1	40.9	43.5	36.6	40.6	37.9	37.8
A2	39.2	38.3	36.7	38.7	37.4	39.4
B1	43.9	36.1	39.1	38.0	38.9	38.8
B2	64.9	40.0	36.0	37.1	38.1	39.0
C1	33.4	40.3	38.9	36.8	40.4	38.8
C2	25.2	40.8	40.1	39.0	40.8	37.7
D1	41.7	39.3	40.2	49.7	41.9	39.1
D2	42.2	40.5	40.2	51.5	40.6	39.6
E1	12.8	20.9	25.6	33.0	34.8	39.0
E2	15.7	12.0	25.6	31.9	30.9	30.3
Mean (A-E)	36.0	35.2	35.9	39.6	38.2	38.0
RSD (A-E)	42.2	29.1	15.8	16.1	8.6	7.2
Mean (A-C)	41.3	39.8	37.9	38.4	38.9	38.6
RSD (A-C)	32.3	6.2	4.4	3.7	3.6	1.7

Table 5.2. Content uniformity data from processing nedocromil sodium trihydrate formulation in FBSVP-B, experiment #1

Sample position	Processing time (seconds)					
	30	60	120	300	600	1200
	Nedocromil sodium trihydrate content (%w/w)					
A1	49.0	46.8	43.7	36.4	36.9	36.2
A2	42.5	47.5	41.2	37.9	39.8	35.8
B1	50.1	44.7	42.7	38.9	37.6	36.7
B2	54.2	43.7	45.0	38.7	37.6	36.9
C1	34.7	34.9	42.5	39.1	35.5	37.2
C2	27.3	33.2	43.8	38.6	36.3	36.9
D1	46.3	43.6	40.9	37.1	36.9	36.3
D2	47.6	44.3	39.8	40.8	37.2	35.7
E1	19.3	19.9	28.9	36.6	39.3	36.7
E2	20.9	34.0	29.4	34.0	38.0	37.1
Mean (A-E)	39.2	39.3	39.8	37.8	37.5	36.6
RSD (A-E)	32.5	22.0	14.6	5.0	3.5	1.5
Mean (A-C)	43.0	41.8	43.2	38.2	37.3	36.6
RSD (A-C)	23.9	14.8	3.0	2.6	3.9	1.5

Table 5.3. Content uniformity data from processing nedocromil sodium trihydrate formulation in FBSVP-B, experiment #2

Sample position	Processing time (seconds)					
	30	60	120	300	600	1200
	Nedocromil sodium trihydrate content (%w/w)					
A1	47.1	48.4	43.2	41.6	41.3	41.8
A2	44.4	44.6	43.2	40.6	40.4	42.3
B1	29.3	40.6	46.3	41.4	40.8	40.9
B2	36.0	41.2	44.8	41.3	42.4	39.3
C1	47.8	44.5	42.5	43.1	40.5	43.0
C2	49.9	42.9	43.6	42.7	40.0	40.2
D1	48.1	44.1	43.2	42.2	39.4	38.1
D2	49.8	45.7	42.8	42.9	38.5	40.9
E1	6.1	5.2	34.4	13.9	26.2	34.1
E2	9.6	30.9	38.4	23.9	17.7	31.7
Mean (A-E)	36.8	38.8	42.2	37.4	36.7	39.2
RSD (A-E)	45.2	32.7	8.1	26.9	22.0	9.4
Mean (A-C)	42.4	43.7	43.9	41.8	40.9	41.3
RSD (A-C)	19.0	6.5	3.1	2.3	2.1	3.3

Table 5.4. Content uniformity data from processing nedocromil sodium trihydrate formulation in FBSVP-B, experiment #3

Sample position	Processing time (seconds)					
	30	60	120	300	600	1200
	Nedocromil sodium trihydrate content (%w/w)					
A1	44.8	44.8	43.1	40.8	43.8	39.0
A2	45.3	44.8	43.6	41.1	39.5	39.6
B1	46.7	42.3	42.6	39.5	39.0	35.8
B2	40.3	40.9	42.5	40.1	40.2	35.5
C1	27.5	41.7	43.5	44.1	41.6	36.7
C2	27.5	43.5	44.2	44.0	42.4	35.7
D1	42.3	39.0	39.2	44.2	39.0	36.0
D2	42.4	40.0	37.2	40.6	41.3	34.7
E1	48.8	47.0	46.8	43.9	40.6	38.3
E2	47.1	46.5	45.0	45.3	42.2	38.5
Mean (A-E)	41.3	43.1	42.8	42.4	41.0	37.0
RSD (A-E)	18.6	6.3	6.5	5.0	3.9	4.7
Mean (A-C)	38.7	43.0	43.2	41.6	41.1	37.1
RSD (A-C)	23.0	3.8	1.5	4.7	4.5	4.9

Table 5.5. Content uniformity data from processing nedocromil sodium trihydrate formulation in FBSVP-B, experiment #4

Sample position	Processing time (seconds)					
	30	60	120	300	600	1200
	Nedocromil sodium trihydrate content (%w/w)					
A1	43.4	42.6	41.1	37.6	38.1	38.8
A2	44.0	43.9	42.6	36.9	37.2	36.3
B1	24.5	37.8	40.9	40.9	38.5	38.0
B2	32.4	32.8	41.8	40.2	37.2	36.8
C1	47.9	46.5	41.9	39.0	38.6	38.0
C2	46.7	45.2	42.4	38.5	38.5	38.0
D1	43.1	40.4	44.6	40.9	36.4	43.7
D2	44.1	40.0	41.7	40.4	37.5	39.2
E1	49.4	27.5	42.4	18.4	40.9	37.8
E2	50.1	30.3	45.8	22.4	41.4	38.9
Mean (A-E)	42.6	38.7	42.5	35.5	38.5	38.6
RSD (A-E)	18.9	16.8	3.6	22.9	4.1	5.3
Mean (A-C)	39.8	41.5	41.8	38.8	38.0	37.6
RSD (A-C)	23.4	12.6	1.6	4.0	1.7	2.4

Table 5.6. Content uniformity data from processing nedocromil sodium trihydrate formulation in FBSVP-B, experiment #5

Experiment number	Processing time (seconds)					
	30	60	120	300	600	1200
	% Relative standard deviation (n=10)					
#1	42.2	29.1	15.8	16.1	8.6	7.2
#2	32.5	22.0	14.6	5.0	3.5	1.5
#3	45.2	32.7	8.1	26.9	22.0	9.4
#4	18.6	6.3	6.5	5.0	3.9	4.7
#5	18.9	16.8	3.6	22.9	4.1	5.3

Table 5.7. Summary of percent relative standard deviation of content uniformity samples taken from positions A, B, C, D and E at different processing times during blending of nedocromil sodium trihydrate formulation in FBSVP-B.

Experiment number	Processing time (seconds)					
	30	60	120	300	600	1200
	% Relative standard deviation					
#1	32.3	6.2	4.4	3.7	3.6	1.7
#2	23.9	14.8	3.0	2.6	3.9	1.5
#3	19.0	6.5	3.1	2.3	2.1	3.3
#4	23.0	3.8	1.5	4.7	4.5	4.9
#5	23.4	12.6	1.6	4.0	1.7	2.4

Table 5.8. Summary of percent relative standard deviation of content uniformity samples taken from positions A, B and C only at different processing times during blending of nedocromil sodium trihydrate formulation in FBSVP-B.

5.2.4 Discussion

The mean drug content was in the range 35 - 45%$^{w}/_{w}$, close to the nominal drug content of 40%$^{w}/_{w}$, at each time point in all experiments. Furthermore the mean drug content was not found to change significantly during the processing period. Since the drug particles were approximately one third the size of the lactose, the results suggest that there was no significant preferential loss of fines from the vessel over time, as had been experienced in previous SVP designs (see section 3.3.3.4).

Overall blend uniformity, indicated by %RSD, was generally reasonable but poor in those areas of the vessel that had been predicted to have poor flow characteristics using CFD simulations (see section 4.5.3). If the data from those samples taken from areas of predicted poor flow were discounted, the calculated %RSD was found to be <5% after 2 minutes mixing in all cases, thus falling marginally within commercially acceptable levels.

There was no evidence of demixing occurring as mixing times were extended up to a period of 20 minutes, indicating a robust mixing process that would lend itself well to commercial validation

5.2.5 Conclusions

The homogeneity of the nedocromil sodium formulation processed in the FBSVP-B was found to attain acceptable levels in samples taken from areas where high air flows were predicted in the CFD simulation of the FBSVP-B and poor in samples taken

from areas of predicted low flow. This gave confidence that the CFD simulations gave valid predictions that could be applied to future vessel designs.

A mixing time of approximately 2 minutes was sufficient to achieve homogeneity in areas of good powder movement and an extension of this time to periods of up to 20 minutes did not adversely affect the mixing quality.

Redesign of the vessel should be undertaken in order to address the problem of poor distribution of air flows throughout the vessel.

5.3 Functionality of a dry powder inhaler formulation processed in FBSVP-B

5.3.1 Experimental conditions and sampling

The samples collected at each time point during blend content uniformity tests (section 5.2) were also characterised for their functionality in terms of delivery of potentially respirable fine particle doses from the samples when loaded into a proprietary DPI device. Two sub-samples of 20 ± 0.5mg from each of the vials containing the samples taken from positions A, B and C were filled into size 3 gelatin capsules. These locations were selected (in preference to locations D or E) since they were expected to be more representative of the bulk properties of the powder blend within the free-moving parts of the powder bed. The capsules were treated as described in section 2.5.

5.3.2 Results

Results from *in-vitro* aerosol impingement testing of the above samples are presented in tables 5.9 to 5.13. A summary table of the %FPF values obtained throughout these experiments is given in table 5.14. Overall mean results are presented in graph 5.2.

Sample number	Processing time (seconds)																	
	30						60						120					
	C+D	S 1	S 2	Rec	DD	FPF	C+D	S 1	S 2	Rec	DD	FPF	C+D	S 1	S 2	Rec	DD	FPF
A1	0.7	3.4	1.9	73.3	5.2	35.7	2.1	3.4	2.5	99.5	5.8	42.2	1.8	3.0	2.7	92.1	5.6	47.2
A2	1.4	3.2	1.7	79.0	4.9	35.2	2.8	3.6	2.6	111.5	6.1	41.8	1.6	3.2	2.7	92.8	5.9	45.7
B1	2.8	3.7	2.6	113.9	6.4	41.5	2.0	2.9	2.6	93.5	5.5	46.6	1.6	3.4	2.7	96.7	6.1	44.7
B2	2.9	3.9	2.4	115.1	6.3	38.1	2.7	3.4	2.6	107.3	5.9	43.1	1.8	2.8	2.8	91.8	5.5	50.1
C1	2.1	3.7	1.6	91.8	5.3	30.3	2.2	3.0	2.6	97.6	5.6	46.0	1.6	3.2	2.7	93.0	5.9	45.8
C2	1.3	3.6	1.5	79.4	5.1	29.5	2.2	3.1	2.6	97.8	5.7	45.3	1.7	2.9	2.8	91.6	5.6	49.0
Mean	1.9	3.6	1.9	92.1	5.5	35.1	2.3	3.2	2.5	101.2	5.8	44.2	1.7	3.1	2.7	93.0	5.8	47.1
SD	0.9	0.3	0.5	18.4	0.6	4.6	0.3	0.2	0.0	6.8	0.2	2.1	0.1	0.2	0.1	1.9	0.2	2.1
RSD	47.7	7.4	23.6	19.9	11.6	13.0	14.2	7.5	1.7	6.7	3.9	4.7	6.1	7.5	1.9	2.0	3.7	4.4

Sample number	Processing time (seconds)																	
	300						600						1200					
	C+D	S 1	S 2	Rec	DD	FPF	C+D	S 1	S 2	Rec	DD	FPF	C+D	S 1	S 2	Rec	DD	FPF
A1	1.5	3.7	2.3	93.0	5.9	38.1	1.7	3.1	2.5	91.2	5.6	44.4	1.4	4.0	2.1	93.7	6.1	34.8
A2	1.9	3.2	2.4	95.0	5.7	42.8	1.3	3.2	2.3	85.4	5.5	41.7	1.4	3.8	2.3	94.3	6.1	37.6
B1	2.6	2.1	2.2	85.6	4.3	50.7	1.4	3.7	2.2	91.2	5.9	37.1	1.5	4.0	2.1	94.0	6.1	34.4
B2	2.3	2.4	2.5	89.1	4.9	51.2	2.3	3.4	2.2	97.4	5.5	39.0	1.8	3.6	1.9	91.2	5.5	34.8
C1	1.5	3.2	2.2	85.1	5.4	41.1	1.5	4.0	2.0	92.6	5.9	33.0	1.5	4.0	2.0	93.1	5.9	33.3
C2	1.7	2.8	2.4	86.1	5.2	45.7	1.9	3.5	2.1	94.9	5.7	37.6	1.7	3.7	2.1	93.0	5.8	36.6
Mean	1.9	2.9	2.3	89.0	5.2	44.9	1.7	3.5	2.2	92.1	5.7	38.8	1.5	3.8	2.1	93.2	5.9	35.2
SD	0.5	0.6	0.1	4.2	0.6	5.3	0.4	0.3	0.2	4.1	0.2	3.9	0.2	0.2	0.1	1.1	0.2	1.6
RSD	23.7	20.1	5.9	4.7	11.4	11.7	21.0	9.3	7.9	4.4	3.2	10.2	10.3	4.5	6.5	1.2	4.1	4.5

Key	
C+D	Dose recovered in capsule and device
S 1	Dose recovered in stage 1
S 2	Dose recovered in stage 2
Rec	Percent total recovery / nominal recovery
DD	Delivered dose (stage 1 + stage 2)
FPF	Fine particle fraction
SD	Standard deviation
RSD	Relative standard deviation

Table 5.9. *In-vitro* functionality data from TSI testing of samples obtained during processing of nedocromil sodium trihydrate formulation in FBSVP-B, experiment #1.

Sample number	Processing time (seconds)																	
	30						60						120					
	C+D	S 1	S 2	Rec	DD	FPF	C+D	S 1	S 2	Rec	DD	FPF	C+D	S 1	S 2	Rec	DD	FPF
A1	2.1	3.9	2.0	100.0	6.0	34.3	2.5	4.1	2.6	114.8	6.7	39.0	2.1	3.5	2.6	103.3	6.2	42.6
A2	2.8	4.2	2.4	116.8	6.6	35.9	2.0	3.9	2.9	110.4	6.8	42.1	3.9	2.3	2.0	103.2	4.4	46.4
B1	2.7	5.0	2.1	122.7	7.1	29.4	2.6	3.7	2.9	113.6	6.5	44.0	3.0	2.9	2.5	104.6	5.4	45.7
B2	3.5	4.2	2.0	122.2	6.3	32.6	1.3	3.4	2.9	94.6	6.3	45.3	2.2	2.8	2.4	92.0	5.2	45.7
C1	0.9	2.3	1.3	55.1	3.5	35.5	1.8	2.9	2.3	86.4	5.2	44.3	3.2	2.5	2.6	103.2	5.1	50.8
C2	1.4	3.7	1.9	87.7	5.6	33.7	1.1	2.2	1.9	65.0	4.1	46.8	2.3	3.5	2.6	105.4	6.1	43.3
Mean	2.2	3.9	1.9	100.7	5.8	33.6	1.9	3.4	2.6	97.5	5.9	43.6	2.8	2.9	2.4	102.0	5.4	45.8
SD	1.0	0.9	0.4	26.3	1.2	2.4	0.6	0.7	0.4	19.6	1.1	2.7	0.7	0.5	0.2	5.0	0.7	2.9
RSD	43.5	23.3	19.1	26.1	21.3	7.1	31.6	21.6	15.5	20.1	18.4	6.2	25.3	16.8	9.7	4.9	12.7	6.3

Sample number	Processing time (seconds)																	
	300						600						1200					
	C+D	S 1	S 2	Rec	DD	FPF	C+D	S 1	S 2	Rec	DD	FPF	C+D	S 1	S 2	Rec	DD	FPF
A1	2.8	2.6	1.9	91.0	4.5	43.0	1.9	2.8	2.5	89.5	5.3	46.9	2.2	2.2	2.6	86.7	4.8	53.6
A2	2.2	2.9	2.2	91.1	5.1	43.2	2.7	2.1	2.8	95.2	4.9	57.3	1.7	2.4	2.7	84.5	5.0	52.9
B1	2.1	3.5	2.3	99.9	5.9	40.1	1.9	2.5	2.8	89.1	5.3	52.2	1.9	2.6	2.6	89.0	5.3	49.9
B2	3.0	2.8	2.4	101.0	5.1	46.3	1.9	2.5	2.6	87.6	5.1	51.4	1.9	3.1	2.1	88.3	5.2	40.0
C1	2.2	2.6	2.6	91.0	5.1	50.0	2.2	2.3	3.0	93.7	5.4	56.8	1.8	2.6	2.6	86.0	5.1	50.0
C2	2.7	2.7	2.3	95.0	5.0	46.0	1.9	2.7	2.2	86.4	5.0	45.1	2.2	2.4	2.2	84.8	4.6	47.0
Mean	2.5	2.8	2.3	94.8	5.1	44.8	2.1	2.5	2.7	90.3	5.2	51.6	1.9	2.6	2.4	86.5	5.0	48.9
SD	0.4	0.4	0.2	4.6	0.4	3.4	0.3	0.3	0.3	3.5	0.2	5.0	0.2	0.3	0.3	1.8	0.3	4.9
RSD	14.3	12.6	9.0	4.9	8.4	7.7	15.6	10.5	10.4	3.9	3.5	9.6	10.5	12.3	10.3	2.1	5.3	10.1

Key
C+D Dose recovered in capsule and device
S 1 Dose recovered in stage 1
S 2 Dose recovered in stage 2
Rec Percent total recovery / nominal recovery
DD Delivered dose (stage 1 + stage 2)
FPF Fine particle fraction
SD Standard deviation
RSD Relative standard deviation

Table 5.10. *In-vitro* functionality data from TSI testing of samples obtained during processing of nedocromil sodium trihydrate formulation in FBSVP-B, experiment #2.

Sample number	Processing time (seconds)																	
	30						60						120					
	C+D	S 1	S 2	Rec	DD	FPF	C+D	S 1	S 2	Rec	DD	FPF	C+D	S 1	S 2	Rec	DD	FPF
A1	2.0	3.7	2.5	102.5	6.2	40.0	2.2	3.9	2.9	112.3	6.8	42.8	2.3	3.2	2.8	104.0	6.0	47.1
A2	2.1	3.8	2.8	108.8	6.6	42.3	2.4	4.1	2.9	117.4	7.0	41.4	2.3	4.0	3.0	116.4	7.0	43.1
B1	0.7	1.7	1.4	47.3	3.1	45.4	0.7	1.8	1.0	44.0	2.9	36.4	2.3	3.3	3.0	107.3	6.2	47.2
B2	1.1	2.7	1.6	67.8	4.3	37.6	1.5	3.7	1.9	88.9	5.6	33.8	2.0	3.4	3.1	106.1	6.5	47.5
C1	2.6	4.0	2.9	119.7	7.0	42.2	2.0	3.4	3.1	106.8	6.5	47.8	2.5	3.3	2.7	106.1	6.0	44.5
C2	2.5	4.7	3.0	127.9	7.7	39.3	2.1	3.0	2.9	100.1	5.9	49.1	2.6	3.4	2.6	107.3	6.0	43.8
Mean	1.8	3.4	2.4	95.7	5.8	41.1	1.8	3.3	2.5	94.9	5.8	41.9	2.3	3.4	2.9	107.9	6.3	45.5
SD	0.8	1.1	0.7	31.5	1.7	2.8	0.7	0.8	0.8	26.8	1.5	6.1	0.2	0.3	0.2	4.4	0.4	1.9
RSD	42.3	31.0	29.4	32.9	30.1	6.7	35.6	25.0	33.1	28.3	26.3	14.5	8.9	8.4	6.6	4.0	6.5	4.2

Sample number	Processing time (seconds)																	
	300						600						1200					
	C+D	S 1	S 2	Rec	DD	FPF	C+D	S 1	S 2	Rec	DD	FPF	C+D	S 1	S 2	Rec	DD	FPF
A1	2.2	3.5	2.5	102.2	6.0	41.6	2.1	3.1	2.5	95.2	5.5	44.4	2.0	3.9	2.3	102.0	6.1	36.6
A2	2.3	3.7	2.6	107.1	6.3	41.7	2.2	3.3	2.7	102.5	6.0	45.4	2.9	3.1	2.3	102.9	5.4	41.7
B1	1.8	3.3	2.5	94.8	5.8	42.5	2.6	3.0	2.6	102.4	5.6	46.6	2.5	2.8	2.4	97.2	5.3	46.4
B2	1.9	3.9	2.5	103.2	6.4	39.2	3.1	2.8	2.3	102.5	5.1	45.9	2.2	3.3	2.3	97.2	5.6	40.8
C1	2.4	3.4	2.7	106.7	6.2	44.2	1.9	3.0	2.5	91.8	5.5	45.3	2.2	3.6	2.5	103.8	6.1	40.5
C2	2.3	3.2	2.4	98.3	5.6	42.3	2.0	3.3	2.4	95.4	5.6	41.6	2.0	3.5	2.8	102.0	6.2	44.4
Mean	2.2	3.5	2.5	102.1	6.0	41.9	2.3	3.1	2.5	98.3	5.6	44.9	2.3	3.4	2.4	100.8	5.8	41.8
SD	0.2	0.2	0.1	4.8	0.3	1.6	0.5	0.2	0.2	4.7	0.3	1.8	0.3	0.4	0.2	2.9	0.4	3.4
RSD	11.4	6.7	5.1	4.7	5.0	3.9	19.9	6.4	6.0	4.8	5.1	3.9	14.6	11.2	8.3	2.9	7.3	8.1

Key	
C+D	Dose recovered in capsule and device
S 1	Dose recovered in stage 1
S 2	Dose recovered in stage 2
Rec	Percent total recovery / nominal recovery
DD	Delivered dose (stage 1 + stage 2)
FPF	Fine particle fraction
SD	Standard deviation
RSD	Relative standard deviation

Table 5.11. *In-vitro* functionality data from TSI testing of samples obtained during processing of nedocromil sodium trihydrate formulation in FBSVP-B, experiment #3.

Sample number	Processing time (seconds)																	
	30						60						120					
	C+D	S 1	S 2	Rec	DD	FPF	C+D	S 1	S 2	Rec	DD	FPF	C+D	S 1	S 2	Rec	DD	FPF
A1	1.9	4.2	2.6	108.4	6.7	37.9	2.3	3.6	2.8	108.9	6.4	43.4	2.7	3.2	2.4	104.0	5.7	43.2
A2	2.1	4.9	2.1	113.0	7.0	30.4	2.2	3.7	2.5	104.4	6.2	40.4	2.2	3.7	2.4	103.4	6.1	39.7
B1	1.6	3.6	2.0	89.3	5.5	35.4	2.9	3.7	2.1	109.4	5.9	36.5	1.4	3.4	2.2	87.7	5.6	40.0
B2	2.4	3.6	2.1	100.7	5.7	36.3	1.8	3.5	2.4	97.0	5.9	41.0	2.3	3.3	2.8	104.5	6.0	45.9
C1	0.6	1.9	1.0	43.8	2.9	35.8	1.8	3.7	2.5	99.2	6.2	40.1	2.3	4.0	2.4	109.6	6.5	37.7
C2	1.1	1.7	1.1	47.6	2.8	39.5	1.9	3.6	2.5	99.9	6.1	40.5	2.0	4.0	2.2	102.9	6.2	35.2
Mean	1.6	3.3	1.8	83.8	5.1	35.9	2.1	3.6	2.5	103.1	6.1	40.3	2.1	3.6	2.4	102.0	6.0	40.3
SD	0.7	1.3	0.6	30.6	1.8	3.1	0.4	0.1	0.2	5.2	0.2	2.2	0.4	0.4	0.2	7.4	0.3	3.8
RSD	41.8	38.6	33.7	36.5	36.2	8.6	19.1	2.2	8.3	5.1	3.2	5.5	19.4	10.2	8.6	7.3	5.5	9.5

Sample number	Processing time (seconds)																	
	300						600						1200					
	C+D	S 1	S 2	Rec	DD	FPF	C+D	S 1	S 2	Rec	DD	FPF	C+D	S 1	S 2	Rec	DD	FPF
A1	2.1	3.4	2.5	99.4	5.9	42.2	2.0	3.4	2.4	98.1	5.8	41.4	1.5	3.6	2.6	95.6	6.2	42.0
A2	1.8	3.7	2.3	96.8	5.9	38.3	2.1	3.1	2.6	98.2	5.7	45.2	1.5	3.3	2.6	93.0	5.9	43.8
B1	1.9	3.5	2.4	97.2	5.9	40.5	1.8	3.8	2.3	99.0	6.1	38.4	1.6	2.7	2.4	83.8	5.1	47.3
B2	1.8	3.3	2.6	95.7	5.9	43.5	1.7	3.6	2.2	93.1	5.8	38.2	1.4	2.5	2.9	84.2	5.4	53.3
C1	2.7	3.6	2.4	108.9	6.0	39.5	3.0	2.6	2.0	95.3	4.6	43.5	1.5	2.8	2.6	86.1	5.4	48.1
C2	2.2	3.6	2.4	103.0	6.0	40.1	2.6	3.2	2.3	101.8	5.5	41.7	1.9	2.4	2.6	85.3	4.9	51.6
Mean	2.1	3.5	2.4	100.2	5.9	40.7	2.2	3.3	2.3	97.6	5.6	41.4	1.6	2.9	2.6	88.0	5.5	47.7
SD	0.4	0.1	0.1	5.0	0.1	1.9	0.5	0.4	0.2	3.0	0.5	2.7	0.2	0.5	0.1	5.0	0.5	4.3
RSD	16.9	3.8	4.1	5.0	1.0	4.6	22.4	12.1	8.5	3.1	9.1	6.6	11.0	16.3	5.4	5.7	8.6	9.1

Key	
C+D	Dose recovered in capsule and device
S 1	Dose recovered in stage 1
S 2	Dose recovered in stage 2
Rec	Percent total recovery / nominal recovery
DD	Delivered dose (stage 1 + stage 2)
FPF	Fine particle fraction
SD	Standard deviation
RSD	Relative standard deviation

Table 5.12. *In-vitro* functionality data from TSI testing of samples obtained during processing of nedocromil sodium trihydrate formulation in FBSVP-B, experiment #4.

Sample number	Processing time (seconds)																	
	30						60						120					
	C+D	S 1	S 2	Rec	DD	FPF	C+D	S 1	S 2	Rec	DD	FPF	C+D	S 1	S 2	Rec	DD	FPF
A1	1.8	4.3	2.1	103.2	6.5	32.7	2.2	4.2	2.5	110.8	6.7	37.6	1.9	3.8	2.1	98.2	6.0	35.9
A2	1.7	5.0	1.7	105.7	6.8	25.3	2.1	4.6	2.7	116.9	7.3	37.3	2.4	3.6	1.9	98.2	5.5	34.9
B1	0.5	2.0	1.0	42.6	3.0	33.3	0.6	2.4	0.9	49.6	3.4	27.7	2.1	3.9	2.2	102.8	6.1	36.1
B2	1.0	3.0	1.7	70.8	4.7	35.4	0.5	2.2	0.9	44.2	3.1	27.6	2.3	3.3	2.2	97.8	5.5	39.7
C1	2.3	4.3	2.1	109.2	6.4	33.2	2.4	5.6	2.3	128.8	7.9	29.4	1.6	4.0	1.9	93.3	5.9	31.8
C2	2.2	4.6	2.0	110.2	6.6	30.7	2.1	5.3	2.4	122.8	7.7	31.1	1.7	4.4	2.3	104.2	6.7	34.2
Mean	1.6	3.9	1.8	90.3	5.6	31.8	1.6	4.1	2.0	95.5	6.0	31.8	2.0	3.8	2.1	99.1	5.9	35.4
SD	0.7	1.2	0.4	27.6	1.5	3.5	0.9	1.4	0.8	38.2	2.2	4.6	0.3	0.4	0.2	3.9	0.4	2.6
RSD	45.3	29.8	24.7	30.6	27.1	11.0	52.5	35.3	42.8	40.0	36.7	14.4	17.2	9.6	7.9	3.9	7.4	7.4

Sample number	Processing time (seconds)																	
	300						600						1200					
	C+D	S 1	S 2	Rec	DD	FPF	C+D	S 1	S 2	Rec	DD	FPF	C+D	S 1	S 2	Rec	DD	FPF
A1	2.3	3.2	2.2	95.8	5.4	40.6	2.1	3.1	2.1	90.5	5.2	40.1	1.9	2.8	2.5	90.5	5.3	46.3
A2	2.0	3.4	2.2	94.7	5.6	39.6	1.8	3.1	2.6	93.4	5.7	46.3	1.9	3.1	2.5	93.1	5.6	44.3
B1	2.4	3.1	2.0	94.3	5.1	39.1	1.7	3.0	2.4	88.3	5.4	44.1	1.9	2.8	2.5	90.4	5.3	47.1
B2	2.3	3.3	2.3	98.4	5.6	41.2	3.2	2.3	1.9	92.7	4.2	45.8	2.0	2.9	2.3	89.6	5.2	44.9
C1	2.2	3.7	2.2	102.0	5.9	37.6	1.8	3.2	2.5	93.0	5.6	43.8	1.8	3.0	2.7	94.1	5.7	47.8
C2	2.1	3.0	2.3	92.8	5.3	43.0	2.0	3.0	2.6	95.3	5.6	46.6	1.9	3.1	2.4	93.2	5.6	43.8
Mean	2.2	3.3	2.2	96.3	5.5	40.2	2.1	2.9	2.3	92.2	5.3	44.5	1.9	3.0	2.5	91.8	5.4	45.7
SD	0.1	0.2	0.1	3.4	0.3	1.8	0.6	0.3	0.3	2.5	0.6	2.4	0.1	0.1	0.1	1.9	0.2	1.6
RSD	5.9	7.2	4.6	3.5	5.0	4.6	27.4	11.3	12.6	2.7	10.9	5.4	2.8	4.6	5.3	2.0	3.6	3.6

Key	
C+D	Dose recovered in capsule and device
S 1	Dose recovered in stage 1
S 2	Dose recovered in stage 2
Rec	Percent total recovery / nominal recovery
DD	Delivered dose (stage 1 + stage 2)
FPF	Fine particle fraction
SD	Standard deviation
RSD	Relative standard deviation

Table 5.13. *In-vitro* functionality data from TSI testing of samples obtained during processing of nedocromil sodium trihydrate formulation in FBSVP-B, experiment #5.

Expt. no.	Sample position	Processing time (seconds) 30	60	120	300	600	1200
		Percent fine particle fraction					
Expt #1	A1	35.7	42.2	47.2	38.1	44.4	34.8
Expt #1	A2	35.2	41.8	45.7	42.8	41.7	37.6
Expt #1	B1	41.5	46.6	44.7	50.7	37.1	34.4
Expt #1	B2	38.1	43.1	50.1	51.2	39.0	34.8
Expt #1	C1	30.3	46.0	45.8	41.1	33.0	33.3
Expt #1	C2	29.5	45.3	49.0	45.7	37.6	36.6
Expt #2	A1	34.3	39.0	42.6	43.0	46.9	53.6
Expt #2	A2	35.9	42.1	46.4	43.2	57.3	52.9
Expt #2	B1	29.4	44.0	45.7	40.1	52.2	49.9
Expt #2	B2	32.6	45.3	45.7	46.3	51.4	40.0
Expt #2	C1	35.5	44.3	50.8	50.0	56.8	50.0
Expt #2	C2	33.7	46.8	43.3	46.0	45.1	47.0
Expt #3	A1	40.0	42.8	47.1	41.6	44.4	36.6
Expt #3	A2	42.3	41.4	43.1	41.7	45.4	41.7
Expt #3	B1	45.4	36.4	47.2	42.5	46.6	46.4
Expt #3	B2	37.6	33.8	47.5	39.2	45.9	40.8
Expt #3	C1	42.2	47.8	44.5	44.2	45.3	40.5
Expt #3	C2	39.3	49.1	43.8	42.3	41.6	44.4
Expt #4	A1	37.9	43.4	43.2	42.2	41.4	42.0
Expt #4	A2	30.4	40.4	39.7	38.3	45.2	43.8
Expt #4	B1	35.4	36.5	40.0	40.5	38.4	47.3
Expt #4	B2	36.3	41.0	45.9	43.5	38.2	53.3
Expt #4	C1	35.8	40.1	37.7	39.5	43.5	48.1
Expt #4	C2	39.5	40.5	35.2	40.1	41.7	51.6
Expt #5	A1	32.7	37.6	35.9	40.6	40.1	46.3
Expt #5	A2	25.3	37.3	34.9	39.6	46.3	44.3
Expt #5	B1	33.3	27.7	36.1	39.1	44.1	47.1
Expt #5	B2	35.4	27.6	39.7	41.2	45.8	44.9
Expt #5	C1	33.2	29.4	31.8	37.6	43.8	47.8
Expt #5	C2	30.7	31.1	34.2	43.0	46.6	43.8
Mean		**35.5**	**40.4**	**42.8**	**42.5**	**44.2**	**43.9**
SD		**4.5**	**5.8**	**5.1**	**3.6**	**5.4**	**6.0**
RSD		**12.6**	**14.4**	**12.0**	**8.4**	**12.2**	**13.6**

Table 5.14. Summary of percent fine particle fraction determined for samples obtained during processing of nedocromil sodium trihydrate formulation in FBSVP-B, experiments #1 to #5.

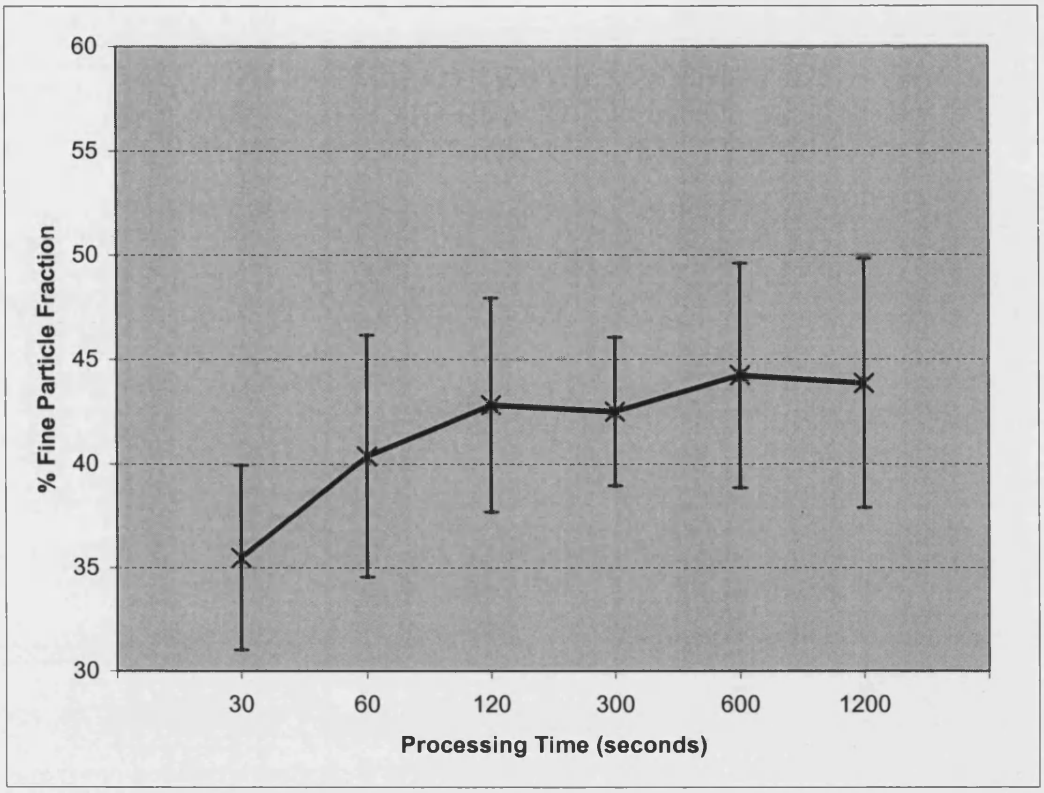

Graph 5.2. Graph showing mean %FPF results from five batches of the nedocromil sodium trihydrate DPI formulation at different processing times in FBSVP-B.

5.3.3 Discussion

As shown in graph 5.2, mean %FPF was found to stabilise after 120 seconds of processing time and was not found to change significantly during a processing time of 20 minutes.

However, considerable variability was found between experiments. Whilst some of this variability may be attributed to the inherent variability of *in-vitro* aerosol

impingement testing, a significant contributor to this can be attributed to the lack of consistent flow conditions throughout the processor, which were seen to cause problems in the milling and mixing studies (see sections 5.1 and 5.2 respectively).

5.3.4 Conclusion

The high shear conditions generated in the FBSVP-B appeared well suited to processing the nedocromil sodium DPI formulation although the presence of areas of low airflow velocity has again caused problems with reproducibility of the process.

6. SWEPT BED SVP DESIGN AND FABRICATION

6.1 Rationale

Although the FBSVP-B design demonstrated considerable promise in providing a processing environment suitable for manufacture of nedocromil sodium trihydrate blends for dry powder inhalation, a number of design flaws were also evident which were analysed and further considered in chapters 4 and 5.

As a result of this assessment further vessel refinements were engineered in order to address the main constraints of the FBSVP-B. Particular consideration was paid to the elimination of dead zones in the vessel, which are described in chapter 5. The strategy for this redesign was to provide high volumes of fluidising air movement that were directed in a more controlled manner in order to prevent areas of low velocity from developing within the processing area.

CFD technology was used as a predictive tool for investigating a number of design alternatives prior to fabrication of the new processor. The refinements that were developed and applied are considered below.

6.2 Design background

It was considered that the presence of dead zones within a powder bed undergoing processing in the FBSVP-B may be avoided by either increasing significantly the volume of fluidising air or by more carefully predicting and controlling the airflow directions.

It was likely that increasing airflow and consequently raising air pressure within the vessel would make particle arrestment from air leaving the vessel more difficult and also exacerbate problems of powder leakage from the vessel. Additionally, it was anticipated that an increasing air input volume would result in less powder being present in the zone of high activity associated with the high pressure air nozzles in the bottom part of the vessel, which in turn was likely to reduce the efficiency of the processing operations. Because of this it was not considered desirable to increase the air input volume but to modify the air input characteristics and consider alternative vessel designs. The basis of these redesigns was directed at targeting the high volume (fluidising) air in a more controlled fashion using CFD simulations as an adjunct in this design.

It was decided to retain the basic geometry of the vessel with a central cone positioned at the base of the cylindrical main vessel but replace the mesh base with a solid base and use high volume air inputs directed from the side close to the solid vessel base in order to 'sweep' away powder gathered on the base.

This method of introducing air for mass powder movement was termed a 'swept bed' system and the new processor was referred to as the Swept Bed Single Vessel Processor (SBSVP). The design of the SBSVP is shown in figures 6.1 and 6.2 and described in the following section.

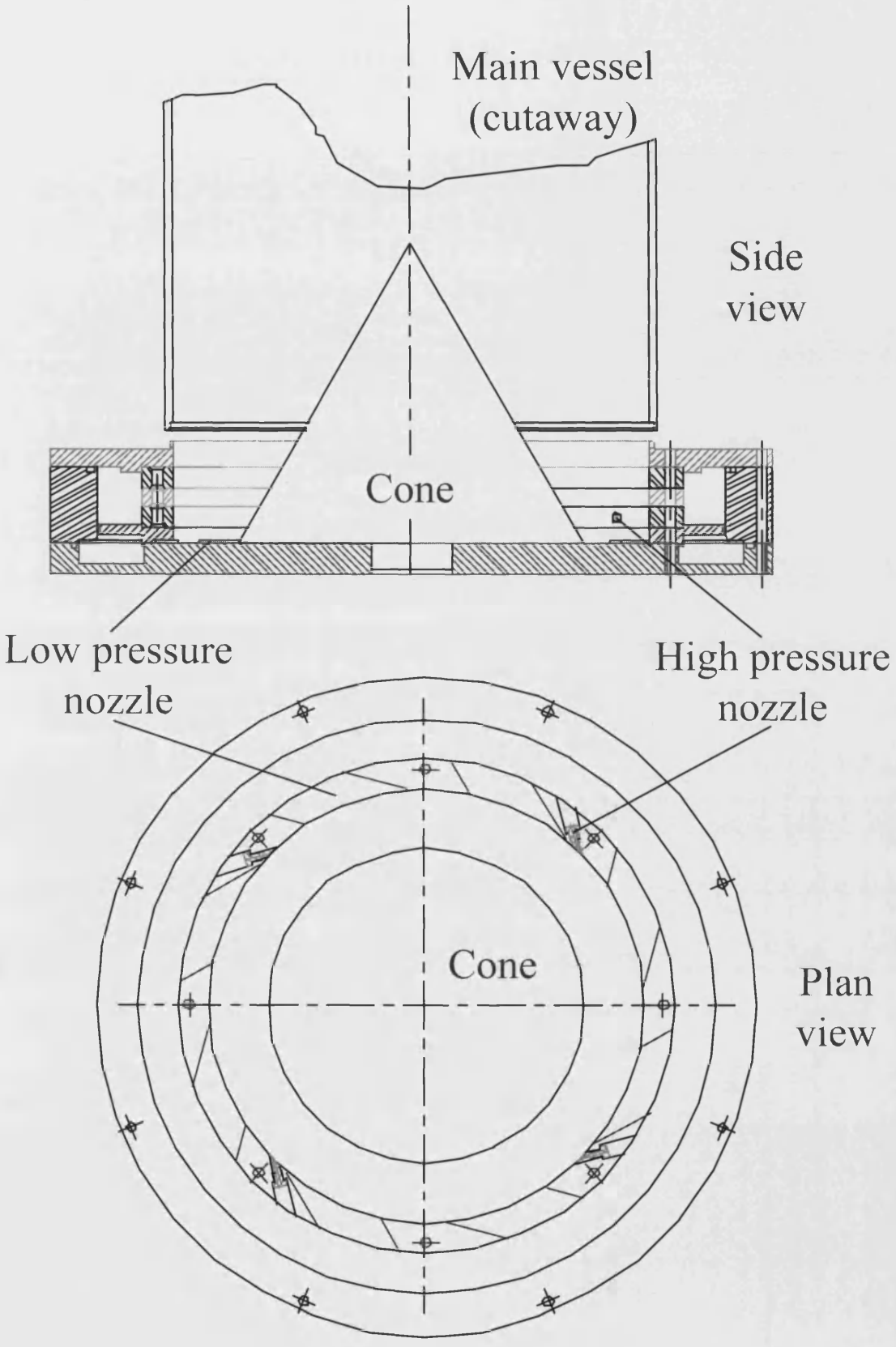

Figure 6.1. Drawing of SBSVP.

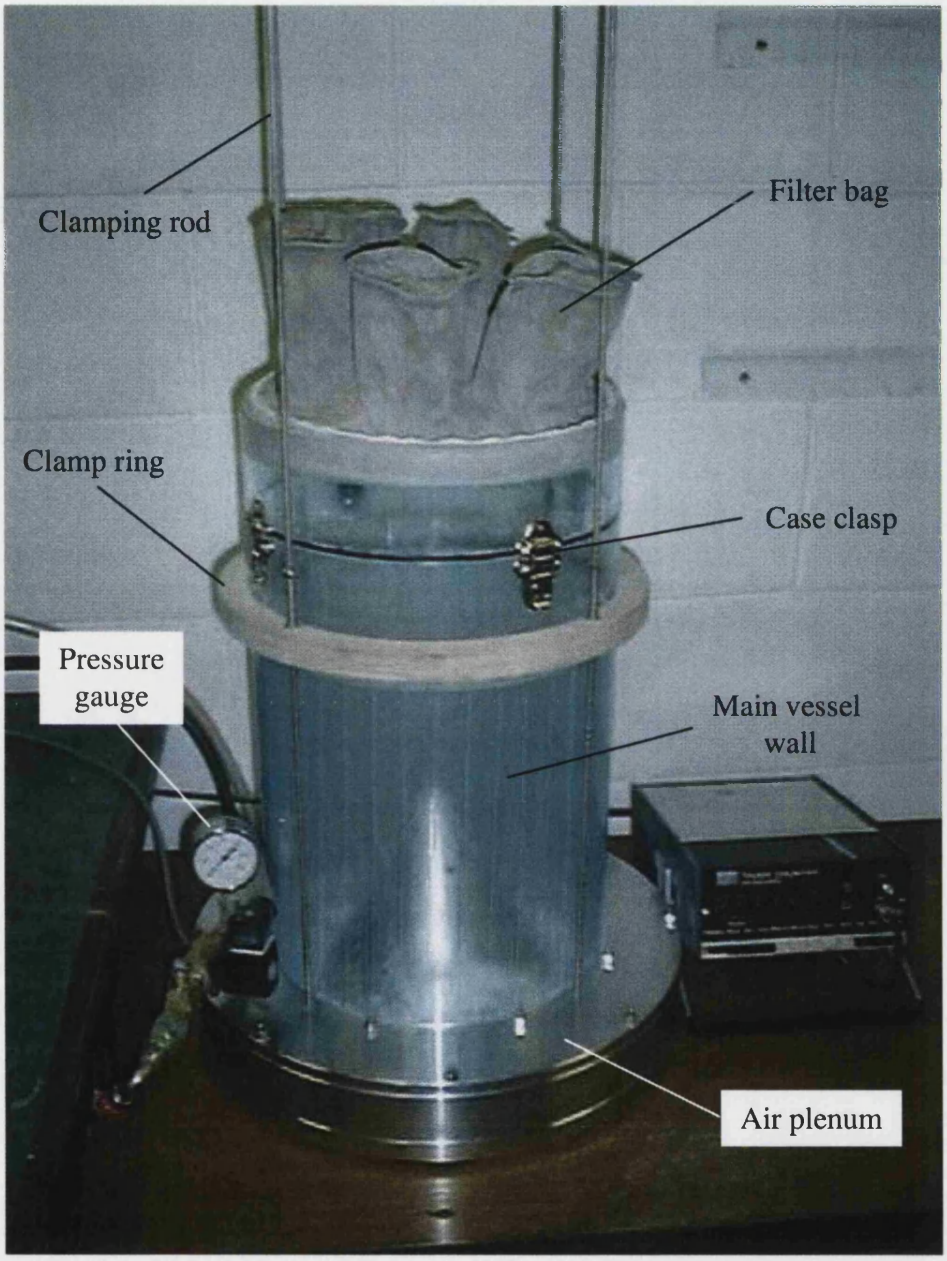

Figure 6.2. Photograph of SBSVP (external side view).

6.3 Design

6.3.1 General arrangement

The SBSVP was constructed from a series of modules so that design modifications could be incorporated into the structure without major reconstruction of the processor. These modules were the air plenum, the base plate, the high pressure air nozzles, the low pressure air nozzles, the vessel walls and the filter assembly. Each of these is described below.

6.3.2 Air plenum

The air plenum sub-assembly comprised the following modular components as shown in figure 6.3:

Air plenum base plate

Nozzle plates (four)

Air plenum top plate

Air plenum outer ring

Central cone

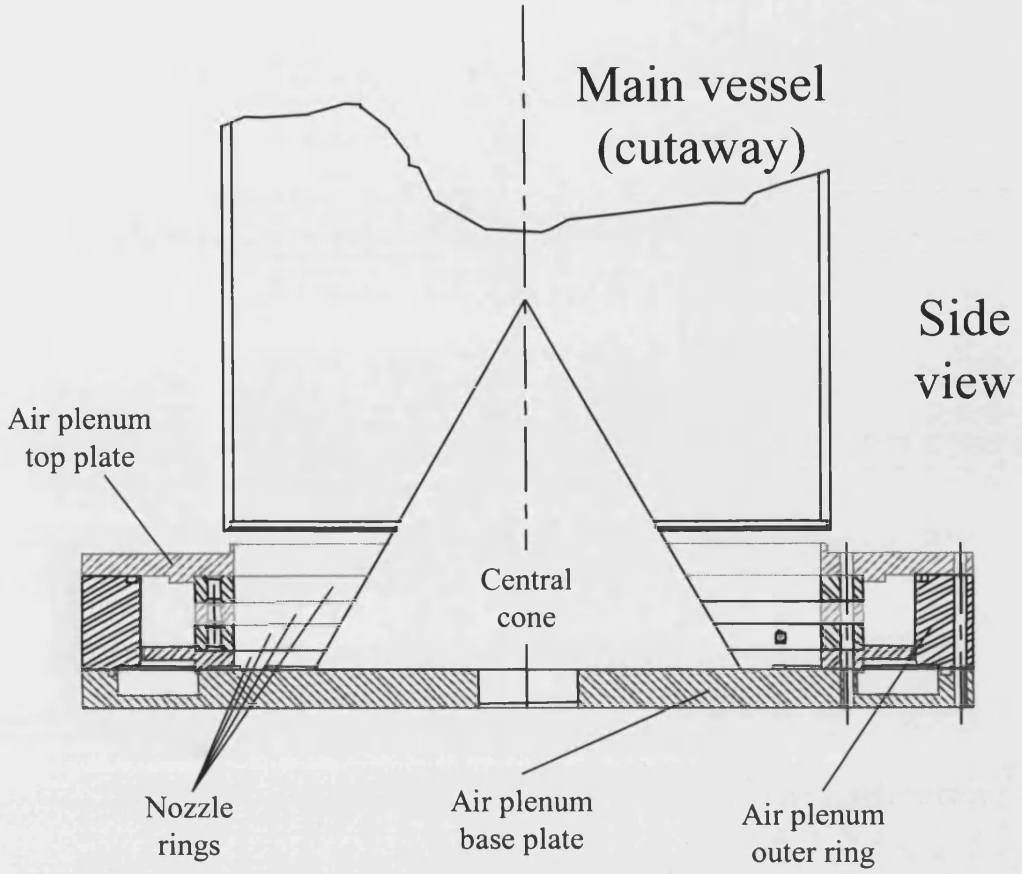

Figure 6.3. Drawing showing SBSVP air plenum components.

Each of these parts was fabricated from aluminium and when assembled together formed the air plenum, which contained the low and high pressure air nozzles and ducting for their air supplies. The air plenum was closed at the bottom by the air plenum base plate and at the top with a flanged ring (the air plenum top plate), which allowed attachment of the cylindrical vessel wall.

The high volume air nozzle ring, three interchangeable high pressure air nozzle rings (see below) and the air plenum outer ring were positioned in-between the top and the base plates and the assembled module held together with sixteen 8mm stainless steel

bolts. The high pressure air nozzle rings were designed such that each interlocked and could be stacked on top of each other on either face and in any order.

The total height of the assembled air plenum was 65mm above the vessel base.

The air plenum was affixed to a stand and connected to the compressed air supplies using standard fittings. The high pressure air nozzles and the high volume air nozzles were provided with compressed air from separate supplies. A pressure gauge and needle valve were placed into each compressed air line to allow the airflow rate to be controlled. The air flow to each set of nozzles was switched on and off using in-line solenoid valves of an appropriate rating. During operation, the high volume air supply was introduced by gradually opening the needle valve over approximately 2 seconds to avoid over pressurising the vessel. The high pressure air supply was introduced immediately at the correct pressure.

A cone was milled from a solid block of aluminium and the surface polished. The dimensions were as follows: height 180mm; base diameter 208mm; slope 60° from horizontal. A cylindrical stub on the base of the cone having a diameter of 50mm and height of 15mm allowed the cone to rest in the centre of the base plate where it was held in position under its own mass. This arrangement provided an annular track of 40mm width between the base of the cone and the side of the air plenum.

6.3.2.1 High pressure air nozzles

One of the three high pressure air nozzle rings was fitted with a series of 24 slots in each of which a high pressure air nozzle could be inserted. The slots allowed the nozzles to be inserted tangentially around the circumference of the nozzle ring as shown in figure 6.4 with each nozzle having a circular opening of 1.0mm diameter. It was possible to mount the ring in alternative positions giving a clockwise or an anti-clockwise direction of air-flow.

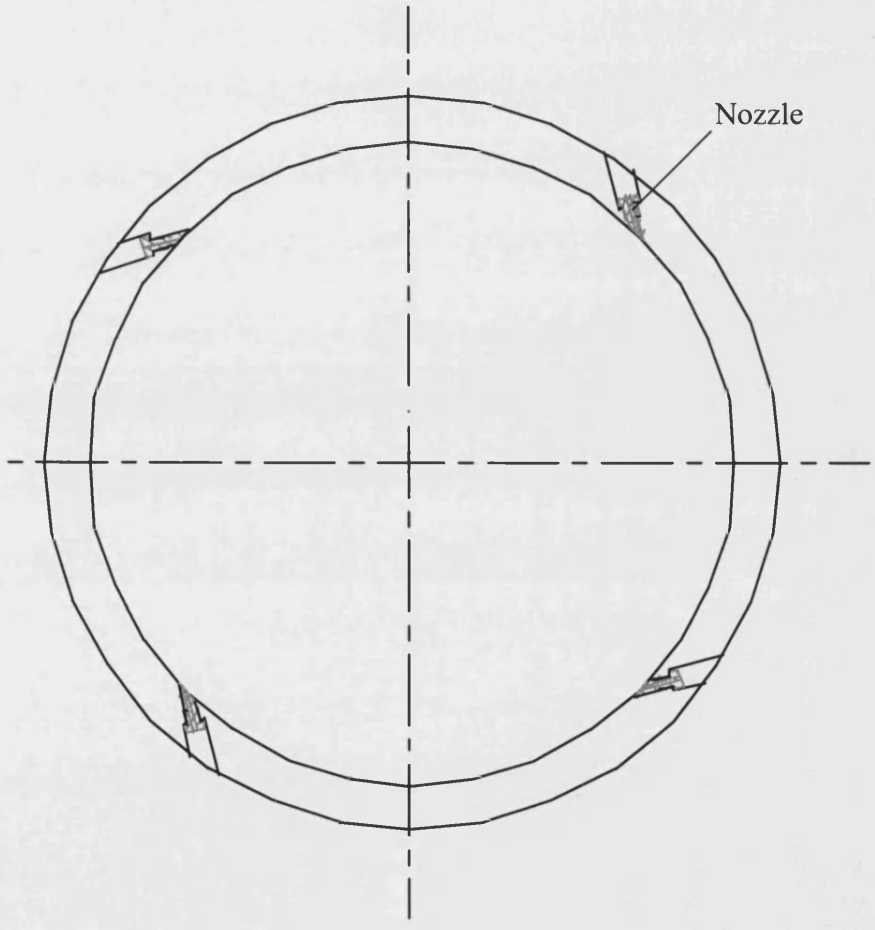

Figure 6.4. Plan view drawing of high pressure nozzle ring showing 4 of 24 nozzles only.

The height of the centre of each nozzle ring when assembled into the air plenum module (and hence the height of the centre of any nozzles in that ring) is shown in table 6.1 below.

Nozzle height	Approximate height of centre of nozzle above vessel base (mm)
Top	40
Middle	26
Bottom	16

Table 6.1. Approximate height of high pressure air nozzles above vessel base.

6.3.2.2 Flat (high volume) air nozzles

The fluidised mesh base used in FBSVP-A and FBSVP-B was replaced with a solid base and a further nozzle ring was fitted with eight flat slots of 2.0mm height and 70mm circumference as shown in figure 6.5. When positioned in the air plenum this formed eight flat nozzles, which enabled high volumes of air to sweep the vessel base. This nozzle ring was designed so that it could be located in one position only so causing air to be directed clockwise.

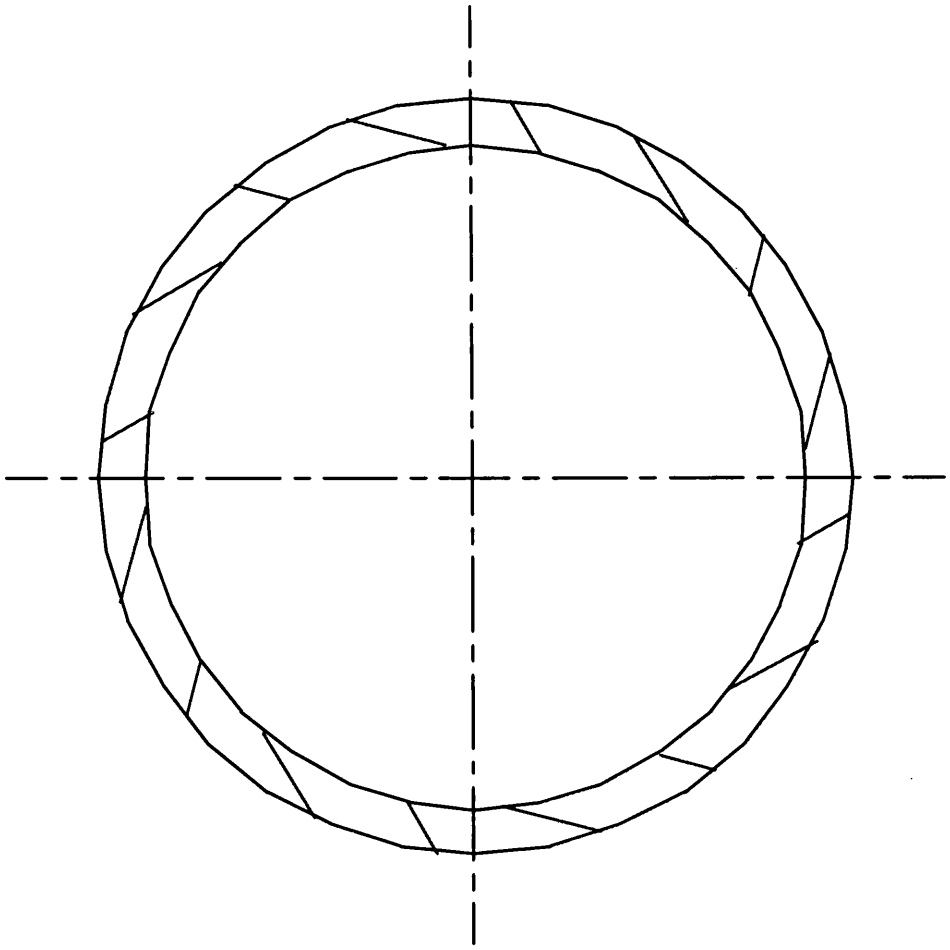

Figure 6.5. Plan view drawing of flat (high volume) nozzle ring.

The optimal angle of the flat (high volume) air nozzles was determined by performing single phase velocity simulations using the CFD software. This software allowed a study of the predicted flow patterns for three alternative nozzle angles; 0°, 15° and 30° to the tangent of the nozzle ring. A schematic diagram of the model input to the CFD software is shown in figure 6.6. The vessel was modelled as a one eighth segment to reduce computational complexity.

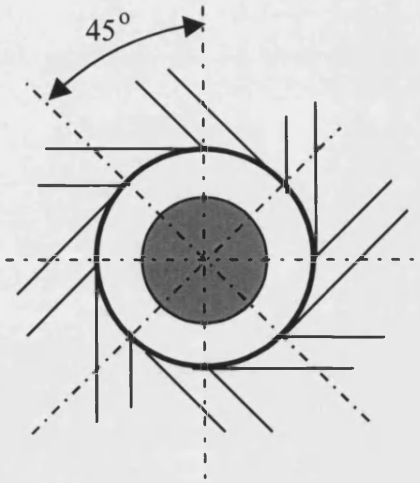

Figure 6.6. Schematic diagram of model used for CFD predictions.

The results of this study are shown in figures 6.7, 6.8 and 6.9.

Figure 6.7 shows the flow simulation for a nozzle angle of 0° to the tangent. The model predicted an area of low velocity close to the cone which could potentially lead to a dead zone in the vessel.

The simulation for a nozzle angle of 15° is shown in figure 6.8. This indicated a good distribution of airflow across the vessel base with a main flow channel in the middle of the annulus. A small region of low velocity was indicated near to the cone.

With the nozzle angle set to 30°, as shown in figure 6.9, the model predicted that all of the base powder was activated to flow. However, it was also predicted that a large proportion of the airflow would impinge on the cone surface, which could lead to a significant reduction in the circulation velocity of the airflow.

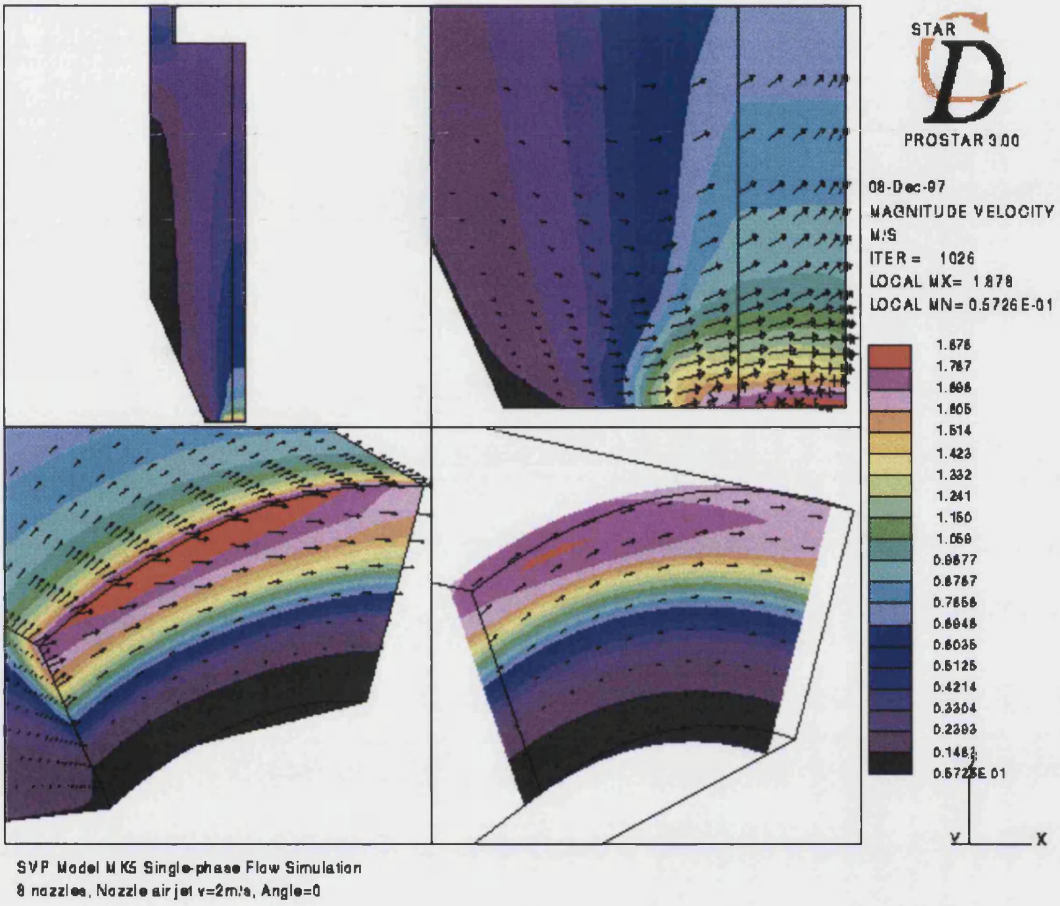

Figure 6.6. Single phase CFD flow simulation model of SBSVP with flat nozzles at 0° from the tangent and nozzle air outlet velocity set at 2msec^{-1}.

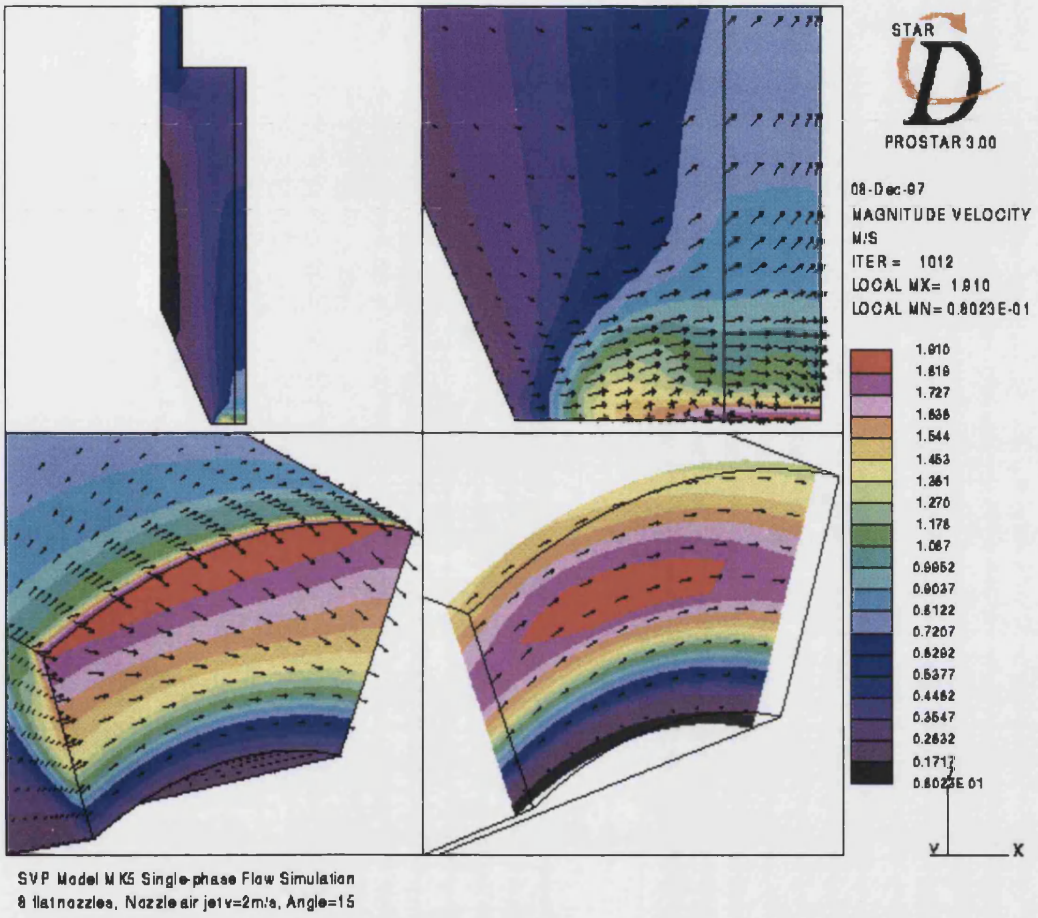

Figure 6.7. Single phase CFD flow simulation model of SBSVP with flat nozzles at 15° from the tangent and nozzle air outlet velocity set at 2msec^{-1}.

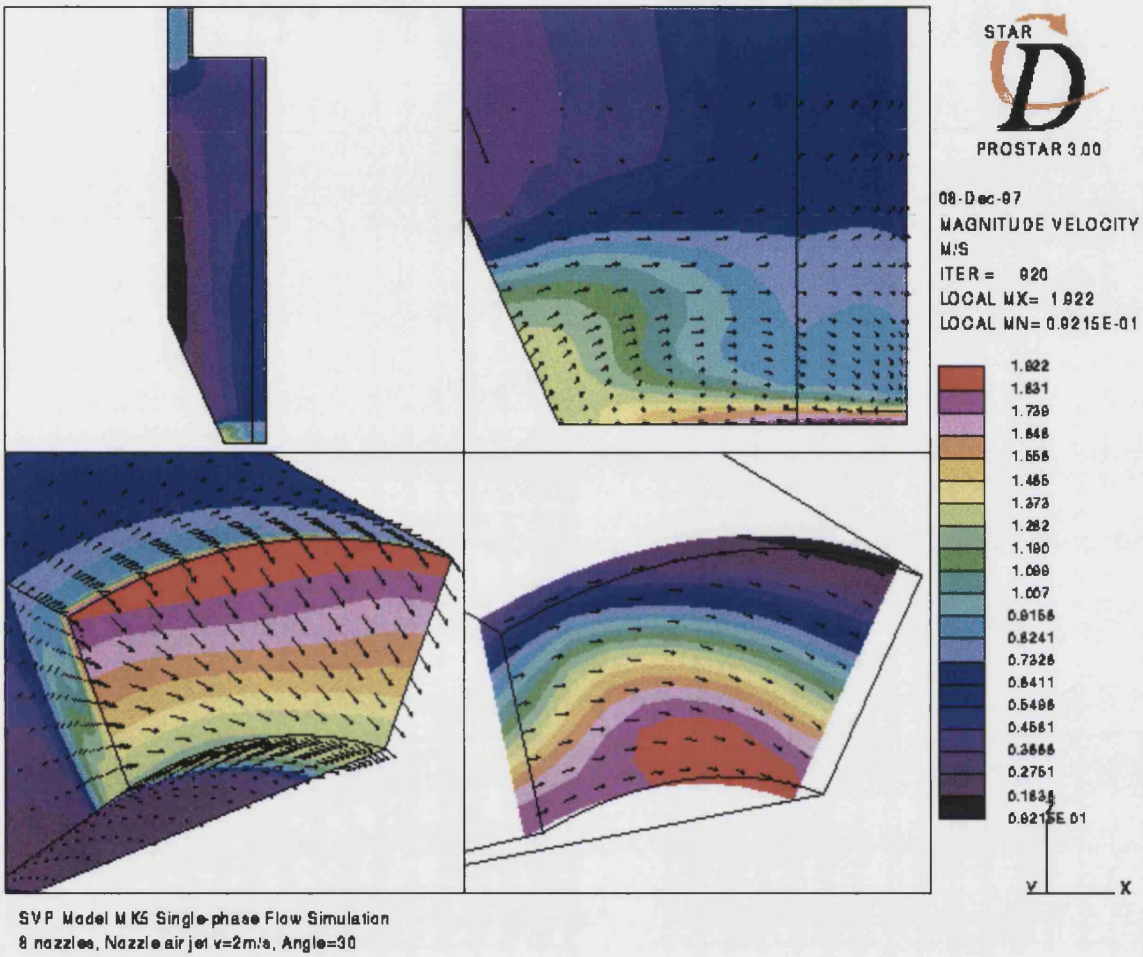

Figure 6.8. Single phase CFD flow simulation model of SBSVP with flat nozzles at 30° from the tangent and nozzle air outlet velocity set at 2msec^{-1}.

As a result of the above considerations it was deduced that the flow conditions predicted for a nozzle angle of 15 degrees would be optimal for this system and consequently this was implemented into the vessel design.

6.3.3 Vessel walls

The vessel walls were constructed from cylindrical Perspex® pipe of 300mm external diameter and 6mm wall thickness. Three sections of wall were fabricated having heights of 150mm, 300mm and 600mm. The top and bottom edges of each section were machined with a groove to enable them to be seated onto the air plenum. It was also possible to interlock the different sections making available the following range of vessel wall heights: 150mm, 300mm, 450mm, 600mm, 750mm, 900mm and 1050mm.

A further section of Perspex® was cut to a length of 100mm and a wooden clamping ring firmly attached to its circumference (see figure 6.2); the clamping section was placed on top of the wall section(s) during assembly of the vessel. Four case clasps were affixed to the top of the clamping section to allow attachment of the filter assembly.

All internal Perspex® wall surfaces were coated with an antistatic tape in a similar manner to that described for FBSVP-B in section 4.3.5.

Four 8mm threaded clamping rods of 1.5m length were attached to the air plenum as shown in figure 6.2. These were inserted through holes in the clamping ring, four springs of suitable size placed onto each rod and nuts tightened over each until sufficient tension was held in the springs to ensure that all sections of the vessel wall were fixed in place and sealed with the top of the air plenum.

6.3.4 Filter assembly

The filter assembly was that used in FBSVP-B. This is described in detail in section 4.3.2.

6.3.5 Airflow determination for high pressure air nozzles

The velocity of the airflow leaving the high pressure air nozzles was measured by using the technique described in section 4.3.1.

The velocity profile of the nozzles was measured for the following nominal air pressures measured in the air plenum:

70, 140, 210, 280 and 350 kPa

A summary of the air velocities at each air plenum pressure setting is shown in table 6.1. These are also summarised in graphical form and a regression analysis of the data presented in graph 6.1.

	Nominal nozzle pressure				
	70 kPa	140 kPa	210 kPa	280 kPa	350 kPa

Nozzle number	Mean velocity $msec^{-1}$	SD	Mean velocity $msec^{-1}$	SD	Mean velocity $msec^{-1}$	SD	Mean velocity $msec^{-1}$	SD	Mean velocity $msec^{-1}$	SD
1	56.0	2.9	76.7	3.2	91.5	6.4	102.5	3.5	140.1	7.3
2	37.7	2.9	56.5	3.2	68.5	5.2	101.7	17.8	151.7	1.6
3	33.7	7.1	47.1	6.2	55.9	3.8	79.4	4.1	145.3	4.7
4	41.3	6.4	89.2	3.3	122.7	5.6	152.1	3.1	147.4	4.0
5	25.0	1.3	35.8	1.6	45.3	5.8	56.6	2.5	64.4	4.0
6	44.4	5.1	57.5	3.3	85.0	13.2	91.4	4.2	106.3	2.8
7	56.2	1.7	70.4	2.1	96.0	5.2	116.1	3.1	150.0	3.1
8	81.6	0.5	111.4	7.9	154.5	3.3	152.3	3.5	154.1	4.0
9	27.7	1.5	64.5	2.5	83.3	2.6	106.5	5.7	102.4	9.0
10	88.2	2.9	110.0	11.5	150.2	5.2	158.1	3.6	162.3	7.2
11	61.1	5.9	88.8	4.6	108.9	13.0	124.7	4.2	140.0	3.8
12	33.0	8.7	57.6	4.5	69.5	0.9	84.2	1.8	113.1	8.8
13	20.8	3.2	37.7	8.1	62.4	7.3	94.9	17.4	129.1	13.7
14	57.3	7.1	84.5	2.3	119.9	10.7	151.4	2.6	150.4	5.9
15	89.4	6.6	115.9	9.0	150.2	3.8	154.1	5.2	149.4	4.4
16	90.1	2.2	115.1	8.5	150.7	3.4	154.3	5.1	154.8	4.3
17	91.5	0.8	111.9	30.0	153.7	5.7	156.4	4.5	156.8	4.2
18	55.9	2.2	73.5	4.9	100.7	8.3	116.1	5.3	131.2	2.0
19	48.9	1.5	71.5	3.0	73.2	24.7	111.3	2.4	140.4	8.1
20	46.0	1.3	71.5	6.2	83.6	3.8	100.5	3.2	108.6	4.2
21	36.2	1.5	74.6	8.9	86.9	4.4	112.5	12.2	144.2	3.8
22	36.9	1.5	54.3	3.2	84.4	9.8	100.9	4.2	114.9	0.7
23	43.2	0.6	61.1	15.5	83.7	6.6	115.7	3.4	129.7	4.8
24	52.1	3.1	73.9	1.5	120.3	19.5	151.5	6.5	145.2	6.4
Approx. overall mean	**52**	**22**	**75**	**24**	**100**	**33**	**119**	**29**	**135**	**23**

Table 6.1. Summary of measured air velocities of each nozzle at different nominal air plenum air pressures in SBSVP.

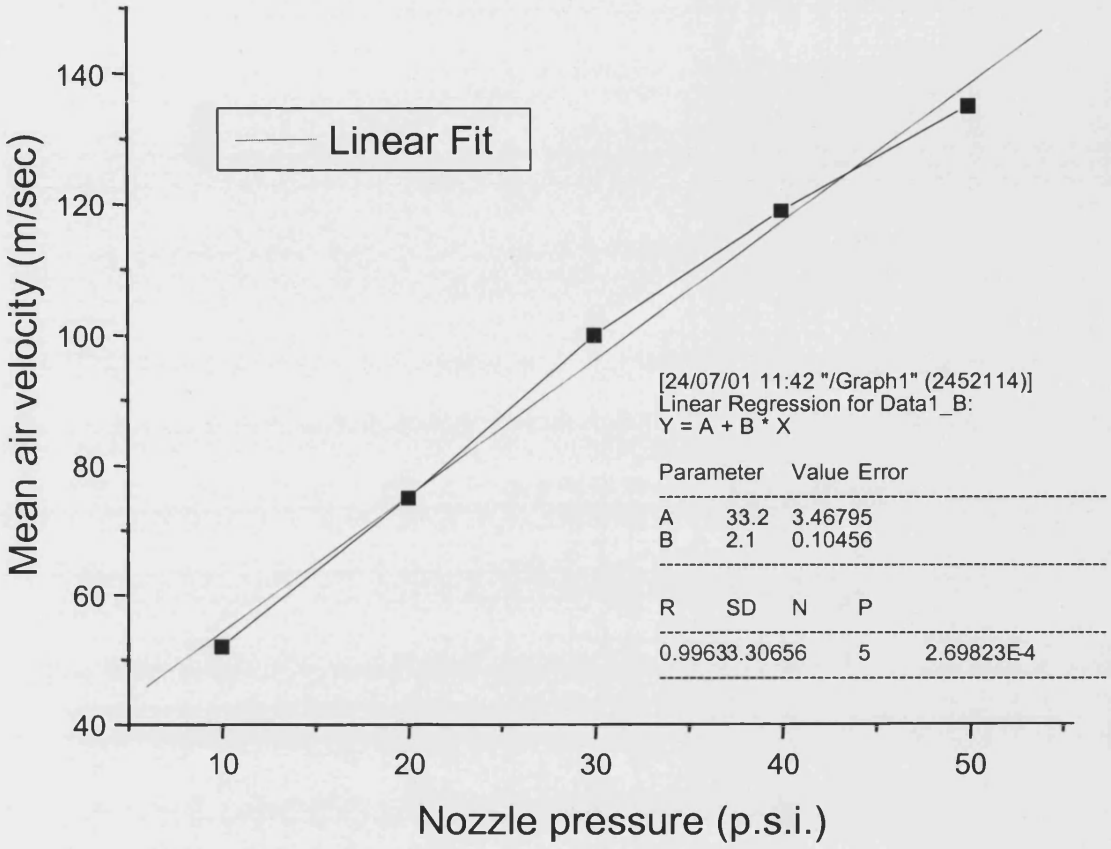

Graph 6.1. Graph showing mean air velocities at each nominal air plenum pressure in SBSVP and regression information for a linear fit of the data.

6.4 Summary of changes in vessel design of SBSVP compared to FBSVP-B

(a) Number of high pressure air nozzles increased from 12 to 24

(b) Three variable height positions for the high pressure air nozzles

(c) Fluidised air flow replaced with flat swept bed air nozzles

(d) Mesh base replaced with a solid base

(e) Vessel fabricated in a modular design to allow variation of individual parts

7. SWEPT BED SVP CHARACTERISATION

7.1 Rationale

Characterisation of the SBSVP was undertaken using similar analytical concepts to those used in the development of FBSVP-A and FBSVP-B and consequently much of the work described in this section is related closely to the studies reported in chapter 5.

7.2 Particle size reduction

7.2.1 Introduction

The aim of this study was to assess the particle size reduction performance of the SBSVP.

The work was conducted in three groups of experiments. The first group compared the performance of the SBSVP with that of the FBSVP models A and B in effecting particle size reduction using the same types of materials under similar processing conditions. In these experiments the SBSVP was operated with both the high pressure air nozzles and the high volume air nozzles engaged in a clockwise direction; this configuration was designated co-current flow.

The second group of experiments studied the effect of reversing the direction of the high pressure nozzles such that they were in opposition to the direction of flow of the high volume air nozzles; this arrangement was termed counter-current flow. The effect of differing nozzle air velocities within this vessel configuration was also investigated.

The final group of experiments varied the height of the high pressure air nozzle ring in the air plenum at a single nozzle air pressure and also examined the effects of co-current and counter-current flow of the high pressure and high volume air nozzle inputs at the different heights.

7.2.2 The effect of changes in high pressure nozzle air velocity on particle size reduction characteristics of SBSVP compared to FBSVP-A and FBSVP-B

7.2.2.1 SBSVP set up

The vessel was cleaned as described for the FBSVP-B (see section 5.1.1).

The air plenum was assembled with the high volume nozzles directed clockwise and the high pressure nozzles directed clockwise and positioned in the middle of the three possible locations (see section 6.3.2).

The 300mm and 150mm sections of vessel wall were attached to the air plenum followed by the clamping section and the filter assembly. The appropriate clasps and clamps were secured as described in section 6.3.3.

The high pressure air was set to the appropriate flow rate adjusting the needle valve with reference to the pressure gauge. The high volume air was set at a flow rate of 25.5 m^3hr^{-1}. The system was manually inspected for leaks before loading of the test material.

7.2.2.2 Experimental conditions

Using the linear regression formula from graph 5.1, it was possible to extrapolate an approximate plenum pressure that would provide equivalent nozzle air velocities to

those tested when investigating particle size reduction in the FBSVP-B (see section 5.1).

The air plenum set pressures and corresponding nozzle air velocity values are shown in table 7.1 below.

FBSVP-B		SBSVP	
Nozzle ring air pressure (kPa)	Approx. mean nozzle air velocity ($msec^{-1}$)	Air plenum set pressure (kPa)	Approx. mean nozzle air velocity ($msec^{-1}$)
70	78	140	75
140	107	245	105
210	138	350	135

Table 7.1. Table showing set pressures required in SBSVP air plenum to provide approximately equivalent nozzle outlet air velocities to those used during FBSVP-A and FBSVP-B particle size reduction experiments.

It was therefore concluded that particle size reduction experiments should be carried out at air plenum set pressures of 140, 245 and350 kPa.

The test material in all particle size reduction experiments was Prismalac 40® lactose (see Section 2.1.2), which was loaded in quantities of 500g. The material was spread around the base of the vessel using a spatula in order to ensure a constant bed height over the annular section.

Ambient environmental temperature and relative humidity conditions were monitored and recorded during all tests.

The flow fields arising during processing were visually monitored and any dead spots or other unusual occurrences recorded.

Three batches of test material were processed at each of the nozzle pressure settings and processing halted to allow samples to be taken for particle size analysis at processing times of 0, 30, 60, 120, 180, 240, 300, 450, 600, 900, 1200, 1500 and 1800 seconds for experiments conducted using 75 and 105 $msec^{-1}$ high pressure nozzle air velocities and 0, 30, 60, 120, 180, 240, 300, 450, 600, 900 and 1200 seconds for experiments performed using a high pressure nozzle air velocity of 135 $msec^{-1}$.

The filter assembly was removed to allow sampling, which was performed following the method described in section 5.1.3. After each set of samples had been taken from the processor, the filter assembly was replaced and shaken to allow adhered material to fall back into the bulk powder bed. The walls of the processor were then knocked with a rubber mallet to allow material adhering to the internal surfaces of the processor to return to the powder bed.

7.2.2.3 Results

Expt. no.	Run 1	Run 2	Run 3	Mean	SD
Milling time (seconds)	Mean mass median particle diameter (μm)				
0	374	371	361	368	6.9
30	216	200	195	204	10.8
60	173	178	171	174	3.5
120	160	121	154	145	20.8
180	138	152	108	133	22.4
240	139	135	70	115	39.0
300	105	37	116	86	43.1
450	42	49	53	48	5.2
600	29	21	48	33	14.0
900	21	22	20	21	1.1
1200	18	21	19	20	1.4
1500	19	18	18	18	0.6
1800	25	17	19	20	4.0

Table 7.2. Mass median particle diameters obtained at different times during milling period of 30 minutes in SBSVP set up under following conditions:

Approximate nozzle air velocity: 75 $msec^{-1}$

High pressure air nozzle height: central position

High pressure air nozzle direction: co-current with high volume air nozzles

Expt. no.	Run 1	Run 2	Run 3	Mean	SD
Milling time (seconds)	Mean mass median particle diameter (μm)				
0	364	333	351	350	15.5
30	161	155	151	156	4.8
60	134	133	123	130	5.9
120	65	58	42	55	11.7
180	38	76	28	47	25.3
240	22	35	30	29	6.4
300	20	33	26	27	6.5
450	21	21	21	21	0.1
600	20	23	22	22	1.8
900	20	22	23	22	1.3
1200	21	21	23	22	1.3
1500	19	23	22	21	2.2
1800	17	23	22	21	3.0

Table 7.3. Mass median particle diameters obtained at different times during milling period of 30 minutes in SBSVP set up under following conditions:

Approximate nozzle air velocity: 105 $msec^{-1}$

High pressure air nozzle height: central position

High pressure air nozzle direction: co-current with high volume air nozzles

Expt. no.	Run 1	Run 2	Run 3	Mean	SD
Milling time (seconds)	Mean mass median particle diameter (μm)				
0	382	398	353	378	22.9
30	137	129	131	132	4.1
60	68	68	34	56	19.7
120	26	20	25	23	3.2
180	23	19	22	21	1.8
240	18	17	22	19	2.6
300	19	17	21	19	1.9
450	18	15	22	18	3.4
600	16	15	23	18	4.1
900	15	15	21	17	3.1
1200	16	15	22	17	3.6

Table 7.4. Mass median particle diameters obtained at different times during milling period of 20 minutes in SBSVP set up under following conditions:

Approximate nozzle air velocity: 135 $msec^{-1}$

High pressure air nozzle height: central position

High pressure air nozzle direction: co-current with high volume air nozzles

7.2.3 The effect of directing the high pressure nozzles to a position in opposition to the direction of the high volume air nozzles on the particle size reduction characteristics of SBSVP

7.2.3.1 SBSVP set up

The SBSVP was configured as described in section 7.2.2.1 except that, in this case, the air plenum was assembled in such a way that the high pressure air nozzle plate directed its airflows in an anticlockwise direction, i.e. counter-current to the high volume airflow from the flat nozzles.

7.2.3.2 Experimental conditions

The experimental conditions were those described in section 7.2.2.1.

7.2.3.3 Results

The results from each set of experiments are shown in tables 7.5 to 7.7.

Expt. no.	Run 1	Run 2	Run 3	Mean	SD
Milling time (seconds)	Mean mass median particle diameter (μm)				
0	389	388	335	371	30.8
30	198	193	188	193	4.9
60	171	162	170	168	4.8
120	157	148	134	147	11.6
180	145	121	114	127	16.2
240	106	101	54	87	28.4
300	124	106	65	98	30.4
450	41	41	24	35	9.5
600	67	45	26	46	20.4
900	31	27	24	27	3.4
1200	24	22	17	21	3.3
1500	22	25	22	23	2.0
1800	19	19	16	18	2.1

Table 7.5. Mass median particle diameters obtained at different times during milling period of 30 minutes in SBSVP set up under following conditions:

Approximate nozzle air velocity: 75 $msec^{-1}$

High pressure air nozzle height: central position

High pressure air nozzle direction: counter-current to high volume air nozzles

Expt. no.	Run 1	Run 2	Run 3	Mean	SD
Milling time (seconds)	Mean mass median particle diameter (μm)				
0	382	452	333	389	59.7
30	145	164	178	162	16.7
60	75	147	170	131	49.5
120	27	97	145	89	59.1
180	42	49	132	74	50.0
240	27	57	114	66	44.1
300	20	32	91	48	38.1
450	20	25	78	41	32.0
600	19	22	29	23	4.8
900	19	19	18	19	0.6
1200	19	18	17	18	1.1
1500	18	18	16	17	1.5
1800	18	16	17	17	0.7

Table 7.6. Mass median particle diameters obtained at different times during milling period of 30 minutes in SBSVP set up under following conditions:

Approximate nozzle air velocity: 105 $msec^{-1}$

High pressure air nozzle height: central position

High pressure air nozzle direction: counter-current to high volume air nozzles

Expt. no.	Run 1	Run 2	Run 3	Mean	SD
Milling time (seconds)	Mean mass median particle diameter (μm)				
0	360	317	329	335	21.9
30	167	186	162	171	12.4
60	156	146	146	149	5.8
120	81	101	110	97	14.5
180	70	50	32	51	19.1
240	35	39	31	35	4.1
300	24	36	26	29	6.5
450	18	19	17	18	0.9
600	15	16	15	16	0.4
900	17	16	15	16	1.3
1200	16	15	15	15	0.7

Table 7.7. Mass median particle diameters obtained at different times during milling period of 30 minutes in SBSVP set up under following conditions:

Approximate nozzle air velocity: 135 $msec^{-1}$

High pressure air nozzle height: central position

High pressure air nozzle direction: counter-current to high volume air nozzles

7.2.4 The effect of changing the height position of the high pressure nozzles on the particle size reduction characteristics of SBSVP

7.2.4.1 SBSVP configuration

The SBSVP was configured as described in section 7.2.2.1 except that, in this case, the air plenum was assembled in such a way that the high pressure air nozzle plate was positioned in either the top position or the bottom position and directed airflows in either an anticlockwise direction, i.e. counter-current to the high volume airflow from the flat nozzles or in a clockwise direction, i.e. co-current with the high volume airflow from the flat nozzles.

7.2.4.2 Experimental conditions

The experimental conditions were those described in section 7.2.2.1.

7.2.4.3 Results

The results from each set of experiments are shown in tables 7.8 to 7.11.

Expt. no.	Run 1	Run 2	Run 3	Mean	SD
Milling time (seconds)	Mean mass median particle diameter (μm)				
0	460	455	460	458	2.6
30	162	158	173	165	7.8
60	131	137	154	141	12.0
120	85	120	132	112	24.7
180	34	76	115	75	40.8
240	43	66	116	75	37.5
300	22	36	100	53	41.5
450	19	18	36	24	10.4
600	18	16	33	22	9.4
900	19	16	22	19	3.0
1200	19	15	21	19	3.1
1500	18	15	22	18	3.5
1800	18	16	21	18	2.5

Table 7.8. Mass median particle diameters obtained at different times during milling period of 30 minutes in SBSVP set up under following conditions:

Approximate nozzle air velocity: 105 $msec^{-1}$

High pressure air nozzle height: bottom position

High pressure air nozzle direction: co-current with high volume air nozzles

Expt. no.	Run 1	Run 2	Run 3	Mean	SD
Milling time (seconds)	Mean mass median particle diameter (μm)				
0	461	465	469	465	3.8
30	176	166	186	176	10.1
60	153	142	162	152	10.3
120	268	107	135	170	86.1
180	114	81	116	104	19.5
240	104	58	92	85	23.5
300	77	31	92	66	31.8
450	27	20	26	24	3.6
600	20	19	23	21	2.0
900	20	18	21	20	1.7
1200	19	17	20	19	1.4
1500	19	17	21	19	1.9
1800	19	16	20	18	1.6

Table 7.9. Mass median particle diameters obtained at different times during milling period of 30 minutes in SBSVP set up under following conditions:

Approximate nozzle air velocity: 105 $msec^{-1}$

High pressure air nozzle height: bottom position

High pressure air nozzle direction: counter-current to high volume air nozzles

Expt. no.	Run 1	Run 2	Run 3	Mean	SD
Milling time (seconds)	Mean mass median particle diameter (μm)				
0	464	471	463	466	4.2
30	179	148	167	165	16.0
60	153	141	143	146	6.3
120	133	107	130	123	14.6
180	118	81	104	101	18.6
240	93	62	33	63	29.8
300	90	46	31	56	30.4
450	28	24	27	26	2.1
600	25	23	22	24	1.5
900	23	21	20	21	1.2
1200	22	22	20	22	1.2
1500	22	22	22	22	0.3
1800	23	21	20	22	1.3

Table 7.10. Mass median particle diameters obtained at different times during milling period of 30 minutes in SBSVP set up under following conditions:

Approximate nozzle air velocity: 105 $msec^{-1}$

High pressure air nozzle height: top position

High pressure air nozzle direction: co-current with high volume air nozzles

Expt. no.	Run 1	Run 2	Run 3	Mean	SD
Milling time (seconds)	Mean mass median particle diameter (μm)				
0	463	444	459	455	10.3
30	199	191	251	213	32.7
60	170	159	187	172	14.2
120	153	140	155	149	8.4
180	136	137	141	138	2.2
240	109	110	119	113	5.3
300	99	105	132	112	17.6
450	25	81	113	73	44.6
600	23	46	67	45	21.6
900	21	24	32	26	5.8
1200	22	22	27	24	2.9
1500	22	20	21	21	1.3
1800	20	18	20	20	1.0

Table 7.11. Mass median particle diameters obtained at different times during milling period of 30 minutes in SBSVP set up under following conditions:

Approximate nozzle air velocity: 105 $msec^{-1}$

High pressure air nozzle height: top position

High pressure air nozzle direction: counter-current to high volume air nozzles

7.2.5 Discussion

Table 7.12 sets out a summary of the results obtained showing the following three sets of conditions:

(a) Nozzles at position M, in a clockwise direction and at three levels of pressure

(b) Nozzles at position M, in an anti-clockwise direction and at three levels of pressure

(c) Nozzles at the two other heights, at a fixed pressure of 245 kPa, and in a clockwise and anti-clockwise direction for each of the two heights.

The results from set (a) indicate that the rate of size reduction increases with increasing pressure but that the same level of size reduction is achieved at the end of the three processes.

Set (b) indicates a much lower difference in the rate of particle size reductions at the various pressures; the final particle size is similar in all cases to the results obtained in set (a).

Set (c) shows similar size reductions in all variations but again the final particle size is similar in all cases to the results obtained in sets (a) and (b).

It is of interest to note that starting material having somewhat different initial particle size characteristics nonetheless follow a similar size reduction pattern resulting in a similar final particle size in all cases.

When compared to the results obtained from FBSVP-A and FBSVP-B (see table 5.3), substantial reductions in final particle size were achieved in all cases. The degree of size reduction was at a level more suited to processing of powders for DPI use.

The variation between particle sizes determined for separate, identical runs was found to be consistently low after approximately 600 seconds processing time. The final deviation in all cases was well within acceptable commercial limits at the end of the process. This contrasts to high variability found during processing in the FBSVP-A and FBSVP-B.

This indicated that the design improvements were effective, providing a robust system lending itself to commercial validation.

7.2.6 Conclusions

The processor has been shown to be suitable for particle size reduction of excipient products for DPI use.

It is conceivable that the processor could be further developed to provide conditions suitable for micronisation of drug materials.

High pressure nozzle air outlet velocity ($msec^{-1}$)	Nozzle air directions	High pressure air nozzle height	Milling time (seconds)												
			0	30	60	120	180	240	300	450	600	900	1200	1500	1800
			Mean mass median particle diameter (μm)												
75	Co	M	368	204	174	145	133	115	86	48	33	21	20	18	20
105	Co	M	350	156	130	55	47	29	27	21	22	22	22	21	21
135	Co	M	378	132	56	23	21	19	19	18	18	17	17		
75	Counter	M	371	193	168	147	127	87	98	35	46	27	21	23	18
105	Counter	M	389	162	131	89	74	66	48	41	23	19	18	17	17
135	Counter	M	335	171	149	97	51	35	29	18	16	16	15		
105	Co	B	458	165	141	112	75	75	53	24	22	19	19	18	18
105	Counter	B	465	176	152	170	104	85	66	24	21	20	19	19	18
105	Co	T	466	165	146	123	101	63	56	26	24	21	22	22	22
105	Counter	T	455	213	172	149	138	113	112	73	45	26	24	21	20

Key:	
Counter - Counter-current	B - Bottom
Co - Co-current	M - Middle
	T - Top

Table 7.12. Summary of changes in mean mass median particle size during particle size reduction experiments in SBSVP.

7.3 Blend content uniformity of a dry powder inhaler formulation processed in SBSVP

7.3.1 Experimental conditions

The SBSVP was set up as described in section 7.1.2 and the high pressure air nozzle pressure set at 140 kPa. All other experimental conditions were as described in section 5.2.1.

7.3.2 Sampling

Sampling was conducted as described in section 5.2.2.

7.3.3 Results

The results from each experiment are shown in tables 7.13 to 7.17 below and a summary of the %RSD calculated from all five experiments is provided in tables 7.18 and 7.19.

Sample position	Processing time (seconds)					
	30	60	120	300	600	1200
	Nedocromil sodium trihydrate content (%w/w)					
A1	39.7	40.6	41.1	39.7	42.4	38.9
A2	38.5	40.7	40.0	39.5	39.2	38.7
B1	39.6	37.3	40.7	39.7	40.0	38.3
B2	38.7	39.2	40.1	38.9	40.8	41.8
C1	41.3	41.3	39.5	39.9	40.5	38.8
C2	38.9	39.2	39.5	39.2	39.5	40.1
D1	39.1	40.5	39.6	39.6	40.3	38.8
D2	37.7	40.7	39.6	39.7	41.6	39.0
E1	39.9	39.6	40.5	39.6	39.5	39.0
E2	42.7	40.6	40.7	39.9	39.6	39.6
Mean (A-E)	39.6	40.0	40.1	39.6	40.3	39.3
RSD (A-E)	3.7	2.9	1.5	0.8	2.6	2.6
Mean (A-C)	39.4	39.7	40.1	39.5	40.4	39.4
RSD (A-C)	2.6	3.7	1.6	0.9	2.9	3.4

Table 7.13. Content uniformity data from processing nedocromil sodium trihydrate formulation in SBSVP, experiment #1

Sample position	Processing time (seconds)					
	30	60	120	300	600	1200
	Nedocromil sodium trihydrate content (%w/w)					
A1	38.7	39.2	40.8	39.7	39.6	38.6
A2	38.9	39.6	41.4	40.1	39.0	38.8
B1	40.0	39.0	39.4	39.7	38.9	38.8
B2	39.2	41.3	41.2	39.8	38.8	38.9
C1	42.1	39.8	39.4	39.6	39.2	38.3
C2	40.0	40.1	40.8	39.7	39.0	38.5
D1	37.8	39.5	39.5	40.8	40.8	38.9
D2	39.0	35.3	40.2	40.2	39.8	39.1
E1	37.7	39.3	38.5	39.8	39.1	38.8
E2	39.6	39.8	39.4	39.8	39.0	39.3
Mean (A-E)	39.3	39.3	40.1	39.9	39.3	38.8
RSD (A-E)	3.2	3.9	2.4	0.9	1.5	0.7
Mean (A-C)	39.8	39.8	40.5	39.8	39.1	38.6
RSD (A-C)	3.1	2.0	2.2	0.4	0.7	0.6

Table 7.14. Content uniformity data from processing nedocromil sodium trihydrate formulation in SBSVP, experiment #2

Sample position	Processing time (seconds)					
	30	60	120	300	600	1200
	Nedocromil sodium trihydrate content (%w/w)					
A1	37.7	40.0	39.1	38.9	37.7	39.3
A2	39.6	39.6	39.3	39.0	38.1	38.5
B1	38.3	40.2	40.0	39.8	38.4	38.3
B2	39.2	40.0	39.6	39.5	38.4	39.2
C1	37.8	40.0	39.9	38.2	38.2	37.9
C2	37.7	40.1	40.7	38.7	38.0	37.9
D1	36.5	39.5	40.2	38.3	38.0	38.1
D2	38.9	39.8	40.4	38.9	38.6	38.1
E1	39.9	39.5	39.3	38.5	38.6	37.9
E2	40.1	39.9	40.2	38.7	38.3	37.1
Mean (A-E)	38.6	39.9	39.9	38.8	38.2	38.2
RSD (A-E)	3.0	0.6	1.4	1.3	0.8	1.7
Mean (A-C)	38.4	40.0	39.8	39.0	38.1	38.5
RSD (A-C)	2.2	0.5	1.5	1.4	0.7	1.7

Table 7.14. Content uniformity data from processing nedocromil sodium trihydrate formulation in SBSVP, experiment #3

Sample position	Processing time (seconds)					
	30	60	120	300	600	1200
	Nedocromil sodium trihydrate content (%w/w)					
A1	38.1	38.8	39.5	38.4	38.1	38.0
A2	39.8	39.1	39.3	38.5	38.3	38.8
B1	38.6	39.2	40.5	39.4	39.8	38.1
B2	40.1	39.2	39.7	38.5	39.0	39.0
C1	38.2	38.8	39.7	38.5	38.6	38.7
C2	38.7	39.1	38.8	38.5	38.7	38.8
D1	38.3	39.4	39.0	38.4	38.9	39.1
D2	37.8	38.7	38.7	39.1	39.2	39.2
E1	40.2	38.4	38.8	38.0	38.0	38.3
E2	40.0	38.8	40.0	38.5	38.5	38.8
Mean (A-E)	39.0	38.9	39.4	38.6	38.7	38.7
RSD (A-E)	2.4	0.8	1.5	1.0	1.4	1.1
Mean (A-C)	38.9	39.0	39.6	38.6	38.8	38.6
RSD (A-C)	2.1	0.5	1.4	0.9	1.5	1.1

Table 7.15. Content uniformity data from processing nedocromil sodium trihydrate formulation in SBSVP, experiment #4

Sample position	Processing time (seconds)					
	30	60	120	300	600	1200
	Nedocromil sodium trihydrate content (%w/w)					
A1	40.2	38.1	38.2	37.5	37.6	37.5
A2	40.1	41.5	38.1	38.7	38.2	37.6
B1	39.1	38.9	38.4	37.6	37.9	37.4
B2	39.0	38.8	38.9	37.9	41.6	37.4
C1	40.2	39.6	37.8	38.1	37.9	37.3
C2	43.1	38.6	38.2	37.8	38.0	37.2
D1	36.5	39.5	38.3	38.3	37.7	38.1
D2	37.6	39.2	38.8	38.3	38.0	37.3
E1	40.8	38.4	38.6	37.9	37.3	37.7
E2	40.3	38.4	38.3	38.5	37.8	38.7
Mean (A-E)	39.7	39.1	38.4	38.0	38.2	37.6
RSD (A-E)	4.5	2.5	0.8	1.0	3.2	1.2
Mean (A-C)	40.3	39.2	38.3	37.9	38.5	37.4
RSD (A-C)	3.7	3.1	0.9	1.1	3.9	0.4

Table 7.16. Content uniformity data from processing nedocromil sodium trihydrate formulation in SBSVP, experiment #5

Experiment number	Processing time (seconds)					
	30	60	120	300	600	1200
	% Relative standard deviation (n=10)					
#1	3.7	2.9	1.5	0.8	2.6	2.6
#2	3.2	3.9	2.4	0.9	1.5	0.7
#3	3.0	0.6	1.4	1.3	0.8	1.7
#4	2.4	0.8	1.5	1.0	1.4	1.1
#5	4.5	2.5	0.8	1.0	3.2	1.2

Table 7.17. Summary of percent relative standard deviation of content uniformity samples taken from positions A, B, C, D and E at different processing times during blending of nedocromil sodium trihydrate formulation in SBSVP.

Experiment number	Processing time (seconds)					
	30	60	120	300	600	1200
	% Relative standard deviation					
#1	2.6	3.7	1.6	0.9	2.9	3.4
#2	3.1	2.0	2.2	0.4	0.7	0.6
#3	2.2	0.5	1.5	1.4	0.7	1.7
#4	2.1	0.5	1.4	0.9	1.5	1.1
#5	3.7	3.1	0.9	1.1	3.9	0.4

Table 7.18. Summary of percent relative standard deviation of content uniformity samples taken from positions A, Band C only at different processing times during blending of nedocromil sodium trihydrate formulation in SBSVP.

7.3.4 Discussion

Comparing the results set out in table 7.17 using SBSVP to those obtained from FBSVP-B shown in table 5.7 it is evident that comparable %RSD levels are substantially different and that the improvements expected through redesign of the vessel have been achieved.

With the SBSVP the %RSD falls to below 5% within 30 seconds and below 2% within 2 minutes thus indicating a rapid speed of mixing.

There is no evidence of demixing occurring during extended mixing times and loss of fine particles is controlled within acceptable limits.

7.3.5 Conclusions

The SBSVP provided suitable mixing conditions for the powder system investigated and has the potential to be developed into a commercial product.

7.4 Functionality of a dry powder inhaler formulation processed in SBSVP

7.4.1 Experimental conditions and sampling

The samples collected during blend content uniformity testing as described in section 7.3 were also used for *in-vitro* aerosol functionality testing. Experimental conditions and sample treatment were otherwise as described in section 5.3.1.

7.4.2 Results

The results are presented in tables 7.19 to 7.24 below. A summary table of the %FPF values obtained throughout these experiments is given in table 7.25. Overall mean results are presented in graph 7.1.

Sample number	Processing time (seconds)																	
	30						60						120					
	C+D	S 1	S 2	Rec	DD	FPF	C+D	S 1	S 2	Rec	DD	FPF	C+D	S 1	S 2	Rec	DD	FPF
A1	1.3	3.4	2.6	91.2	6.0	43.9	1.5	3.4	2.9	97.1	6.3	45.9	1.4	3.0	3.1	93.2	6.1	50.8
A2	0.7	3.1	3.0	85.6	6.1	49.2	1.6	2.9	3.3	97.5	6.2	52.6	1.4	3.0	3.1	93.7	6.1	50.4
B1	1.4	3.2	3.0	95.7	6.2	48.0	1.4	3.1	2.9	93.7	6.1	48.4	1.5	3.3	2.8	94.0	6.0	46.2
B2	1.4	3.3	2.7	92.6	6.0	45.3	1.5	3.4	2.9	98.0	6.4	46.2	1.6	3.0	3.1	95.8	6.1	50.6
C1	1.5	3.9	2.4	97.4	6.3	38.0	1.6	3.3	2.9	98.2	6.3	47.0	1.5	3.1	3.1	96.4	6.3	50.3
C2	1.6	3.5	2.7	97.5	6.2	43.1	1.4	3.2	2.8	93.2	6.0	46.7	1.4	3.3	2.9	96.2	6.3	46.9
Mean	1.3	3.4	2.7	93.3	6.1	44.6	1.5	3.2	3.0	96.3	6.2	47.8	1.4	3.1	3.0	94.9	6.1	49.2
SD	0.3	0.3	0.2	4.6	0.1	4.0	0.1	0.2	0.2	2.3	0.1	2.5	0.1	0.1	0.1	1.4	0.1	2.1
RSD	22.4	8.5	8.5	4.9	2.3	9.0	5.2	5.7	5.2	2.3	2.2	5.2	4.9	4.6	4.4	1.5	1.7	4.3

Sample number	Processing time (seconds)																	
	300						600						1200					
	C+D	S 1	S 2	Rec	DD	FPF	C+D	S 1	S 2	Rec	DD	FPF	C+D	S 1	S 2	Rec	DD	FPF
A1	1.4	3.0	3.0	93.3	6.0	49.8	1.5	3.2	2.9	94.3	6.1	47.1	1.4	2.8	3.2	92.9	6.1	53.3
A2	1.5	3.1	3.3	98.8	6.4	52.0	1.4	3.4	2.8	95.3	6.2	45.1	1.5	2.6	3.4	93.2	6.0	57.2
B1	1.3	3.0	3.2	94.4	6.2	52.1	1.5	2.6	3.5	95.1	6.1	57.4	1.4	2.5	3.3	89.9	5.8	56.4
B2	1.5	3.1	3.1	96.4	6.2	50.1	1.5	2.8	3.4	96.4	6.2	54.5	1.5	2.8	3.3	93.9	6.0	54.3
C1	1.5	2.9	3.0	92.2	5.9	50.8	1.4	2.7	3.3	92.6	6.0	55.0	1.5	2.5	3.4	92.4	5.9	57.4
C2	1.4	3.3	2.9	94.4	6.2	47.4	1.5	2.8	3.1	92.0	5.8	52.6	1.6	2.5	3.3	91.4	5.8	56.9
Mean	1.4	3.1	3.1	94.9	6.2	50.4	1.5	2.9	3.2	94.3	6.1	52.0	1.5	2.6	3.3	92.3	5.9	55.9
SD	0.1	0.1	0.2	2.4	0.2	1.7	0.0	0.3	0.3	1.7	0.1	4.8	0.1	0.1	0.1	1.4	0.1	1.7
RSD	5.0	4.0	5.0	2.5	2.9	3.4	3.1	10.7	9.3	1.8	2.3	9.3	5.0	5.5	2.2	1.5	2.0	3.0

Key	
C+D	Dose recovered in capsule and device
S 1	Dose recovered in stage 1
S 2	Dose recovered in stage 2
Rec	Percent total recovery / nominal recovery
DD	Delivered dose (stage 1 + stage 2)
FPF	Fine particle fraction
SD	Standard deviation
RSD	Relative standard deviation

Table 7.19. *In-vitro* functionality data from TSI testing of samples obtained during processing of nedocromil sodium trihydrate formulation in SBSVP, experiment #1.

Sample number	Processing time (seconds)																	
	30						60						120					
	C+D	S 1	S 2	Rec	DD	FPF	C+D	S 1	S 2	Rec	DD	FPF	C+D	S 1	S 2	Rec	DD	FPF
A1	1.4	3.3	2.8	93.3	6.1	46.0	1.4	3.4	2.7	94.7	6.1	44.6	1.6	2.8	3.2	94.8	6.0	53.5
A2	1.5	3.4	2.6	93.0	6.0	42.8	1.5	3.2	3.2	97.9	6.3	50.1	1.6	3.2	3.1	98.8	6.3	48.7
B1	1.4	3.0	2.8	90.5	5.8	48.1	1.5	3.0	3.0	94.8	6.1	50.0	1.5	2.9	3.2	95.8	6.2	52.4
B2	1.7	2.9	3.1	96.2	6.0	51.3	1.6	2.8	3.1	94.6	5.9	52.7	1.6	3.2	2.8	94.3	6.0	46.6
C1	1.5	3.3	2.7	93.2	6.0	45.1	1.4	3.1	2.9	94.1	6.1	48.3	1.5	3.1	3.1	96.7	6.2	49.8
C2	1.5	3.2	3.1	97.3	6.3	48.9	1.6	3.0	3.0	95.0	6.0	50.5	1.9	2.8	3.4	100.8	6.2	54.4
Mean	1.5	3.2	2.8	93.9	6.0	47.0	1.5	3.1	3.0	95.2	6.1	49.4	1.6	3.0	3.1	96.9	6.1	50.9
SD	0.1	0.2	0.2	2.5	0.1	3.0	0.1	0.2	0.2	1.4	0.1	2.7	0.1	0.2	0.2	2.5	0.1	3.0
RSD	7.0	5.8	7.3	2.6	2.4	6.4	5.2	6.5	5.2	1.5	2.3	5.5	7.9	6.2	6.4	2.6	2.0	5.9

Sample number	Processing time (seconds)																	
	300						600						1200					
	C+D	S 1	S 2	Rec	DD	FPF	C+D	S 1	S 2	Rec	DD	FPF	C+D	S 1	S 2	Rec	DD	FPF
A1	2.0	2.4	3.1	93.2	5.5	56.3	1.6	2.8	3.0	91.8	5.8	52.4	1.5	2.6	3.4	94.6	6.1	56.7
A2	1.6	2.9	3.3	97.9	6.2	53.8	1.4	2.6	3.2	90.1	5.8	54.6	1.6	2.6	3.2	92.4	5.8	55.1
B1	1.5	2.9	3.4	98.1	6.3	53.8	1.5	2.7	3.2	93.4	5.9	54.1	1.5	2.8	3.2	94.6	6.0	53.4
B2	1.5	2.9	3.2	94.3	6.1	52.5	1.5	2.8	3.1	92.3	5.9	52.2	1.8	2.7	3.1	94.9	5.8	52.6
C1	1.7	2.8	3.2	96.0	6.0	53.7	1.9	2.4	3.4	95.4	5.8	58.7	1.3	2.9	3.1	90.8	5.9	52.0
C2	1.6	2.8	3.3	95.1	6.1	53.7	1.8	2.6	3.1	93.1	5.7	53.8	1.5	2.9	3.0	93.4	5.9	50.4
Mean	1.6	2.8	3.2	95.8	6.0	54.0	1.6	2.7	3.2	92.7	5.8	54.3	1.5	2.8	3.2	93.5	5.9	53.4
SD	0.2	0.2	0.1	2.0	0.3	1.2	0.2	0.1	0.1	1.8	0.1	2.4	0.1	0.1	0.2	1.6	0.1	2.3
RSD	10.8	6.9	3.4	2.1	4.7	2.3	11.0	5.6	4.3	1.9	1.4	4.3	9.7	4.8	5.0	1.7	1.9	4.2

Key	
C+D	Dose recovered in capsule and device
S 1	Dose recovered in stage 1
S 2	Dose recovered in stage 2
Rec	Percent total recovery / nominal recovery
DD	Delivered dose (stage 1 + stage 2)
FPF	Fine particle fraction
SD	Standard deviation
RSD	Relative standard deviation

Table 7.20. *In-vitro* functionality data from TSI testing of samples obtained during processing of nedocromil sodium trihydrate formulation in SBSVP, experiment #2.

Sample number	Processing time (seconds)																	
	30						60						120					
	C+D	S 1	S 2	Rec	DD	FPF	C+D	S 1	S 2	Rec	DD	FPF	C+D	S 1	S 2	Rec	DD	FPF
A1	1.6	3.1	2.9	94.5	6.0	48.6	1.3	3.3	3.1	97.5	6.5	48.4	1.7	3.0	2.9	95.2	5.9	49.9
A2	1.2	3.5	2.6	91.8	6.1	43.0	1.6	3.3	3.1	100.3	6.5	48.2	1.4	2.9	3.3	94.7	6.2	53.0
B1	1.3	3.5	2.8	95.4	6.3	44.8	1.5	3.1	3.1	95.6	6.2	50.4	1.4	2.8	3.3	93.7	6.1	53.5
B2	1.3	3.5	2.9	96.0	6.4	45.6	1.5	3.4	3.1	99.3	6.5	47.3	1.4	2.9	3.1	93.2	6.0	52.0
C1	1.6	3.4	2.5	94.2	5.9	42.7	1.6	3.0	3.1	96.9	6.1	50.6	1.4	3.1	3.1	94.1	6.2	50.4
C2	1.3	3.1	2.9	91.2	6.0	48.2	1.2	3.1	3.1	93.3	6.2	50.1	1.5	2.9	3.2	93.7	6.0	52.3
Mean	1.4	3.3	2.8	93.8	6.1	45.5	1.4	3.2	3.1	97.1	6.3	49.1	1.5	2.9	3.1	94.1	6.1	51.8
SD	0.2	0.2	0.2	2.0	0.2	2.5	0.1	0.2	0.0	2.5	0.2	1.4	0.1	0.1	0.1	0.7	0.1	1.4
RSD	12.7	5.7	6.1	2.1	3.2	5.5	9.9	5.2	0.9	2.6	2.6	2.8	8.7	2.8	3.7	0.8	1.6	2.8

Sample number	Processing time (seconds)																	
	300						600						1200					
	C+D	S 1	S 2	Rec	DD	FPF	C+D	S 1	S 2	Rec	DD	FPF	C+D	S 1	S 2	Rec	DD	FPF
A1	1.4	2.9	3.2	94.9	6.1	52.8	1.5	2.7	3.3	94.6	6.0	54.7	1.6	2.9	2.9	93.8	5.9	50.3
A2	1.6	2.8	3.2	95.0	6.0	53.8	1.7	2.6	3.2	92.9	5.8	55.3	1.5	2.7	3.2	91.8	5.9	54.0
B1	1.5	3.0	3.0	93.5	6.0	49.9	1.8	2.5	3.4	95.9	5.9	57.4	1.7	2.5	3.2	92.1	5.7	55.9
B2	1.5	3.0	3.3	97.6	6.3	51.8	1.5	3.0	3.0	93.8	6.0	50.2	1.7	2.8	3.0	92.3	5.7	51.6
C1	1.5	2.7	3.3	93.9	6.0	55.0	1.6	2.5	3.3	92.1	5.8	57.5	1.6	2.6	3.2	92.0	5.8	55.1
C2	1.6	2.6	3.5	95.5	6.1	57.6	1.6	2.7	3.2	93.5	5.9	54.4	1.4	2.8	2.9	88.7	5.7	50.8
Mean	1.5	2.8	3.3	95.1	6.1	53.5	1.6	2.7	3.2	93.8	5.9	54.9	1.6	2.7	3.1	91.8	5.8	52.9
SD	0.1	0.2	0.2	1.4	0.1	2.7	0.1	0.2	0.1	1.3	0.1	2.6	0.1	0.2	0.1	1.7	0.1	2.4
RSD	4.5	6.4	5.1	1.5	2.2	5.0	6.5	7.0	4.2	1.4	1.8	4.8	8.1	5.6	4.2	1.8	1.4	4.5

Key	
C+D	Dose recovered in capsule and device
S 1	Dose recovered in stage 1
S 2	Dose recovered in stage 2
Rec	Percent total recovery / nominal recovery
DD	Delivered dose (stage 1 + stage 2)
FPF	Fine particle fraction
SD	Standard deviation
RSD	Relative standard deviation

Table 7.21. *In-vitro* functionality data from TSI testing of samples obtained during processing of nedocromil sodium trihydrate formulation in SBSVP, experiment #3.

Sample number	Processing time (seconds)																	
	30						60						120					
	C+D	S 1	S 2	Rec	DD	FPF	C+D	S 1	S 2	Rec	DD	FPF	C+D	S 1	S 2	Rec	DD	FPF
A1	1.4	3.8	2.5	96.6	6.4	39.8	1.5	2.8	3.3	94.4	6.1	54.0	1.5	2.9	3.2	95.1	6.1	52.2
A2	1.3	3.5	2.8	96.1	6.3	44.8	1.4	3.0	3.1	93.3	6.0	50.9	1.5	2.8	3.1	93.5	5.9	52.6
B1	1.5	3.5	2.8	97.3	6.3	44.6	1.5	3.3	3.2	98.8	6.4	49.1	1.5	3.2	3.0	95.5	6.1	48.2
B2	1.4	3.7	2.7	97.0	6.3	41.9	1.6	3.2	3.0	97.2	6.2	47.7	1.6	2.8	3.2	95.1	6.0	53.0
C1	1.6	3.1	2.8	94.4	5.9	47.8	1.5	3.3	2.9	97.2	6.3	47.0	1.6	3.0	3.2	97.3	6.2	51.4
C2	1.4	3.5	2.7	95.5	6.2	42.8	1.4	3.3	3.0	96.5	6.3	47.4	1.4	2.8	3.3	93.1	6.1	53.8
Mean	1.4	3.5	2.7	96.1	6.3	43.6	1.5	3.1	3.1	96.2	6.2	49.4	1.5	2.9	3.2	95.0	6.1	51.9
SD	0.1	0.2	0.1	1.1	0.2	2.7	0.1	0.2	0.1	2.0	0.2	2.7	0.1	0.1	0.1	1.5	0.1	2.0
RSD	6.3	6.8	4.8	1.1	2.5	6.3	3.4	7.1	4.2	2.1	2.4	5.5	4.3	5.1	3.2	1.6	1.5	3.8

Sample number	Processing time (seconds)																	
	300						600						1200					
	C+D	S 1	S 2	Rec	DD	FPF	C+D	S 1	S 2	Rec	DD	FPF	C+D	S 1	S 2	Rec	DD	FPF
A1	1.5	3.0	3.0	92.9	6.0	50.1	1.6	3.0	3.1	96.3	6.1	50.5	1.6	2.5	3.4	93.3	5.9	57.3
A2	1.4	3.1	3.1	95.0	6.2	50.2	1.6	3.0	3.0	94.1	5.9	50.1	1.3	3.0	3.1	93.2	6.1	50.8
B1	1.6	2.7	3.2	94.0	5.9	53.8	1.6	2.7	3.1	92.3	5.8	53.9	1.4	2.9	3.1	92.2	5.9	52.1
B2	1.3	3.1	3.2	95.3	6.3	50.5	1.3	3.0	3.0	91.6	6.1	50.2	1.5	2.9	3.2	94.3	6.0	52.5
C1	1.7	2.8	3.0	94.3	5.8	51.9	1.4	3.1	3.0	94.1	6.1	49.6	1.4	2.7	3.3	92.0	5.9	54.9
C2	1.4	3.1	2.8	90.7	5.9	47.9	1.5	3.1	2.8	93.5	5.9	47.7	1.4	2.8	3.3	92.9	6.1	54.1
Mean	1.5	3.0	3.0	93.7	6.0	50.7	1.5	3.0	3.0	93.7	6.0	50.3	1.4	2.8	3.2	93.0	6.0	53.6
SD	0.1	0.2	0.1	1.7	0.2	2.0	0.1	0.2	0.1	1.6	0.1	2.0	0.1	0.2	0.1	0.8	0.1	2.3
RSD	9.2	5.2	4.5	1.8	3.0	3.9	8.9	5.3	3.5	1.8	2.0	4.0	6.7	6.2	3.3	0.9	1.6	4.3

Key	
C+D	Dose recovered in capsule and device
S 1	Dose recovered in stage 1
S 2	Dose recovered in stage 2
Rec	Percent total recovery / nominal recovery
DD	Delivered dose (stage 1 + stage 2)
FPF	Fine particle fraction
SD	Standard deviation
RSD	Relative standard deviation

Table 7.22. *In-vitro* functionality data from TSI testing of samples obtained during processing of nedocromil sodium trihydrate formulation in SBSVP, experiment #4.

Sample number	Processing time (seconds)																	
	30						60						120					
	C+D	S 1	S 2	Rec	DD	FPF	C+D	S 1	S 2	Rec	DD	FPF	C+D	S 1	S 2	Rec	DD	FPF
A1	1.4	3.7	2.8	97.9	6.4	42.9	1.3	3.1	3.2	96.0	6.4	50.9	1.6	3.2	3.1	98.4	6.3	49.1
A2	1.4	4.0	2.7	101.3	6.7	40.3	1.4	2.9	3.3	94.1	6.2	53.7	1.4	3.3	3.1	96.6	6.3	48.4
B1	1.2	3.4	2.9	93.7	6.3	45.7	1.3	3.0	3.3	94.4	6.3	52.5	1.4	2.8	3.3	93.2	6.0	53.9
B2	1.4	3.3	2.9	95.0	6.2	47.2	1.5	2.7	3.3	93.9	6.0	55.0	1.5	3.2	3.0	95.9	6.2	48.0
C1	1.4	3.5	2.8	96.8	6.3	44.2	1.8	2.8	3.1	95.7	5.9	52.0	1.4	3.2	3.0	95.0	6.2	48.5
C2	1.5	3.7	2.7	99.7	6.5	42.0	1.4	3.0	3.3	95.8	6.3	52.2	1.5	3.1	3.3	98.5	6.4	52.1
Mean	1.4	3.6	2.8	97.4	6.4	43.7	1.4	2.9	3.2	95.0	6.2	52.7	1.5	3.1	3.1	96.3	6.2	50.0
SD	0.1	0.3	0.1	2.8	0.2	2.5	0.2	0.2	0.1	0.9	0.2	1.4	0.1	0.2	0.1	2.0	0.1	2.4
RSD	7.0	7.0	3.2	2.9	2.6	5.7	12.8	5.4	2.7	1.0	3.1	2.7	5.2	5.7	4.8	2.1	2.1	4.9

Sample number	Processing time (seconds)																	
	300						600						1200					
	C+D	S 1	S 2	Rec	DD	FPF	C+D	S 1	S 2	Rec	DD	FPF	C+D	S 1	S 2	Rec	DD	FPF
A1	1.4	3.1	3.1	94.5	6.2	49.9	1.7	2.7	3.1	93.2	5.8	53.6	1.5	2.5	3.3	90.9	5.7	56.8
A2	1.5	2.9	3.3	95.7	6.1	53.1	1.4	2.8	3.0	90.1	5.8	52.1	1.4	2.9	3.2	93.6	6.1	53.2
B1	1.4	2.9	3.0	91.5	5.9	50.9	1.6	2.9	2.9	93.1	5.8	49.7	1.6	2.8	3.1	93.1	5.9	52.8
B2	1.4	2.9	3.2	93.9	6.1	52.3	1.4	2.7	3.0	89.5	5.7	53.1	1.6	2.4	3.3	90.8	5.6	58.0
C1	1.4	2.9	3.2	93.4	6.1	52.4	1.5	3.0	3.0	93.2	6.0	50.7	1.5	2.7	3.1	91.4	5.8	53.0
C2	1.5	2.7	3.1	91.0	5.8	53.0	1.5	2.9	3.2	94.7	6.1	53.0	1.4	3.1	3.2	97.7	6.4	50.9
Mean	1.4	2.9	3.1	93.4	6.0	51.9	1.5	2.8	3.1	92.3	5.9	52.0	1.5	2.7	3.2	92.9	5.9	54.1
SD	0.1	0.1	0.1	1.8	0.1	1.3	0.1	0.1	0.1	2.1	0.1	1.6	0.1	0.3	0.1	2.6	0.3	2.7
RSD	4.4	3.8	3.2	1.9	2.4	2.4	8.2	4.3	3.5	2.2	2.4	3.0	5.4	9.9	2.6	2.8	4.5	5.0

Key	
C+D	Dose recovered in capsule and device
S 1	Dose recovered in stage 1
S 2	Dose recovered in stage 2
Rec	Percent total recovery / nominal recovery
DD	Delivered dose (stage 1 + stage 2)
FPF	Fine particle fraction
SD	Standard deviation
RSD	Relative standard deviation

Table 7.23. *In-vitro* functionality data from TSI testing of samples obtained during processing of nedocromil sodium trihydrate formulation in SBSVP, experiment #5.

Expt. no.	Sample position	Processing time (seconds) 30	60	120	300	600	1200
		Percent fine particle fraction					
Expt #1	A1	43.9	45.9	50.8	49.8	47.1	53.3
Expt #1	A2	49.2	52.6	50.4	52.0	45.1	57.2
Expt #1	B1	48.0	48.4	46.2	52.1	57.4	56.4
Expt #1	B2	45.3	46.2	50.6	50.1	54.5	54.3
Expt #1	C1	38.0	47.0	50.3	50.8	55.0	57.4
Expt #1	C2	43.1	46.7	46.9	47.4	52.6	56.9
Expt #2	A1	46.0	44.6	53.5	56.3	52.4	56.7
Expt #2	A2	42.8	50.1	48.7	53.8	54.6	55.1
Expt #2	B1	48.1	50.0	52.4	53.8	54.1	53.4
Expt #2	B2	51.3	52.7	46.6	52.5	52.2	52.6
Expt #2	C1	45.1	48.3	49.8	53.7	58.7	52.0
Expt #2	C2	48.9	50.5	54.4	53.7	53.8	50.4
Expt #3	A1	48.6	48.4	49.9	52.8	54.7	50.3
Expt #3	A2	43.0	48.2	53.0	53.8	55.3	54.0
Expt #3	B1	44.8	50.4	53.5	49.9	57.4	55.9
Expt #3	B2	45.6	47.3	52.0	51.8	50.2	51.6
Expt #3	C1	42.7	50.6	50.4	55.0	57.5	55.1
Expt #3	C2	48.2	50.1	52.3	57.6	54.4	50.8
Expt #4	A1	39.8	54.0	52.2	50.1	50.5	57.3
Expt #4	A2	44.8	50.9	52.6	50.2	50.1	50.8
Expt #4	B1	44.6	49.1	48.2	53.8	53.9	52.1
Expt #4	B2	41.9	47.7	53.0	50.5	50.2	52.5
Expt #4	C1	47.8	47.0	51.4	51.9	49.6	54.9
Expt #4	C2	42.8	47.4	53.8	47.9	47.7	54.1
Expt #5	A1	42.9	50.9	49.1	49.9	53.6	56.8
Expt #5	A2	40.3	53.7	48.4	53.1	52.1	53.2
Expt #5	B1	45.7	52.5	53.9	50.9	49.7	52.8
Expt #5	B2	47.2	55.0	48.0	52.3	53.1	58.0
Expt #5	C1	44.2	52.0	48.5	52.4	50.7	53.0
Expt #5	C2	42.0	52.2	52.1	53.0	53.0	50.9
Mean		**44.9**	**49.7**	**50.8**	**52.1**	**52.7**	**54.0**
SD		**3.1**	**2.7**	**2.3**	**2.3**	**3.2**	**2.4**
RSD		**6.8**	**5.3**	**4.6**	**4.3**	**6.1**	**4.4**

Table 7.24. Summary of percent fine particle fraction determined for samples obtained during processing of nedocromil sodium trihydrate formulation in SBSVP, experiments #1 to #5.

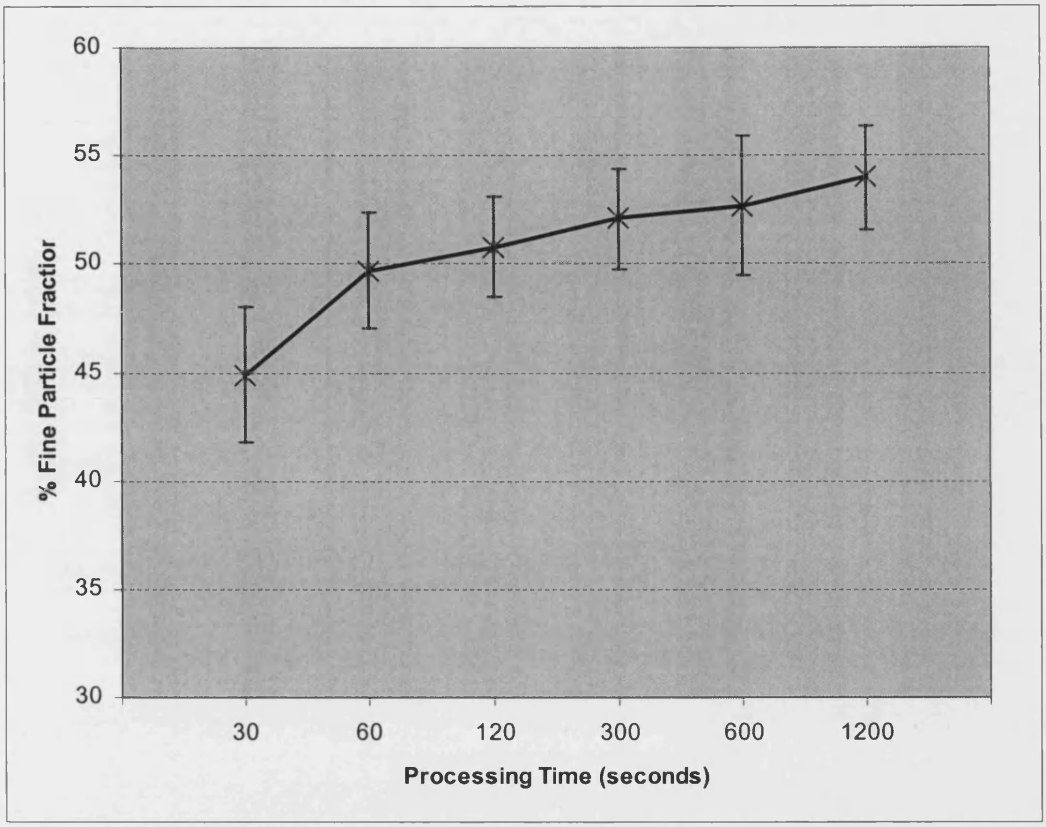

Graph 7.1. Graph showing mean %FPF results of five batches of nedocromil sodium DPI formulation at different processing times in FBSVP-B.

7.4.3 Discussion

A comparison of the results set out in table 7.24 using SBSVP to those obtained from FBSVP-B shown in table 5.14 indicates that comparable %FPF levels are substantially different and that the improvements expected through redesign of the vessel have been achieved.

The mean standard deviation value during the last 900 seconds of processing time for the SBSVP was 2.6% and the mean %FPF was 52.9%. This compares to a value of 5.0% for the mean standard deviation value during the last 900 seconds of processing time in the FBSVP-B and a %FPF of 43.5%.

After 60 seconds of processing the %FPF remained constant over a period of 20 minutes processing time. This robustness is considered highly desirable in production of DPI blends.

Comparison of graphs 7.1 and 5.2 clearly illustrate the improvements achieved in the redesign of the vessel.

7.4.4 Conclusions

The environment generated within the SBSVP provided suitable conditions of high shear which were suitable for robust and reliable production of nedocromil sodium blends for dry powder inhalation.

It is considered that the SBSVP could be developed for commercial application in processing of a DPI formulations in a manner well suited to meet the validation requirements of cGMP.

8. GENERAL DISCUSSION

More specific discussions are presented with each part of the experimental work in sections 3.3.3.4, 5.1.5, 5.2.4, 5.3.3, 7.2.5, 7.3.4 and 7.4.3.

8.1 Overview of design development and comparison with conventional processes

An initial processor was developed, the FBSVP-A, which was characterised for its performance in reducing the particle size of two grades of lactose and for dry blending of a lactose/fine particle sodium chloride powder system.

Although some particle size reduction was observed and mixing performance was found to be superior to a turbulent tumbling method, large areas of low powder activity were observed in certain regions of the vessel. In addition to these problems it was found that the cyclone system employed for arrestment of particles from air exiting from the vessel was inefficient which, along with other leakages, caused a large proportion of fine material to be lost from the processor.

In order to address these faults the vessel was redesigned by replacing the cyclone separator with a bag filter and lowering the high pressure air nozzles, resulting in the fabrication of a new processor, the FBSVP-B. These design modifications were found to greatly increase the degree of fluidisation of the powder bed, thus reducing regions of low activity, although these were not completely eliminated. The problems

of escape of excessive amounts of powder from the vessel were largely solved by the inclusion of the filter bag.

A CFD simulation model was constructed for the processor in which a number of areas of low flow activity were predicted.

The FBSVP-B was characterised for its performance in size reducing a lactose material, which was selected to allow a direct comparison to be made with the comminuting performance of the FBSVP-A.

One minor modification to the vessel was the application of antistatic tape to all polymeric vessel surfaces since these were found to become electrostatically charged during operation (i.e. vessel walls and central cone). This was found to assist in reducing the amount of material adhered to the vessel wall and also to reduce the degree of adhesion of material that did become attached to the walls during processing.

The perceived extent and rate of milling were increased in the redesigned vessel and this was attributed to two factors; these were firstly improved milling efficiency due to repositioning of the air nozzles close to the vessel base and secondly a reduction in the expulsion of fine material from the vessel as a result of replacing the cyclone with a filter bag.

In investigating the use of the FBSVP-B for processing a DPI nedocromil sodium formulation it was found that selected parts of the vessel were able to produce

homogeneous blends but that samples from those areas of the processor that were predicted by the CFD simulations to exhibit poor flow characteristics were considerably less homogeneous. It was therefore concluded that the CFD model was able to predict the flow characteristics of the processor and that a redesign was necessary in order to eliminate areas of low flow activity.

The functionality of the nedocromil sodium blends was also evaluated in terms of *in-vitro* aerosol particle characteristics. The results obtained for %FPF were somewhat variable but compared well to alternative techniques of blending reported in other studies (Clarke, 1998) for a similar formulation as did those for blend homogeneity.

In Clarke's investigations content uniformities characterised by RSDs of 1.35% and 2.28% were obtained from blends manufactured using hand blending in a pestle and mortar and blends processed in a high shear mixer respectively. The mean %RSD for blends after 2 minutes of processing in the FBSVP-B was 2.72%.

The %FPF results for blends produced in the FBSVP-B displayed a mean value of 43% which compared to 33% FPF in Clarke's pestle and mortar mixing and 50% FPF for blends produced in a high shear blender. This was thought to indicate that the shear levels generated in the FBSVP-B were somewhere in-between those generated in pestle and mortar mixing and processing in a bladed high shear system.

In order to address the need for greater shear forces, improve flow activity throughout the vessel environment and hence increase blend content uniformity, a further vessel was designed using CFD technology to optimise air input trajectories.

This redesigned equipment was termed the SBSVP and employed high volume air transmitted tangentially to the powder bed rather than vertical fluidising air. In addition, the number of high pressure air nozzles was doubled from 12 to 24. The total energy input from these nozzles was much increased compared to those in the FBSVP-B as the air velocity output from each nozzle was maintained at the same level as that provided by FBSVP-B nozzles by increasing the pressure and volume of the supply air. It was also possible to alter the height and direction of these nozzles to achieve optimal performance.

The increased energy supplied to the processing environment within the new vessel was apparent by a dramatic increase in the rate and extent of milling when similar lactose materials to those investigated in previous vessels were presented to the processor for size reduction testing. Median particle size of lactose granules was found to reduce from 460μm to 23μm within 2 minutes in the SBSVP at the optimal vessel configuration compared to a maximum reduction in the median size of similar material to 141 μm in 20 minutes processing in the FBSVP-B.

When applied to processing of the nedocromil sodium DPI formulation, the SBSVP again showed improved characteristics over its predecessor.

Activation of the powder bed was extensive, resulting in rapid attainment of blend homogeneity; %RSDs were obtained that were consistently below 5% after only 30 seconds of processing time. A mean RSD of 1.5% was attained at mixing times in excess of two minutes.

The increased shear available in the SBSVP also had a beneficial effect on *in-vitro* aerosol deposition characteristics of the blends. These were characterised by a mean %FPF of 51% after two minutes mixing, rising to 54% after twenty minutes. Variability between blends was low and changes in functionality over extended mixing times were small.

This robustness in the process was considered highly desirable since other DPI formulations have been known to be particularly susceptible to deterioration in performance due to mixing time effects.

8.2 Future work

Since the nedocromil sodium formulation appeared to be influenced by the amount of shear imparted into it during mixing, a future study could investigate the effects of increasing the high pressure air nozzle velocity on blend performance.

The performance of a range of DPI powder systems using different drugs for processing in the SVP equipment would also make a useful study.

It is possible that the SVP equipment could be further developed to produce wet granulation products; this could provide an alternative to bladed high shear systems which if successful could potentially offer closer control of processing conditions.

A number of modifications to the vessel configuration and fabrication could be considered in future work.

It is thought that fabrication of the processor from mirror polished stainless steel may decrease adhesion of material to the vessel walls and also allow control of electrostatics during production of DPI or other powder blends.

Further studies might also involve optimisation of the vessel height, which could be variable for different operations.

The application of CFD technology to vessel design has proved particularly successful and it is anticipated that further work would benefit immensely from increased use of this tool.

For example, CFD models may be developed that predict the effects of changes to the swept bed or high pressure nozzle characteristics.

A particularly interesting area is the use of CFD in predicting the movement of solid and also liquid particles under the influence of fluid flows. Two phase and three phase models could therefore be constructed to further investigate and optimise vessel performance.

It is anticipated that further development of the vessel could potentially result in a capability for performing micronisation of drug and/or excipient particles, thus providing a complete processing environment for powders for inhalation.

9. CONCLUSIONS

A series of three novel air driven powder processors was developed and each characterised for its performance in processing pharmaceutical powder systems.

The first vessel, the FBSVP-A, operated using a fluidised bed and tangential high pressure air nozzles to provide powder agitation. The processor was found to provide some particle size reduction performance when used to mill two different grades of granular lactose. Processing of a simple binary ordered mix to within acceptable blend homogeneity parameters was also found to be possible within this vessel.

However, the FBSVP-A was found to exhibit large regions of powder stagnation during normal operation, leading to inefficiency in particle size reduction and mixing performance. This was found to be due largely to difficulties with the efficiency of cyclone separation apparatus employed for particle arrestment.

It was concluded that modifications to the equipment were required and a second processor was therefore developed, the FBSVP-B.

Characterisation of the FBSVP-B indicated that particle size reduction characteristics were slightly improved over the previous design.

Manufacture of a nedocromil DPI formulation was carried out and the FBSVP-B found to produce blends of poor overall content uniformity. *In-vitro* aerosol

performance of the blends was found to be less efficient and more variable than that of blends produced using conventional high shear techniques.

It was concluded that increased levels of shear energy were required in the processing environment to improve dispersal of the formulation components.

It was apparent that areas of powder stagnation were also occurring in the FBSVP-B. These were observed in CFD simulation predictions of the fluid flows in the vessel. A further redesign was therefore deemed necessary.

Furthermore it was recognised that the concurrence of CFD flow predictions with observed conditions provided verification of the capability of this software to reliably predict complex fluid flows in this application and CFD simulation models were therefore used as an aid in redesigning the vessel.

The final vessel design, the SBSVP, utilised high volume tangential air flows in place of vertical fluidising air and contained an increased number of tangential high pressure air nozzles compared to the FBSVP-B. Design of the high pressure air nozzles was determined by CFD simulations

Particle size reduction in the SBSVP was found to be rapid and extensive. It is concluded that further refinement of the vessel design would result in a processor with satisfactory milling performance in producing fine particle excipients for inhalation products and that it may eventually be possible to utilise equipment based around this design for micronisation of drug powders for inhalation.

On characterisation of the performance of the SBSVP for blending the type of nedocromil formulations examined in the previous design, it was found that the processor produced very homogeneous mixtures with comparable *in-vitro* aerosol performance to optimal processing using conventional techniques.

Hence it was concluded that a processor utilising controllable fluid dynamics and designed with the aid of CFD modelling technology was capable of providing uniform high shear conditions, ideal for consistently producing nedocromil sodium trihydrate blends for inhalation and potentially having a use as an alternative to conventional mixing equipment for DPI and other pharmaceutical blend production.

10. REFERENCES

Akbarieh, M. and Tawashi, R. (1987). Morphic features of solid particles after micronisation in the fluid energy mill. *International Journal of Pharmaceutics.* **35**, 81-89.

Akiyama, T. and Tada, I. (1984). Mixing characteristics of the positive and negative pressure air mixers. *Industrial Engineering and Chemical Process Design and Development.* **23**, 737-741.

Akiyama, T. and Tada, I. (1985). Entropy generation and work due to the jetting air stream in air mixers. *Industrial Engineering and Chemical Process Design and Development.* **24,** 961-966.

Akiyama, T., Peters, L.K., Kageyama, S., Hosoi, M. and Yokota, I. (1982). Mixing characteristics of particulate material in a negative pressure air mixer. *Industrial Engineering and Chemical Process Design and Development.* **21**, 664-670.

Akiyama, T., Zhang, J.Q., Egawa, M. and Kojima, H. (1986). Mixing of fine particles by means of a negative pressure air mixer. *Industrial Engineering and Chemical Process Design and Development.* **25**, 682-687.

Albus, F.E. (1964). The modern fluid energy mill. *Chemical Engineering Progress.* **60**(6), 102-106.

Allen, T. (1990). Particle size measurement. Fourth Edition. Chapman and Hall. London, U.K.

Anon. (1966). Mixing of powders with compressed air. *British Chemical Engineering.* **11**(7), 725.

Ashton, M.D. and Valentin, F.H.H. (1966). The mixing of powders and particles in industrial mixers. *Transactions of the Institution of Chemical Engineers.* **44**, T166-T188.

Ashurst, I., Malton, A., Prime, D. and Sumby, B. (2000). Latest advances in the development of dry powder inhalers. *Pharmaceutical Science and Technology Today* **3**(7), 246-256.

Asking, L. and Olsson, B. (1997). A model for the effect of inhalation device flow resistance on the peak inspiratory flow rate and its application in pharmaceutical testing. *Journal of Aerosol Medicine.* **7**, 201-204.

Bates, M.J. and Ball, J.G., (1993). Design of a single vessel pharmaceutical processor under computer control. Project report A08. Department of Mechanical Engineering. University of Bath, Bath, U.K.

Berressem, P. (1999). The birth of new delivery systems. *Chemistry in Britain.* 29–32.

British Pharmacopoeia, (1993). HMSO: London.

Cairns, H., Cox, D., Gould, K.J., Ingall, A.H. and Suschitzky, J.L. (1985). New anti-allergic pyrano[3,2-g]quinoline-2,8,-dicarboxylic acids with potential for the topical treatment of asthma. *Journal of Medicinal Chemistry.* **28**, 1832–1842.

Clarke, M.J. (1998). An investigation into the interparticle forces governing the performance of nedocromil sodium as a dry powder inhalation system. Ph.D. Thesis, University of Bath, Bath, U.K.

Clarke, M.J., Potter, U.J., Gilpin, C., Tobyn, M.J. and Staniforth, J.N. (1998). Imaging of hygroscopic ultrafine pharmaceutical powders using low temperature and environmental scanning electron microscopy. *Pharmacy and Pharmacology Communications.* **4**, 419–425.

Crompton, G.K. (1982). Problems patients have using pressurised aerosol inhalers. *European Journal of Respiratory Diseases.* **63**(suppl. 119), 101–104.

Davidson, J.F., Clift, R. and Harrison, D. (Eds.). (1985). Fluidization. Second Edition. Academic Press, London, U.K.

Dotson, J.M. (1962). Extending the range of jet mills. *Industrial and Engineering Chemistry.* **54**(2), 62-65.

French, D.L., Edwards, D.A. and Niven R.W. (1996). The influence of formulation on emission, deaggregation and deposition of dry powders for inhalation. *Journal of Aerosol Science.* **27**(5), 769–783.

Ganderton, D. and Kassem, N.M. (1992). Dry powder inhalers. In: Ganderton, D. and Jones, T. (eds.), Advances in Pharmaceutical Sciences. Vol. 6 Academic press. London 165–191.

Gerrity, T.R. (1990). Pathophysiological and disease constraints on aerosol delivery. In Byron, P.R., (ed.), Respiratory Drug Delivery, CRC Press Inc, Florida. 1–38.

Ghosh, B. (1993). Fluidized-bed jet milling of ceramics. *Ceramic Engineering and Science Proceedings.* **14**(1-2), 264-270.

Gonda, I. (1988). Therapeutic aerosols. In: Aulton, M.E. (ed.), Pharmaceutics: The Science of Dosage Form Design. Churchill Livingstone, Edinburgh. 341–358.

Gonda, I. (1992). Targeting by deposition. In: A.J. Hickey (ed.), Pharmaceutical Inhalation Technology. Marcel Dekker, New York, 61–82.

Hallworth, G.W. and Westmoreland, D.G. (1987). The twin impinger; A simple device for assessing the delivery of drugs from metered dose pressurised aerosol inhalers. *Journal of Pharmacy and Pharmacology.* **39**, 966–972.

Harnby, N. (1967). A comparison of the performance of industrial solids mixers using segregating materials. *Powder Technology.* **1**, 94-102.

Hauser, G. (1992). Hygienic design of moving parts of machines in the food industry. ICHEME Symposium. Series No. 126. 435-445.

Hersey, J.A. (1975). Ordered Mixing: A new concept in powder mixing practice. *Powder Technology.* **11**, 41–44.

Hickey, A.J., Concessio, N.M., Van Oort, M.M. and Platz, R.M. (1994). Factors influencing the dispersion of dry powders as aerosols. *Pharmaceutical Technology.* **August**, 58–82.

Hickey, A.J. and Dunbar, C.A. (1997). A new millennium for inhaler technology. *Pharmaceutical Technology.* **June**, 116–125.

Hinds, W.C. (1982). Aerosol technology: properties, behaviour and measurement of airborne particles. Wiley Interscience: New York.

Holgate, S.J. (1996). The efficacy and therapeutic position of nedocromil sodium. *Respiratory Medicine.* **90**, 391–394.

Holm, P. (1987). Effect of impeller and chopper design on granulation in a high speed mixer. *Drug Development and Industrial Pharmacy.* **13**(9-11), 1675-1701.

Holzner, P.M. and Müller, B.M. (1995). Particle size determination of metered dose inhalers with inertial separation methods: apparatus a and b (bp), four stage impinger and anderson mark II cascade impactor. *International Journal of Pharmaceutics.* **116**, 11–18.

Johnson, K.A. (1997). Preparation of peptide and protein powders for inhalation. *Advanced Drug Delivery Reviews.* **26**, 3–15.

Khankari, R., Chen, L. and Grant, D.J.W. (1998). Physical characterisation of nedocromil sodium hydrates. *Journal of Pharmaceutical Sciences.* **87**(9), 1052–1061.

Kontny, M.J. and Mulski, C.A. (1989). Gelatin capsule brittleness as a function of relative humidity at room temperature. *International Journal of Pharmaceutics.* **54**, 79–85.

Krambrock, W. (1976). Mixing & homogenising of granules bulk material in a pneumatic mixer unit. *Powder Technology.* **15**, 199-206.

Lantz, R.J. and Schwartz, J.B. (1981). Mixing. In: H.A. Lieberman and L. Lachman (Eds.). Pharmaceutical Dosage Forms. Volume 2: Tablets. Marcel Dekker Inc., New York, U.S.A. 1-53.

Leach, C. (1999). Site directed aerosol delivery of hfa-beclomethasone to the lungs. *Drug delivery to the Lungs IX*, The Aerosol Society, London, U.K., 7–11.

Leach, C.L. (1995). Approaches and challenges to the use of freon propellants replacements. *Aerosol Science and Technology.* **22**(4), 328–334.

Leschonski, K. and Menzel, U. (1986). Experimental investigations on single plate fluid energy milling. 1st World Congress Particle Technology, Nurnberg, Germany. Preprints. Part II: Comminution. 297-323.

Lord, J.D. and Staniforth, J.N. (1996). Particle size effects on packing and dispersion of powders. In: Byron, P.R., Dalby, R.N. and Farr, S.J. (eds.), Respiratory Drug Delivery V, Interpharm Press, Buffalo Grove, IL., 75–84.

Louey, M.D., Mulvaney, P. and Stewart, P.J. (2000). Investigation of mechanisms of action of ternary components in dry powder formulations. Respiratory Drug Delivery VII. **II**, 439–442.

Lucas, P., Anderson, K. and Staniforth, J.N. (1998). Protein deposition from dry powder inhalers: fine particle multiplets as performance modifiers. *Pharmaceutical Research.* **15**(4), 560–567.

MacGregor, S.A., Newnes, L.B., Li, M, Staniforth, J.N., Tobyn, M.J., Kay, G.R., Horrill, M.D., Lamming, R.C. and Hajee, D.W., Wong, D., Chippendale, K.E., Page,T. (1999). The application of computational fluid dynamics to the development of a pharmaceutical processor. *Proceedings of the Institute of Mechanical Engineers* **213** B, 737-740.

Makin, L.A., Rowley, G. and Fletcher, E.J. (1997). An investigation of carrier particle type, electrostatic charge and relative humidity on *in-vitro* drug deposition from dry powder inhaler formulations. *Pharmaceutical Sciences* **3**, 583–586.

McDonald, D.P. (1971). Micronisation. *Manufacturing Chemist and Aerosol News.* (May), 39.

Miles, J.E.P. and Schofield, C. (1970). Performance of several industrial mixers using non-segregating free flowing powders. *Transactions of the Institution of Chemical Engineers.* **48**, T85-T89.

Nair, P.B.R. and Ramanujam, M. (1986). Modelling of grinding in a fluid energy mill. 1st World Congress Particle Technology, Nurnberg, Germany. Preprints. Part II: Comminution. 359-372.

Nair, P.B.R. and Ramanujam, M. (1991). Classification function in fluid energy grinding. *Powder Technology.* **68**, 79-84.

Newman, S.P. and Clarke, S.W (1983). Therapeutic aerosols I – physical and practical considerations. *Thorax.* **38**, 881–886.

Niven, R.W. (1995). Delivery of biotherapeutics by inhalation aerosol. *Critical Reviews in Therapeutic Drug Carrier Systems.* **12**(2&3), 151-231.

Nyce, J., Leonard, S.A. and Gillum, A.M. (2000). Respirable antisense oligonucleotides (RASONs): formulation and delivery in theory and fact. Respiratory Drug Delivery VII. **I**, 13–17.

Parrott, E.L. (1976). Milling. In: L. Lachman, H.A. Lieberman and J.L. Kanig (Eds.). The Theory and Practice of Industrial Pharmacy. Second Edition. Lea and Febiger, Philadelphia, U.S.A. 466-485.

Patton, J.S. (1996). Mechanisms of macromolecule absorption by the lungs. *Advanced Drug Delivery Reviews.* **19**, 3-36.

Peart, J. (1996). Electrostatic charge interactions in pharmaceutical dry powder aerosols. Ph.D. Thesis, University of Bath, Bath, U.K.

Pharmaceutical Handbook (1980). 19th edition, The Pharmaceutical Press, London.

Prem, H. (1984). Jet grinding in the fluidised bed. *Proceedings of the 9th Annual Powder and Bulk Solids Conference* . 649-663.

Prem, H. and Eddington, D. (1988). Contamination - free processing of pyrophoric rare earths and abrasive ceramic powders. *Proceedings of the 8th Industrial Minerals International Congress* . 204-211.

Prior, M.H., Prem, H. and Rhodes, M.J. (1990). Size reduction. In: M.J. Rhodes (Ed.). Principles of Powder Technology. John Wiley and Sons, Chichester, U.K. 227-297.

Rees, J.E. (1977). Mixing of particulate solids to ensure homogeneity of dosage forms: The need for a critical approach to pharmaceutical process development. *Estratto da Bollettino Chimico Farmaceutico.* **116**, 445.

Rowe, P.N. and Nienow, A.W. (1976). Particle mixing and segregation in gas fluidised beds. A review. *Powder Technology.* **15**, 141-147.

Rumpf, H. (1959). Loading theory of impact size reduction. *Chemie-Ing.-Tech.* **31**(5), 323-337.

Rumpf, H. (1960). Principles of impact size reduction and their application to jet grinding. *Chemie-Ing.-Tech.* **32**(3), 129-135.

Schæfer, T. (1988). Equipment for wet granulation. *Acta Pharmaceutica Suecica.* **25**(4-5), 205-228.

Scott, R.A. (1957). Mixing of solids. In: H.W. Cremer and T. Davies (Eds.). Chemical Engineering Practice. Volume 3: Solid Systems. Butterworths Scientific Publications, London, U.K. 362-379.

Shakhova, N.A. and Minayev, G.A. (1972). Aerodynamics of jets discharged into fluidised beds. *Heat Transfer - Soviet Research.* **4**(1).

Simon, E.J. (1975). Fluid bed processing of bulk solids. Presented at: *Third* International Powder Technology and Bulk Solid Conference. Powtech '75. Harrogate, U.K. (Thurs 20th Feb).

Smit, W.A.J. (1986). Jet milling of heat sensitive materials. 1st World Congress Particle Technology, Nurnberg, Germany. Preprints. Part II: Comminution. 345-357.

Smith, P.L. (1997). Peptide delivery via the pulmonary route: a valid approach for local and systemic delivery. *Journal of Controlled Release.* **46**, 90–106.

Smith, S.J. and Bernstein, J.A. (1996). Therapeutic uses of lung aerosols. In Hickey, A.J. (ed.), Inhalation Aerosols: Physical and Biological Basis for Therapy. Marcel Dekker, Inc., New York, U.S.A. 234–269.

Staniforth, J.N. (1981). Total mixing. *International Journal of Pharmaceutical Technology and Product Manufacture.* **2**(1), 7–12.

Staniforth, J.N. (1982). Advances in powder mixing and segregation in relation to pharmaceutical processing. *International Journal of Pharmaceutical Technology and Product Manufacture.* **3**(suppl), 1–12.

Staniforth, J.N. (1987). Out of order chaos. *Journal of Pharmaceutical and Pharmacology.* **39**, 329–334.

Staniforth, J.N. (1996). Pre-formulation aspects of dry powder aerosols. In: Byron, P.R., Dalby, R.N. and Farr, S.J. (eds.), Respiratory Drug Delivery V, Interpharm Press, Buffalo Grove, IL., 65–73.

Stanley-Wood, N.G. (1990). Size enlargement. In: M.J. Rhodes (Ed.). Principles of Powder Technology. John Wiley and Sons, Chichester, U.K. 193-226.

Steckel, H. and Müller, B.W. (1997). *In-vitro* evaluation of dry powder inhalers II: Influence of carrier particle size and concentration on *in-vitro* deposition. *International Journal of Pharmaceutics.* **154**, 31–37.

Stewart, P.J. (1986). Particle interactions in pharmaceutical systems. *Pharmacy International.* **7**, 146–149.

Tansey, I.P. (1997). Changing to CFC-free inhalers: The technical and clinical challenges. *The Pharmaceutical Journal.* **259**, 896–898.

Teichmann, E. (1967). Possibilities and limitations of mechanical mixing of solids with special reference to pneumatic mixing. *Verfahrenstechnik.* **1**(5), 225-230.

Timsina, M.P., Martin, G.P., Marriott, C., Ganderton, D. and Yianneskis, M. (1994). Drug delivery to the respiratory tract using dry powder inhalers. *International Journal of Pharmaceutics.* **101**, 1–13.

Travers, D.N. and White, R.C. (1971). The mixing of micronised sodium bicarbonate with sucrose crystals. *Journal of Pharmacy and Pharmacology.* **23**, 260S–261S.

Trofast, E.A.C. and Falk, E.J. (1996). Agglomeration of finely divided powders. U.S. Patent No. 5551489.

Versteeg, H.K. and Malalasekera, W. (1995). Introduction to computational fluid dynamics: the finite volume method, Longman, Harlow, Essex, U.K.

Versteeg, H.K., Hargrave, G., Harrington, L., Shrubb, I. And Hodson, D. (2000). The use of Computational Fluid Dynamics (CFD) to predict pMDI air flows and aerosol plume formation. Respiratory Drug Delivery VII. **I**, 257–264.

Vidgren, M., Kärkkäinen, A., Karjalainen, P., Nuutinen, J. and Paronen, P. (1988). *In-vitro* and *in-vivo* deposition of drug particles inhaled from pressurised aerosol and dry powder inhaler. *Drug Development and Industrial Pharmacy* **14**(15–17), 2649–2665.

Vidgren, M.T., Paronen, T.P., Kärkkäinen, A. and Karjalainen, P. (1987). Effect of extension devices on the drug deposition from inhalation aerosols. *International Journal of Pharmaceutics*. **39**, 107–112.

Whitehead, A.B. (1985). Distributor characteristics and bed properties. In: J.F. Davidson, R. Clift and D. Harrison (Eds.). Fluidization. Second Edition. Academic Press, London, U.K. 173-199.

Williams, J.C. (1968). The mixing of dry powders. *Powder Technology*. **2**, 13-20.

Wong, D.Y.T., Wright, P. and Aulton, M.E. (1995a). Effect of drug/carrier ratio on the mixing and dispersion of dry powder inhalations of nedocromil sodium. Proceedings 1st World Meeting on Pharmaceutics. Biopharmaceutics and Pharmaceutical Technology, Budapest. 767–768.

Wong, D.Y.T., Wright, P. and Aulton, M.E. (1995b). Influence of drug particle size on the performance of dry powder inhalers. 14th Pharmaceutical Technology Conference, Barcelona, Spain. 86–97.

Yang, T.T. and Kenyon, D. (2000). Use of an agglomerate formulation in a new multidose dry powder inhaler. *Respiratory Drug Delivery VII.* **II**, 503–505.

Yoon, S.H. (1994). Scale-up method for a horizontal - type jet mill. *Advanced Powder Technology*. **5**(1), 53-59.

Zanen, P., Go, L.T. and Lammers, J-W., (1994). The optimal particle size for β-adrenergic aerosols in mild asthmatics. *International Journal of Pharmaceutics.* **107**, 211–217.

Zanen, P., van Spiegel, P I., van der Kolk, H., Tushuizen, E. and Enthoven, R. (1992). The effect of inhalation flow on the performance of a dry powder inhalation system. *International Journal of Pharmaceutics.* **81**, 199–203.

Zeng, X.M., Martin, G.P., Tee, S-K. and Marriott, C. (1998). The Role of Fine Particle Lactose on the Dispersion and Deaggregation of Saltbutamol Sulphate in an Air Stream *In-vitro. International Journal of Pharmaceutics.* **176**, 99–110.

ELSEVIER

International Journal of Pharmaceutics 181 (1999) 243–254

international journal of pharmaceutics

Design of a fluid energy single vessel powder processor for pharmaceutical use

Graham R. Kay [a,*], John N. Staniforth [a], Michael J. Tobyn [a], Michael D. Horrill [a], Linda B. Newnes [b], Stuart A. MacGregor [b], Ming Li [b], Gerald Atherton [b], Richard C. Lamming [c], David W. Hajee [c]

[a] *Pharmaceutical Technology Group, Department of Pharmacy and Pharmacology, University of Bath, Bath BA2 7AY, UK*
[b] *Department of Mechanical Engineering, University of Bath, Bath BA2 7AY, UK*
[c] *School of Management, University of Bath, Bath BA2 7AY, UK*

Received 26 May 1998; received in revised form 14 January 1999; accepted 24 January 1999

Abstract

This study introduces a motionless novel single vessel powder processor designed to carry out all of the unit operations in the preparation of powders for tableting. The processor used controllable fluid dynamics to provide the energy for each unit operation. The vessel design was evaluated using a computational fluid dynamics model which indicated the flow necessary for the intended processing operations to take place. The processor performance was evaluated experimentally for two unit processes: particle size reduction and dry powder mixing. The processor was found capable of reducing the size of lactose granules from a median particle diameter of 459 μm to a median particle diameter of 182 μm within 5 min under optimal process conditions. It was found that a formulation containing lactose granules (373 μm median particle diameter) and a model drug, sodium chloride (30 μm), could be mixed to an improved degree of homogeneity in comparison with equivalent powders blended using a conventional turbulent tumbling technique. It was concluded that a processor having controllable fluid dynamics offered the potential to perform multi-task processing of powders.

Keywords: Particle size reduction; Powder mixing; Single vessel processing; Granulation; Equipment design

1. Introduction

The most commonly used techniques in preparing powders for tableting are wet granulation and direct compression (Armstrong, 1988). Direct compression is the simpler technique, requiring

* Corresponding author. Tel.: +44-1225-826826 (ext. 4831); fax: +44-1225-826114.
E-mail address: prpgrk@bath.ac.uk (G.R. Kay)

0378-5173/99/$ - see front matter
PII: S0378-5173(99)00033-2

only the blending of the drug with specialised excipients prior to tablet compaction. In many cases, however, the properties of pharmaceutical powders do not allow successful tableting, and these powder systems require modification, most commonly by employing a wet granulation process. Conventional wet granulation techniques can involve up to eight separate unit operations (see Fig. 1), each requiring transfer of material from one processing vessel to another (Armstrong, 1988). Modern processing equipment, such as fluid bed granulators and high-speed mixer/granulators, are able to combine some of the unit operations, thereby reducing the number of material transfers. The benefits of this approach include increased economy, improved quality assurance and, in some cases, enhanced product functionality (Cliff, 1991; Kay, 1997). A number of attempts have been made to minimise the number of processing vessels required (Poska, 1991; Robin et al., 1994), however, the technology to perform all of the sub-operations required for wet granulation processing between ingredient dispensing and compaction of the final granules into tablets is not yet available.

This study introduces a number of prototype designs which were developed with the requirement of carrying out the following sub-operations within a single vessel: drug and excipient milling, dry mixing, wet massing/granulation, drying, granule milling and secondary blending. A further design constraint was that all powder movement within the vessel should be carried out without the presence of moving parts within the vessel chamber. In this preliminary work, the characterisation of a novel single vessel processor (SVP) for the unit processes of particle size reduction and dry powder mixing is considered.

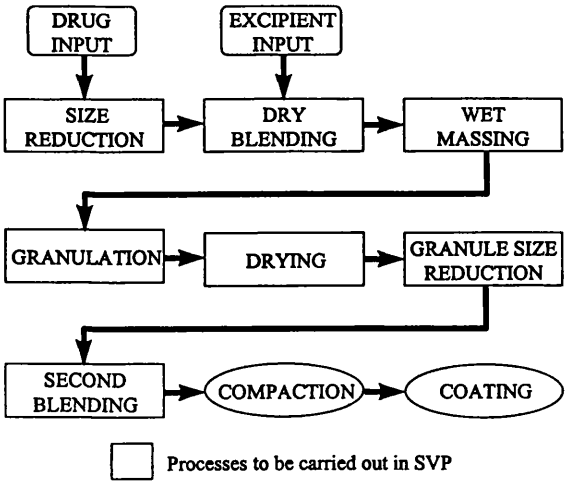

Fig. 1. A summary of the sub-operations performed during tablet manufacture using wet granulation.

A number of different techniques may be used in milling pharmaceutical powders, the most common being ball milling, hammer milling, cone milling and fluid energy milling (Lantz, 1990). Fluid energy or jet mills operate by the acceleration of particles using high pressure jets of a gaseous fluid (usually air), so that they collide with each other or a part of the grinding chamber, causing comminution by particle impact and attrition. In some processing applications, such as ordered mixing (Staniforth, 1980) and dry powder inhalation products (Johnson, 1997), powder particles must be milled to sizes below 5 μm, which is usually achieved by fluid energy milling (Hallworth, 1987). This method of milling also has the advantage that no moving parts come into contact with the product.

The most widely used mixers in pharmaceutical dry mixing operations are tumbling and bladed agitator mixers (Lantz and Schwartz, 1990). A further group of powder mixers is that which employs fluid flows providing either agitation (Akiyama et al., 1986) or fluidization (Krambrok, 1976). This group of mixers is able to mix powders very quickly (Miles and Schofield, 1970) and also without contact of moving parts with the pharmaceutical materials. The use of fluid flows in fluid bed granulation and drying is a well established technique (Kristensen and Schaefer, 1987).

It was therefore intended to investigate whether fluid flows could be used to achieve a combination of the milling, mixing and granulation processes by developing a processor based on controllable fluid dynamics.

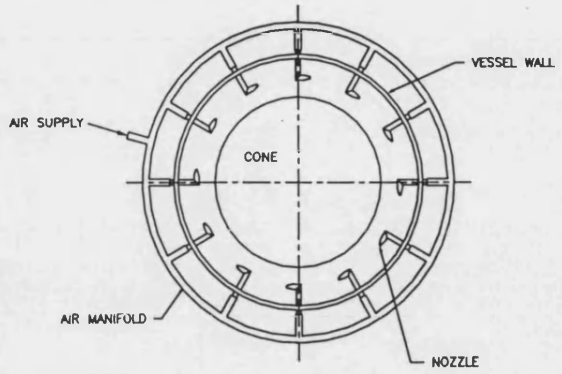

Plan View.

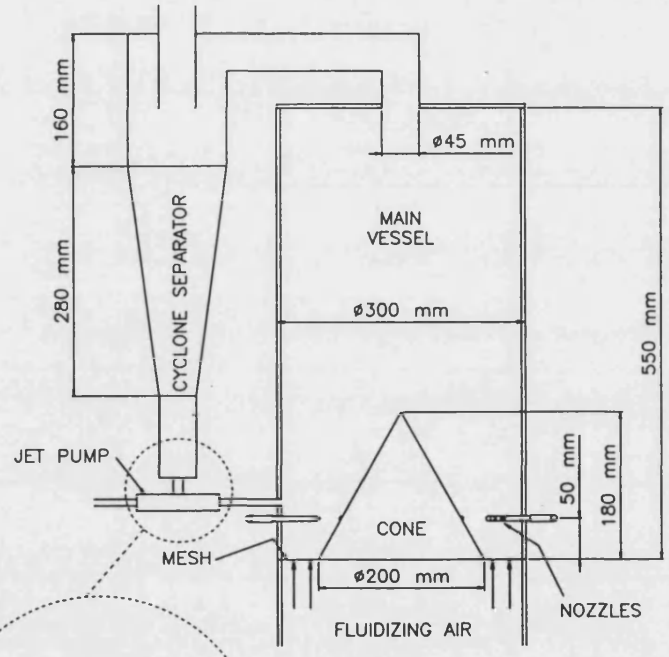

Side View.

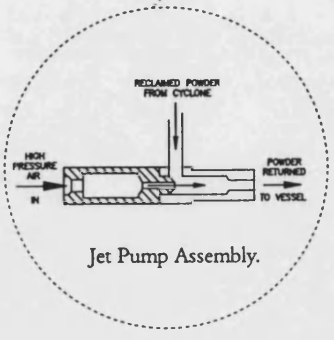

Jet Pump Assembly.

Fig. 2. The SVP Mark IV.

2. Prototype design

2.1. Pre-prototype development

An initial prototype was constructed using a Perspex cylinder, approximately 300 mm in diameter and 250 mm high. Six L-shaped nozzles positioned in a circular arrangement around the base of this vessel provided a vortex air motion which was intended to be similar to the flow pattern found in a bladed system such as a conventional high-speed mixer/granulator (Holm, 1997). It was found that a conical structure, placed in the centre of the base, was able to eliminate a region of low particulate movement in this part of the vessel and some particle size reduction and limited powder mixing was found to occur.

In order to increase the movement of particles around the base of the vessel, it was found that the addition of fluidizing air, directed through the base, was able to reduce frictional contact between the particles and the base sufficient to allow improved size reduction and mixing characteristics (Bates and Ball, 1993). In this case the central cone was replaced by a 'honeycomb' distributor plenum.

2.2. The SVP Mark IV

Following these initial investigations, a prototype processor, the 'SVP Mark IV', (Kay, 1997) was constructed as shown in Fig. 2.

A hollow cylinder of clear Perspex of wall thickness 6 mm was used for the main vessel wall so that powder movements could be observed during operation of the processor. This was fitted with a mesh base of 100 μm aperture diameter. This provided support for powder within the vessel, whilst allowing uniform fluidization of the powder bed when air was introduced through the base. A lid provided with a rubber o-ring seal was attached to the top of the vessel using four case clasps. A polyethylene cone was fixed to the centre of the vessel base to prevent the formation of a dead area in this part of the vessel.

Fluidizing air was ducted into the bottom of the vessel from a centrifugal fan (Type D28, 0.75 kW, Robert Stahlschmidt Elektromotorenwerk, Germany) of fan diameter 180 mm, blade width 12 mm and blade angle 20°. This could be operated at a maximum rotational speed of 2800 rpm, which produced a calculated maximum air flow rate of 0.0456 m^3/s.

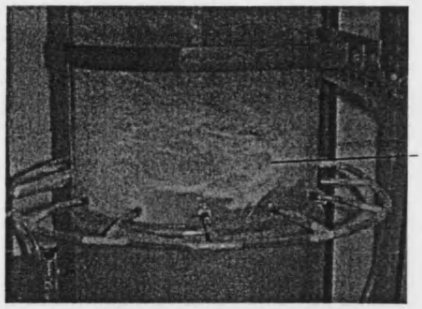

Fig. 3. Photograph of flow patterns of lactose powder generated during the operation of the SVP Mark IV.

Twelve L-shaped high pressure jet nozzles of 1 mm output diameter were located around the base of the vessel and connected to a compressed air manifold. A compressed air feed of approximately 550 kPa was able to supply each nozzle at a validated (Kay, 1997) pressure of up to 30 psi (207 kPa). The design of the nozzles was such that they could be adjusted for angle and depth within the vessel as required. A needle valve allowed control of the nozzle output pressure.

The attachment of a cyclone separator to the vessel lid enabled the removal of entrained particles from air leaving the vessel during operation of the air inputs. The gas outlet of the cyclone was allowed to vent to atmosphere and the dust outlet was attached to a jet pump. High pressure air was directed through the jet pump nozzle, causing air to be drawn through the top hole. This produced a suction effect which returned powder from the cyclone dust outlet back into the main vessel.

The Mark IV SVP was found to provide more uniform and widespread powder movement than previous designs and powder losses from the vessel were also greatly reduced. The powder flow patterns achieved within the vessel can be seen in Fig. 3. A further advantage of the Mark IV design over the previous designs was that it was not

necessary to maintain a fluidizing air input at all times, thus making it easier to control the process and to remove powder at the end of processing.

3. Particle size reduction

3.1. Materials

Two grades of granular lactose (α-lactose monohydrate) were selected as model test materials. These were of similar particle size ranges, but were prepared by different methods and consequently could be expected to exhibit different physical strength properties.

The first test material was a pharmaceutical quality commercially-available granular lactose (CAGL), CrystaLac 40 (Meggle, Wasserberg, Germany). The second material was granulated lactose manufactured using SorboLac 400 lactose powder (Meggle, Wasserberg, Germany). This particular grade of material has a higher specific surface area and finer particle size than CAGL. The granulation was performed in a high-speed mixer/granulator, using water (20% w/w compared to dry powder) as a binding liquid. The granules were fluid-bed dried to a moisture content of less than 5% w/w and granules outside the sieve fraction 250–500 μm were discarded. This material was termed high-speed mixer/granulated lactose (HSMGL).

3.2. Methods

Either CAGL or HSMGL material in 500g lots were placed in the SVP vessel and size reduction carried out over 30 min. Three lots of each material were processed in the SVP at nozzle pressures of 10, 20 or 30 psi. (69, 138 and 207 kPa, respectively) and the nozzle output air pressures were validated using a pressure transducer (type P722-022 pressure sensor, Schaevitz, UK.).

Representative samples of approximately 1.5 g were obtained from four positions in the powder bed using a sampling thief at each of the following times after the initialisation of size reduction: 0, 1, 2, 3, 4, 5, 7.5, 10, 15, 20, 25 and 30 min. Particle size analysis was performed in triplicate with low angle laser light scattering (LALLS) equipment (Malvern Mastersizer X, Malvern Instruments, Malvern, UK) using a dry powder feeder technique.

Scanning electron microscopy (SEM) was used to produce images of particles at different stages of milling. The specimens were prepared by mounting a representative powder sample onto a conducting carbon-coated adhesive pad fixed to an aluminium stub. The sample was then coated with a layer of gold using a sputter coater (EHV model S150B, Edwards High Vacuum, Sussex, UK). Specimens prepared in this manner were examined using a scanning electron microscope (JEOL T330 SEM, Japanese Electron Optics, Tokyo, Japan) operating with an incident beam of 10 keV at a working distance of 25 mm.

Table 1
Summary of change in median particle diameter during milling of CAGL in the SVP Mark IV at different nozzle pressures

Nozzle pressure (psi)	Median particle diameter (μm)											
	Milling time (min)											
	0	1	2	3	4	5	7.5	10	15	20	25	30
10	459	401	415	390	330	314	283	272	230	236	221	199
20	459	345	358	287	261	281	211	233	196	194	174	167
30	459	297	227	197	199	182	180	172	163	157	160	157

Table 2
Summary of change in median particle diameter during milling of HSMGL in the SVP Mark IV at different nozzle pressures

Nozzle pressure (psi)	Median particle diameter (μm)											
	Milling time (min)											
	0	1	2	3	4	5	7.5	10	15	20	25	30
10	373	355	304	317	339	274	297	241	195	151	154	127
20	373	316	251	249	198	188	163	141	121	118	115	109
30	373	245	238	202	164	155	134	131	107	115	117	107

3.3. Results and discussion

Data describing the changes in median particle diameter during milling are summarised in Tables 1 and 2 for CAGL and HSMGL, respectively.

Fig. 4 shows the change in size distribution of CAGL when milled over 30 min at a nozzle pressure of 30 psi. It can be seen from this graph that after 1 min of milling, firstly that the modal size of the CAGL was reduced and secondly it exhibited a unimodal distribution. This latter observation is noteworthy since milling operations usually result in bimodal distributions and may therefore be indicative of a non-standard size reduction mechanism.

The effect of milling time at a nozzle pressure of 30 psi on the particle size distribution of HSMGL can be seen in Fig. 5. In this case, the size distribution takes on a bimodal character after 1 min milling time. This is a classical response profile for the early stages of a milling process.

On this evidence, it is suggested that in the case of CAGL, most of the agglomerates were reduced to their constituent crystallites within the first minute of milling at 30 psi; the stage of milling at which all, or nearly all, individual crystallites have been liberated from the agglomerates is termed the 'point of complete deagglomeration' (POCD) and is considered to be a key SVP process parameter.

In contrast to CAGL, the HSMGL agglomerates appear to be broken down less easily into their constituent crystallites and hence, after a milling time of 1 min, exhibit a bimodal distribution in which many of the agglomerates are still largely intact, but a proportion of them have been broken into individual crystallites. This implies that the bond strength between crystallites in HGMGL are stronger than those in CAGL. This theory is further supported by the SEM photomicrographs (Figs. 6 and 7), which show a larger proportion of agglomerates in the HSMGL after 1 min of milling than are present in CAGL.

Further examination of Fig. 4 presents a downward trend for the modal size of CAGL. However, after about 1 min milling time, the modal and median sizes are less affected by increasing milling time. This suggests that most of the agglomerates have been broken down into their constituent crystals after 1 min and any further reduction in particle size is probably due to fragmentation of the individual crystallites by edge abrasion as shown in Fig. 8.

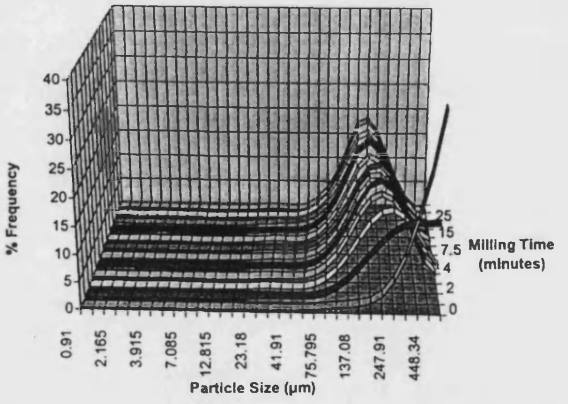

Fig. 4. Relationship between particle size distribution of CAGL and milling time in the SVP Mark IV at a nozzle pressure of 30 psi.

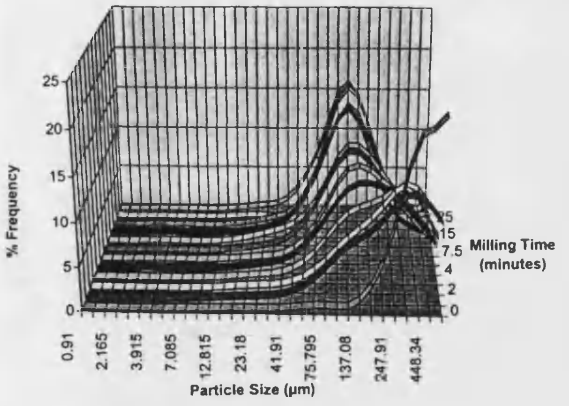

Fig. 5. Relationship between particle size distribution of HSMGL and milling time in the SVP Mark IV at a nozzle pressure of 30 psi.

This mechanism may suggest that fragmentation of the component crystals would lead to the formation of a fine particle fraction in the later stages of milling and hence a bimodal size distribution. However, there is no evidence in the particle size data to suggest this is the case. This may be explained by a preferential removal of fines by the SVP since observation of the SVP during milling indicated that a certain amount of fine particulate material was entrained in the air leaving the cyclone separator.

The effect of reducing the milling nozzle pressure was investigated. As expected, the rate of milling was reduced with decreasing nozzle pressures for both materials. The times taken to reach the POCD for CAGL and HSMGL at different nozzle pressures and the median particle diameter of the materials at these times are summarised in Table 3.

The milling data suggests that for CAGL, the maximum milling capability of the SVP was to mill the material to a median particle diameter of approximately 160 μm. This appears to have been achieved at nozzle pressures of 30 and 20, but not at 10 psi. The maximum milling capability of the SVP for HSMGL appears to be to a median particle diameter of approximately 110 μm. It is speculated that different milling conditions, such as higher nozzle pressures or changing the geometry of the vessel, may result in an increase in the

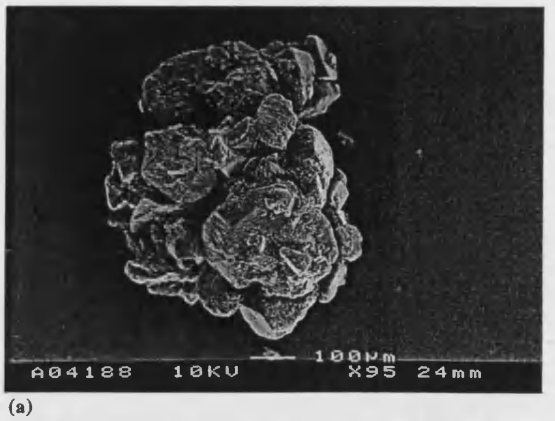

(a)

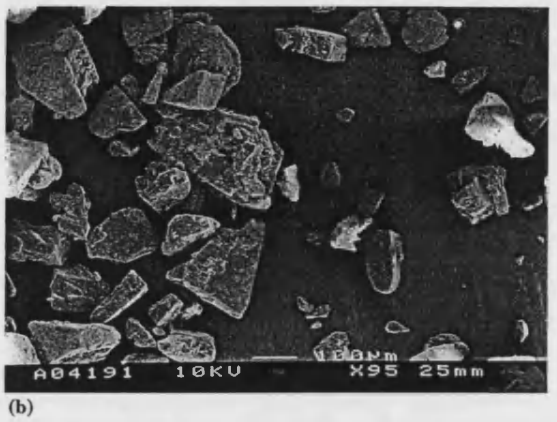

(b)

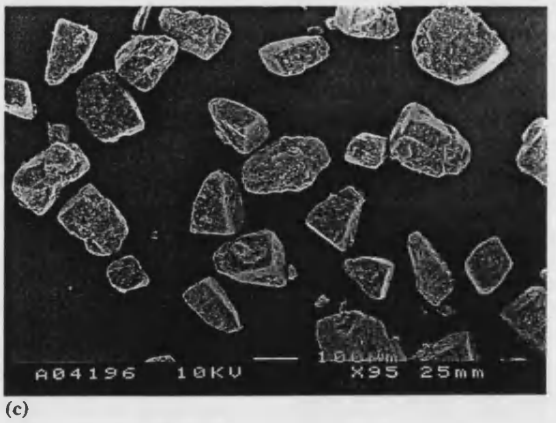

(c)

Fig. 6. Scanning electron micrographs of CAGL before and after milling at a nozzle pressure of 30 psi: (a) unprocessed particle, (b) after 1 min processing, and (c) after 30 min processing.

(a)

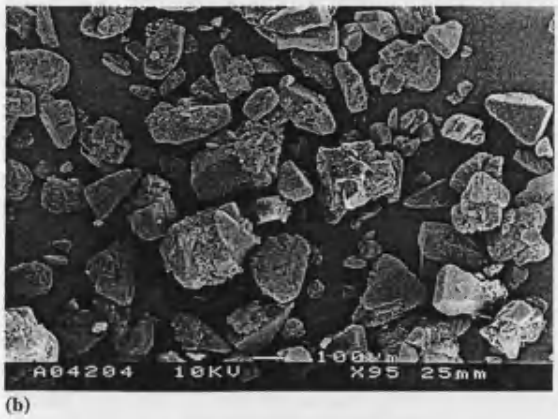

(b)

(c)

Fig. 7. Scanning electron micrographs of HSMGL before and after milling at a nozzle pressure of 30 psi: (a) unprocessed particle, (b) after 1 min processing, and (c) after 30 min processing.

milling capacity as well as an increase in the rate of milling.

4. Mixing

4.1. Materials

Lactose powder (CrystaLac 40, Meggle, Wasserberg, Germany) was used as the major component (90%) and sodium chloride crystals (Lot No. 40414 40408011, Aldrich Chemical, Gillingham, Dorset, UK) the minor model drug component (10%) of a 500 g binary powder mix. Sodium chloride was selected as a model drug to allow conductivimetric analysis over a wide concentration range without requiring sample dilutions. The median particle diameter of the lactose was 373 μm and that of the sodium chloride was 30 μm as measured by LALLS.

This difference in the particle diameters of the two components was deliberately selected so as to encourage the formation of interactive mixes in which finer particles become adhered to the surfaces of coarser, 'carrier' particles.

4.2. Methods

The efficiency of the SVP for mixing two dry powders was compared with other mixing techniques with known efficiencies: geometric mixing and turbulent tumbling mixing.

4.2.1. Geometric mixing

Geometric mixing, or trituration, was performed by placing 50 g sodium chloride crystals and 50 g lactose granules into a large mortar and mixing thoroughly by hand for 5 min using a pestle. A further 100 g lactose was added and similarly mixed, followed by a 200 g quantity of lactose, which was also mixed for 5 min. The final 100 g of lactose was added and the whole mixture thoroughly mixed for a further 15 min.

4.2.2. Turbulent tumbling mixing

Milled sodium chloride crystals (50 g) and lactose granules (450 g) were placed into a 2 l glass jar and its lid was sealed. This was then posi-

tioned in a Turbula mixer (type T2C, Glen Creston, Stanmore, Middlesex, UK), which was operated at speed II for 30 min.

4.2.3. Operation of the SVP

Lactose granules (450 g) were placed into the bottom of the SVP, on top of which 50 g of sodium chloride was gently loaded. The fluidizing fan was turned on at its maximum speed providing an air volume throughput of approximately 2 m^3/h and the jet nozzles supplied with air at a pressure of 30 psi.

These conditions were maintained for a period of 30 min after which the air supply was terminated and the powder removed from the vessel for sampling and analysis.

4.2.4. Powder sampling

The material obtained from each mixing experiment was emptied onto a clean, flat surface with a minimum of agitation, so that samples could be taken from the resulting powder heap. Thirty samples of approximately 500 mg were taken at random from the mixture using a sample thief.

4.2.5. Model drug assay

The samples (500 mg) were placed in a 50 ml volumetric flask, then dissolved and diluted to 50 ml using freshly distilled, deionised water at 25°C. A conductivity meter (type CDM80, Radiometer, Denmark) and cell (type CDC104, Radiometer, Denmark) was calibrated, then each sample solution was assayed for sodium chloride content based on the conductivity of the solution. Controls showed that, as expected, lactose did not add to the conductivity.

4.3. Results and discussion

As expected, the most efficient mixing of the materials tested was obtained by manual geometric mixing, which provided a coefficient of variation of 0.93%. The value of using this technique was to provide evidence that a homogeneous mixture could be obtained using the materials under investigation. The results using manual geometric mixing may be considered as a benchmark for other mixing techniques. Since the method of homogeneity testing can be considered to give values that are a composite for mixing and segregation, any segregation phenomena that occur during the mixing process are taken into account.

It is notable that the results indicate a mean content which is slightly less than the theoretical value of 10.0% sodium chloride. This may have occurred through agitation of the material causing a loss of fine particles to the external environment since the mixing vessel was not enclosed during the mixing process. Since this lost fine material would have been predominantly composed of sodium chloride particles this may account for the low content.

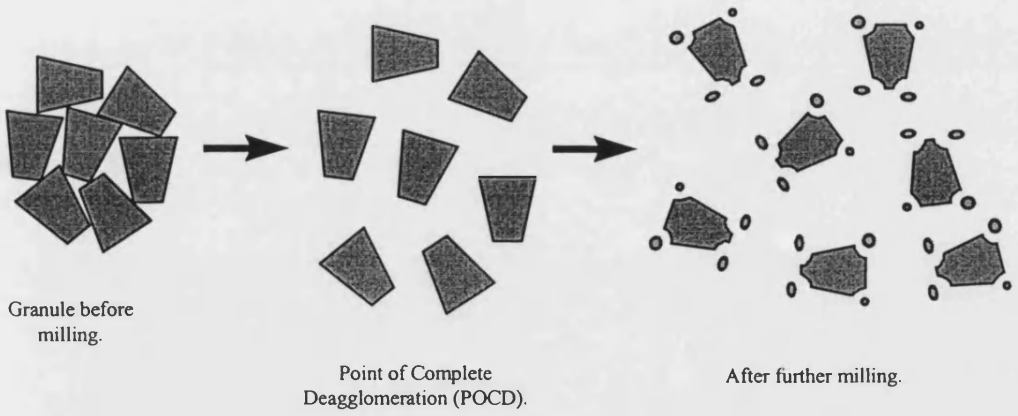

Fig. 8. Proposed milling mechanism of CAGL and HSMGL in the SVP Mark IV.

Table 3
Summary of time taken to reach POCD and median particle diameter at POCD for CAGL and HSMGL at different nozzle pressures

Material	Nozzle pressure (psi)	Time taken to reach POCD (min)	Median particle diameter at POCD (μm)
CAGL	30	1	297
HSMGL	30	5	155
CAGL	20	3	287
HSMGL	20	10	141
CAGL	10	5	314
HSMGL	10	20	151

The quality of mix obtained by using the turbulent tumbling technique was poor, being characterised by a coefficient of variation of 15.20%. This was probably due to a lack of internal shear forces, particularly between initial fine particle agglomerates of sodium chloride, provided by tumbling mixing. These forces are necessary for the formation of interactive powder mixtures.

The effect of the shearing force which is imparted onto a powder mixture containing two components, one of which is much finer than the other is shown diagrammatically in Fig. 9. This figure shows an agglomerate of the fine component, which is mixed with larger carrier particles. A low shear force takes the easiest route through the powder, which in this case is around the exterior of the carrier particles and the fines agglomerate. A high shear force is able to pass between individual particles in the agglomerate and hence break it up so that it may be distributed over the carrier surfaces and form an interactive mix. The geometric manual mixing technique imparts a large shear force on the powder by the grinding action of the mortar and pestle. This causes the adhesive component (sodium chloride) to be redistributed onto the carrier particle surface.

Aggregates, which may be of a similar particle size to the carrier lactose particles, remain intact in the turbulent tumbling technique due to this lack of shear, so reducing the homogeneity of the mix.

It was considered that the high shear conditions created by the high pressure air nozzles within the SVP would be able to break up the agglomerates during the mixing evaluation in a similar fashion to that which would be expected in a bladed mixer.

A value for the coefficient of variation of less than 5% is generally considered necessary in most pharmaceutical powder mixing processes (Kay, 1997). The SVP provided a mixing capability characterised by an average coefficient of variation of 2.49%. As shown in Table 4, this is represents an improved mixing efficiency over turbulent tumbling mixing. The motion of powder within the SVP during its operation was observed to display large regions of recirculating flow, which enable mixing to occur (see Fig. 3).

The SVP design was tested using a computational fluid dynamics (CFD) model (STAR_CD, Version 3, Computational Dynamics, London, UK). The model allowed different flow regimes to

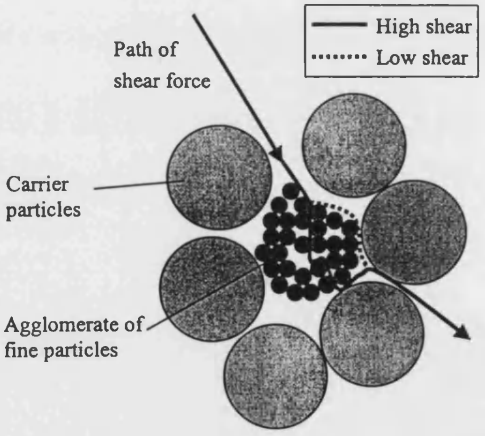

Fig. 9. Schematic representation of the path of the shear force following application of high and low shear forces in interactive mixing.

Table 4
Coefficient of variation obtained from each mixing technique

Mixing method	Coefficient of variation (%)	Mean content (%)
Manual geometric mixing	0.93	9.41
Turbulent tumbling mixing	15.20	9.49
Mixing in the SPV Mark IV	2.49	8.17

be studied, an example of which is shown in Fig. 10, and indicated relatively few dead regions where particles could settle (MacGregor et al., 1998). Experimental testing showed that the CFD predictions appeared to be exhibited by the SVP. The lack of dead spots predicted in the CFD model was also considered to exist experimentally and was assumed to be a major reason for enhanced mixing efficiency. The combination of fluidizing air, which was supplied to all of the flat regions of the vessel base, with the swirling flow fields generated by the high pressure air nozzles ensured that the flow patterns within the SVP attained sufficiently turbulent conditions and fluctuating velocities within the powder bed to perform the mixing process. The high shear created by the action of the high pressure air nozzles facilitated the mixing of a binary powder system consisting of powders of widely differing particle sizes, thus enabling the formation of interactive powder mixes.

5. Conclusion

A prototype SVP was designed with the aid of a computational fluid dynamics model and was found to be capable of performing the sub-operations of granule size reduction and dry powder mixing. There was also some evidence that the SVP was capable of providing primary size reduction of materials. The flow patterns induced in powder within the processor could be readily observed and displayed a strong swirling flow field which was well fluidised.

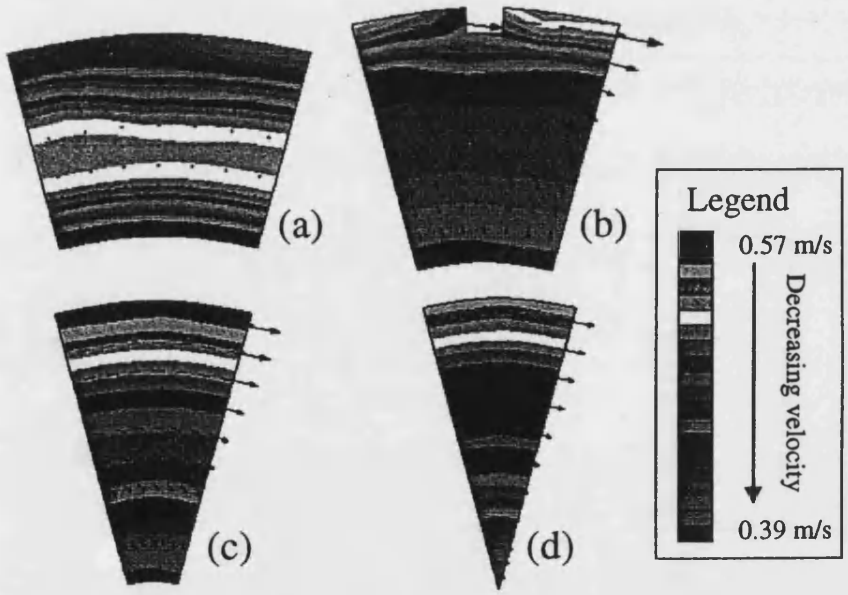

Fig. 10. Example of the CFD model of the SVP Mark IV for single phase flows. The model shows 1/12 cross-sections of the vessel in the plan view at (a) the base of the vessel, (b) 50 mm from the base (nozzle outlet height), (c) 100 mm from the base, and (d) 180 mm from the base (apex of the cone). The arrows indicate the direction of the airflow. Relative flow velocity magnitudes are indicated by reference to the colours in the legend.

Particle size reduction was found to be rapid for the batch size investigated; the speed and extent of granule size reduction was considered to be at least equivalent to that which could be attained using conventional techniques of secondary size reduction in granulation. It is envisaged that greater size reduction could be obtained by increasing the nozzle pressures.

The mixing achieved within the SVP was found to be rapid and more homogeneous than that achievable with a similar powder system using a conventional low shear mixing technique.

The principle of using controllable fluid dynamics to perform multi-task processing of powders has been demonstrated. The SVP offers the potential for the batchwise preparation of powders for tableting and capsule filling within a single vessel.

One problem that was encountered with the current SVP design was in separating very fine particles from the gas stream using a cyclone separator. In order to improve this aspect of processing, it is anticipated that future designs will require the addition of a fibrous filter system.

The SVP concept is considered to form the basis for a continuous bladeless processor, capable of integration into a closed, automated and controllable manufacturing system in which raw materials can be processed into final dosage forms without manual intervention.

References

Akiyama, T., Zhang, J.Q., Egawa, M., Kojima, H., 1986. Mixing of fine particles by means of a negative pressure air mixer. Ind. Eng. Chem. Proc. Des. Dev. 25, 682–687.

Armstrong, N.A., 1988. Tableting. In: Aulton, M.E. (Ed.), Pharmaceutics. The Science of Dosage Form Design. Churchill Livingstone, London, pp. 647–668.

Bates, M.J., Ball, J.G., 1993. Design of a single vessel pharmaceutical processor under computer control. Project report A08. Department of Mechanical Engineering, University of Bath, Bath, UK.

Cliff, M.J., 1991. Tablet processing facility design for the future. Pharm. Eng. 11 (1), 15–20.

Hallworth, G.W., 1987. The formulation and evaluation of pressurised metered-dose inhalers. In: Ganderton, D., Jones, T.M. (Eds.), Drug Delivery to the Respiratory Tract. Ellis Horwood, Chichester UK, pp. 87–118.

Holm, P., 1997. High Shear Mixer Granulators. In: Parikh, D.M. (Ed.), Handbook of Pharmaceutical Granulation Technology. Marcel Dekker, New York, pp. 151–204.

Johnson, K.A., 1997. Preparation of peptide and protein powders for inhalation. Adv. Drug Deliv. Rev. 26, 3–15.

Kay, G.R., 1997. Design and Characterisation of a Single Vessel Pharmaceutical Powder Processor. MPhil Thesis. Department of Pharmacy and Pharmacology, University of Bath, Bath, UK.

Krambrok, W., 1976. Mixing and homogenising of granular bulk material in a pneumatic mixer unit. Powder Technol. 15, 199–206.

Kristensen, H.G., Schaefer, T., 1987. Granulation. A review of pharmaceutical wet granulation. Drug Dev. Ind. Pharm. 13 (4-5), 803–872.

Lantz, R.J., 1990. Size reduction. In: Lieberman, H.A., Lachman, L., Schwartz, J.B. (Eds.), Pharmaceutical Dosage Forms: Tablets, vol. 2, 2nd edn. Marcel Dekker, New York, pp. 107–200.

Lantz, R.J., Schwartz, J.B., 1990. Mixing. In: Lieberman, H.A., Lachman, L., Schwartz, J.B. (Eds.), Pharmaceutical Dosage Forms: Tablets, vol. 2, 2nd edn. Marcel Dekker, New York, pp. 1–71.

MacGregor, S.A., Newnes, L.B., Ming, L. et al. 1998. The use of computational fluid dynamics in the design of a pharmaceutical processor, Int. Symp. on Computational Technologies for Fluid/Thermal/Chemical Systems with Industrial Applications, Joint ASME/JSME Pressure Vessels and Piping Conference, 26-30 July 1998, San Diego, CA.

Miles, J.E.P., Schofield, C., 1970. Performance of several industrial mixers using non-segregating free flowing powders. Trans. Inst. Chem. Eng. 48, T85–T89.

Poska, R., 1991. Integrated mixing, granulating and microwave drying: a development experience. Pharm. Eng. 11 (1), 9–13.

Robin, P., Lucisano, R.P., Pearlswig, D.M., 1994. Rationale for the selection of a single pot manufacturing process using microwave/vacuum drying. Pharm. Technol. 18, 28–36.

Staniforth, J.N., 1980. Ordered mixing of drugs with particulate excipients. PhD Thesis, University of Aston, Birmingham, UK.

The application of computational fluid dynamics to the development of a pharmaceutical processor

S A MacGregor[1]*, L B Newnes[1], M Li[1], J N Staniforth[2], M J Tobyn[2], G R Kay[2], M D Horrill[2], R C Lamming[3], D W Hajec[3], D Wong[4], K E Chippendale[5] and T Page[5]
[1]Department of Mechanical Engineering, University of Bath, UK
[2]Department of Pharmacy and Pharmacolgy, University of Bath, UK
[3]School of Management, University of Bath, UK
[4]Rhone Poulenc Rorer
[5]Aeromatic Fielder

Abstract: The use of computational fluid dynamics (CFD) in the design of a pharmaceutical processor is described. A simple computational model of the process vessel was developed using a single-phase flow. The results of this preliminary study showed good agreement with experimental tests. The model was further developed to consider the effect of solid particles on the processes occurring within a single vessel pharmaceutical processor. Having obtained converged solutions, the model was used to optimize the design of the processor. The model was used to develop new designs of the vessel. The design optimization was done on the basis of comparisons with conventional pharmaceutical processing equipment. Optimization of the process parameters is important, as they are known to affect the functionality of the final product. The study reported here discusses one step in the design process, showing how changes to the inlet configuration can be modelled to show the potential for improved performance.

Keywords: CFD, pharmaceutical processors, powders

1 INTRODUCTION

In the preparation of powders for tabletting, techniques such as wet granulation and direct compression are widely used. Conventional wet granulation techniques may involve as many as seven individual subprocesses. Initially the excipients and drug substance are screened. The drug and excipients are then mixed. In the next phase liquid is added and granules are formed. This is followed by a drying phase before final size reduction (forced screening) and mixing are completed. These processes are often carried out in separate vessels, thus making the overall process inefficient and with reduced quality due to the need for transportation of materials, holding the powders *in situ* and long changeover times between batches. In an attempt to rationalize the process by reducing the number of processing vessels or process steps, there are examples of single-vessel processors, which combine some but not all of the individual subprocesses [1–3].

The current study focuses on the design of a single vessel in which all seven subprocesses are carried out. Computational fluid dynamics (CFD) has been used extensively in the design phase of the processor. The use of CFD is now commonplace and there are many examples of its application [4–6].

2 PHYSICAL MODEL

A schematic diagram of the single-vessel processor is shown in Fig. 1. The vessel consists of a cylindrical section that has a cone at the base. The purpose of the cone is to fill the central region to avoid the settling out of powder in regions where the velocity is low. There are two sets of air inlets to the vessel. One, which provides air for fluidizing the powder, is of low velocity but has a high volume flowrate. The fluidizing air not only lifts the powder from the base of the vessel but also provides some of the air motion, which enhances the mixing and size reduction processes. The second set

The MS was received on 15 April 1999 and was accepted after revision for publication on 21 April 1999.
**Corresponding author: Department of Mechanical Engineering, Faculty of Engineering and Design, University of Bath, Claverton Down, Bath BA2 7AY, UK.*

supplies the ring of high-pressure nozzles around the periphery of the vessel, just above the base. These high-velocity jets provide energy for the various unit subprocesses. The outlet from the vessel passes through a cyclone dust separator, where any powder that escapes from the processing section is collected and returned to the main vessel through a jet pump. In future designs it is anticipated that the cyclone separator will be replaced by a more effective filtration system, which is more effective with small-diameter particles, i.e. a bag filter.

A second design was developed in which the fluidized bed was replaced by a series of 'flat' tangential nozzles. Again the nozzles not only provided the air to lift the particles off the base of the vessel but also provided the initial bulk motion for the particles within the vessel.

3 COMPUTATIONAL MODELS

The CFD model was constructed using the code STAR_CD and consisted of a three-dimensional axisymmetrical sector of the vessel. The computational grid consisted of 4000 cells and is shown in Fig. 2. Near the exit of the vessel the velocity gradients are significant and hence the grid has been refined in this region. Similarly, near the base of the vessel where the size reduction and mixing processes are most intense, the grid has also been refined. In order to model the high-pressure nozzles, the nozzle inlet velocity magnitude and direction have been set at the wall. It was not necessary to model the actual geometry of the nozzles as they were small by comparison with the rest of the vessel and thus had little effect on the overall flow field.

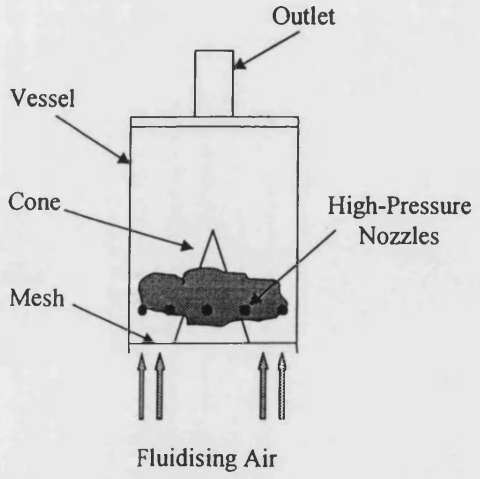

Fig. 1 Schematic diagram of a single-vessel processor

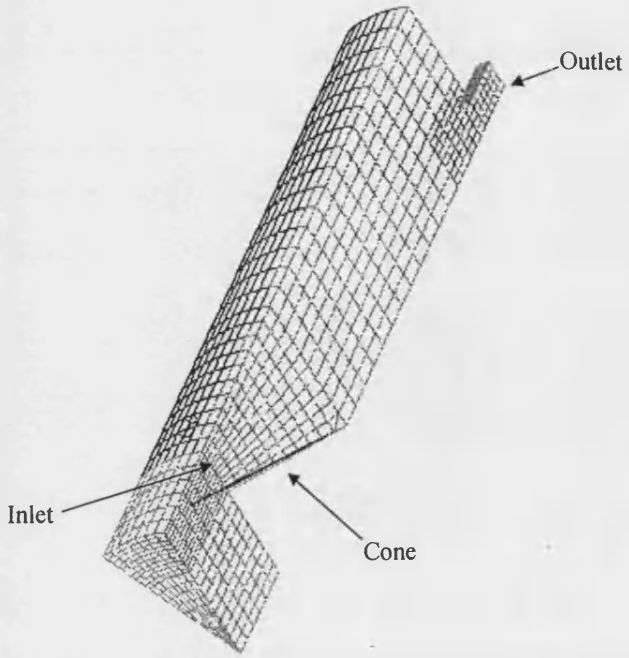

Fig. 2 Computational model of a single-vessel processor

The software offered a number of options in the use of turbulence models. However, it was found that the best convergence and most consistent results were achieved using a $k-\varepsilon$ model. The model was run for both single- and two-phase flow cases. In the latter the solids loading was varied between 10 and 40 per cent by volume. For a solids loading of 10 per cent it was relatively easy to achieve consistent convergence. Although this level of solids loading was not representative of an actual processor, it was useful in order to check the validity of the results. A solids loading of 40 per cent was considered to be representative of the loading that would be present in an industrial-scale system. However, it was more difficult to achieve converged solutions. In the main volume the bottom two layers of the computational grid are loaded with particles. This investigation focused on particles that had a diameter of 50 μm. This particle size lies within the range of powders used in the pharmaceutical industry for tablet production. In later models various size distributions were used. However, this was found to have only a minimal effect on the results. The major factor was the actual size of the solid particles. It should be noted that only the particle movement has been considered in this study. No attempt has been made to model the particle–particle interactions in terms of particle break-up or agglomeration.

The values for the fluidizing and nozzle velocities were selected based on preliminary experimental testing. Only the results for two-phase flows are presented in the current study.

4 RESULTS

Two cases are presented, although many other cases have been considered and modelled. Figure 3a shows the case for a vessel with a fluidized bed. The fluidizing velocity was set at a value of 0.2 m/s, while the inlet velocity for the high-pressure jets was 3.68 m/s. These values were found to give the best results. It is clear from Fig. 3a that a large region of recirculating flow dominates the flow field. Particles are carried up the central region of the vessel. As they reach the upper part of the vessel, the influence of the inlet jets is reduced and the majority of the particles are carried in the recirculating flow back to the base near the wall.

Near the top of the vessel there is a region where the flow accelerates due to the outlet pipe. This is clearly seen in single-phase predictions carried out on this geometry. Some particles may be carried out of the vessel with this flow. This is especially so of any smaller particles that may be present. Loss of particles from the main vessel causes the process to become inefficient, as these particles must be collected and recycled to the main vessel. It may also result in final mixtures that have poor homogeneity, as many of the excipients, which are being mixed in the vessel, will have different size ranges.

In Fig. 3b the flow field is predicted for the case where the fluidized bed has been replaced by a series of tangential inlets. Comparing Figs 3a and b shows

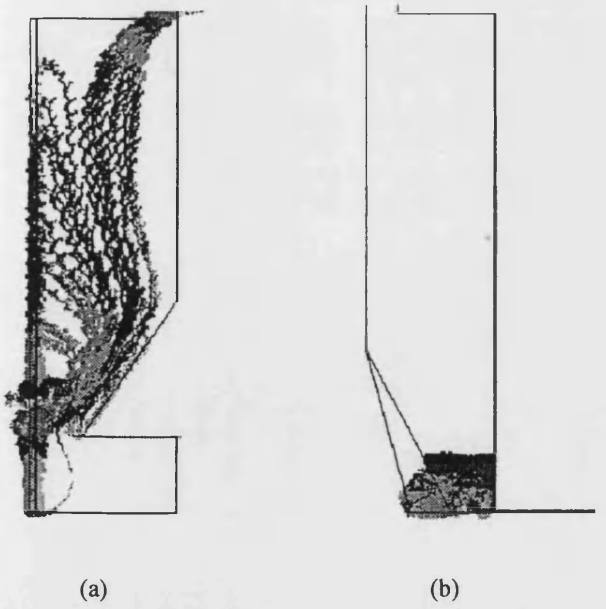

(a) (b)

Fig. 3 Predicted particle tracks for a vessel with fluidized bed and tangential inlets

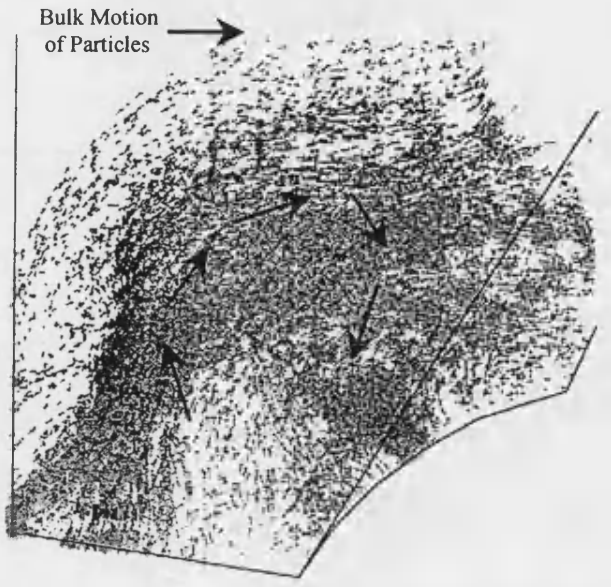

Fig. 4 Enlarged three-dimensional particle tracks for a vessel with tangential inlets

that the behaviour of the particles is completely different in the two cases considered. In the latter case the particles are concentrated in the region close to the base of the vessel. Very little solid material is able to penetrate the upper part of the vessel. There are a number of advantages associated with this flow field from the point of powder processing. Concentrating the powder in the base means that it is difficult for solid particles to escape from the vessel. It might be possible to reduce the height of the vessel as the process is confined to a relatively small volume. By concentrating the solid material in a particular region of the vessel it ensures that there are many particle interactions, which are essential to generate both good mixing and size reduction. In a final design it may well be advantageous to combine the best features from both flow fields, i.e. the large recirculation region which enhances the mixing processes and regions where the particle concentration is high, thus ensuring many particle collisions, etc., when size reduction is required.

The results of the predictions for the case with tangential inlets rather than a fluidized bed showed that with some inlet conditions there was a possibility that there could be problems with powder deposition [7]. These predictions were made on the basis of powder concentration throughout the vessel. Regions with high concentrations of solids were found to coincide with regions where powder collected during experimental testing.

Figure 4 shows a three-dimensional enlarged view of the particle tracks for the vessel with tangential

ports around the base. The particles are seen to move up the side of the cone and then radially outwards before returning to the base of the vessel. The particle motion generated by the air inlet jets is similar to that seen in conventional mixer and granulators.

5 CONCLUSIONS

The use of computational fluid dynamics has been considered for the optimization of the design of a single-vessel pharmaceutical processor. The results from an investigation were presented, which showed that by predicting flow field parameters and particle dynamics it was possible to improve the geometry of a powder processor. It was also possible to assess the effects of inlet conditions. By considering both flow vector plots and particle trajectories the performance of new design proposals can be compared with that of conventional pharmaceutical processors. It is possible to show that the proposed design will achieve the levels of performance required for the new design to be successful. The use of CFD to design the processor removes the need to build and test expensive prototype equipment.

REFERENCES

1 **Robin, P., Lucisanol, J.** and **Pearlswig, B. M.** Rationale for selection of a single-pot manufacturing process using microwave/vacuum drying. *Pharm. Technol.*, 1994, **18**, 28.

2 **MacGregor, S. A., Staniforth, J. N., Newnes, L. B.** and **Kay, G. R.** A preliminary study of a single vessel pharmaceutical processor. *Proc. Instn Mech. Engrs, Part E, Journal of Process Mechanical Engineering*, 1996, **210**(E2), 121–124.

3 **Newnes, L. B., Staniforth, J. N.** and **MacGregor, S. A.** Flexible pharmaceutical powder production. *IJCIM*, 1996, **9**(3), 227–233.

4 **MacGregor, S. A., Syred, N.** and **Morgan, D. J.** *Coal Fired Cyclone Combustors. Coal Combustion: Science and Technology of Industrial and Utility Applications*, 1988, pp. 657–664 (Hemisphere Publishing, New York).

5 **Biffin, M.** Improved cyclone dust separators for hot gas clean up. PhD thesis, University of Wales, 1984.

6 **Gupta, A. K., Lilley, D. G.** and **Syred, N.** *Swirl Flows*, 1984 (Abacus Press).

7 **MacGregor, S. A., Newnes, L. B., Li, M., Staniforth, J. N., Tobyn, M. J., Kay, G. R., Horrill, M. D., Lamming, R. C.** and **Hajee, D. W.** Computational study of deposition in powder processors. In 2nd International Symposium on *Computational Technologies for Fluid/Thermal/Chemical Systems with Industrial Applications*, ASME-PVP, Boston, 1999.